FUGRO

Geophysical Results Report

North Sea OWF Zone West (Lot 2) Geophysical Survey | Danish North Sea

F176286-REP-GEOP-001 05 | 16 August 2022
Final
Energinet Eltransmission A/S

ENERGINET

Document Control

Document Information

Project Title	North Sea OWF Zone West (Lot 2) Geophysical Survey
Document Title	Geophysical Results Report
Fugro Project No.	F176286
Fugro Document No.	F176286-REP-GEOP-001
Issue Number	05
Issue Status	Final
Fugro Legal Entity	Fugro Netherlands Marine
Issuing Office Address	Prismastraat 4, Nootdorp, 2631RT, The Netherlands

Client Information

Client	Energinet Eltransmission A/S
Client Address	Tonne Kjærsvej 65, DK-7000 Fredericia, Denmark
Client Contact	Martin Bak Hansen
Client Document No.	N/A

Document History

Issue	Date	Status	Comments on Content	Prepared By	Checked By	Approved By
01	11 Mar 2022	Complete		JSZ/MF/FB/MvC	BBK	AP
02	12 May 2022	Final		JSZ	BBK	AP
03	17 May 2022	Final Revised		JSZ	JF	AP
04	07 June 2022	Final		JSZ	JF	AP
05	06 August 2022	Final		JF	JF	AP

Project Team

Initials	Name	Role
AP	A. Padwalkar	Project Manager
JSZ	Julia Szudzinska	Project Lead Geophysicist
MF	Maddalena Falco	Geophysicist
FB	Floortje Burgers	Geophysicist
MvC	Marijn van Cappelle	Geologist
JU	Jordy Uzio	Geologist
BBK	Bogusia Klosowska	Principal Geologist
MvL	Martine van der Linde	Geophysics Group Leader
JF	Jennifer Fowler	Project Reporting and Deliverables Manager

FUGRO
Fugro Netherlands Marine Limited
Prismastraat 4
Nootdorp
2631 RT
The Netherlands

Energinet Eltransmission A/S
Tonne Kjærsvej 65
DK-7000 Fredericia
Denmark Bldg

16 August 2022

Dear Sir/Madam,

We have the pleasure of submitting the 'Geophysical Results Report' for the 'Energinet Denmark North Sea OWF Zone West (Lot 2) Geophysical Survey'. This report presents the results of the Geophysical Survey.

This report was prepared by Julia Szudzinska, Maddalena Falco, Floortje Burgers and Marijn van Cappelle under the supervision of Jennifer Fowler (Project Reporting and Deliverables Manager).

We hope that you find this report to your satisfaction; should you have any queries, please do not hesitate to contact us.

Yours faithfully,

Jennifer Fowler
Project Reporting and Deliverables Manager

Executive Summary

Interpretative Site Investigation		
Survey Dates	Geophysical	24 May to 11 October 2021
	Grab samples	17 October to 19 October 2021
Equipment	Geophysical	Multibeam echo sounder (MBES), side scan sonar (SSS), magnetometer (MAG), sub-bottom profiler (SBP), 2D ultra ultra high resolution seismic (2D-UUHR)
	Grab samples	Seafloor grab samples were acquired using a Dual Van Veen grab sampler
Coordinate System		Datum: European Terrestrial Reference System 1989 (ETRS89) Projection: UTM Zone 32N, CM 9°E

Bathymetry
Water depths range from 29.2 m to 49.7 m. The site is characterised by gentle seafloor slopes, on average ranging between approximately 0° and 5°. Localised gradients exceeding 10° were observed in areas of seafloor scour and areas of potential debris.

Seafloor Morphology
Morphological features were observed on the seafloor, which included: sand waves; ripples; large ripples; areas of boulders; possible pingo remnants or archaeological sites of interest; ridges; possible biogenic features; rock dump; trawl marks, which are evidence of an extensive fishing activity and are present across the entire site.

Substrate Type
Following the classification presented in the Danish Råstofbekendtgørelsen (BEK no. 1680 of 17/12/2018, Phase IB), there were two substrate types identified within the OWF West Zone site: 1a – silty soft bottom; comprising mainly mud and sandy mud and muddy sand; 1b – solid sandy bottom; comprising mainly gravel and coarse sand, muddy sand, and sand; 2a – Sand, gravel and pebbles – few larger stones; 2b –sand, gravel and pebbles – seabed cover of larger stones 1% to 10%; 3 – Sand, gravel and pebbles – seafloor cover of larger stones 10% to 25%.

Seafloor Sediments
Based on the results on the backscatter data and grab sampling campaign, the dominant seafloor sediment in the OWF Zone West site is sand, with areas of higher component of finer sediment defined as muddy sand and mud and sandy mud. Areas of gravel and coarse sand were identified where the Holocene sediment is relatively thin. The till/diamicton class corresponds with areas where Unit U30 is exposed or close to the seafloor.

Seabed Targets and Potential Site-Specific Hazards	
Wrecks	Fallwind wreck was observed in the central western part of the site (EA_R_SSS_00580). A potential wreck marked in ENC database was observed in the northern part of the site (EA_P_SSS_00591). Both wrecks can be seen in SSS, MBES and MAG datasets.
Cables	Two (2) telecommunication cables are crossing the OWF Zone West site – Havfrue and TAT14. Both cables are orientated in NW – SE direction and were observed only in the magnetometer data.
Pipeline	One (1) gas pipeline is crossing the OWF Zone West site – EuroPipe. It is intermittently exposed and was observed in SSS, MBES, MAG and SBP datasets.
Man-made objects	164 targets were identified as man-made objects on SSS, MBES and MAG datasets (including wrecks, cables, pipeline, rock dumps and debris).
Boulders and coarse materials	In total 18412 targets were picked and classified as (possible) boulders. The boulders are spread evenly across the entire OWF West Zone site except for the area stretching from SW to NE in the northern part of the site where the unit U10 is thicker.

	The areas where the boulder density reached at least 40 boulders in a seafloor area measuring 100 m x 100 m were defined as boulder fields.
Other targets	The seafloor targets were identified from SSS, MBES, and MAG datasets. In total, 3145 magnetic anomalies and 18596 side-scan sonar targets were observed across the site. SSS targets were rationalised to the MBES position where relevant. No targets were noted on the MBES that were not also seen on other sensor(s).
Mobile seafloor sediments	Areas of sand waves, large ripples and ripples were identified within the OWF site. During the acquisition seafloor mobility was observed where large ripples and ripples are present, however there was no evidence of sand waves mobility.
Geological Features	
Acoustic blanking	Acoustic blanking is locally present in Unit U20.
Seismic anomalies	Seismic anomalies with a high amplitude and reverse polarity are present at two levels (level 1 and level 2) in Unit U90.
Glacial deformation	Glacial deformation was observed at two levels, in BSU and in Unit U24. In the north, the BSU contains a well-defined thrust-faults forming a thrusted complex, with a detachment surface at approximately 140 m MSL. In the north, Unit D24 is deformed to a various degree. Deformation includes folding and thrust-faults.
Faults	Normal faults and an inverted normal fault with a generally north-south orientation are present in the BSU.
Shallow Geology	
Unit U10	Unit U10 is present across most of the site and forms a few metres-thick layer of Holocene sediments. In the north of the site Unit U10 is thicker, reaching a maximum thickness of 22 m.
Unit U20	Unit U20 forms spatially variable channels, with a maximum thickness of 120 m. In the north, Unit U20 has a sheet-like geometry locally. In the southern part of the site, the unit forms one large channel with a west-south-west to east-north-east orientation connected with many small channels forming a tributary network. In the north of the site the unit forms one very deep, narrow channel with a north-west to south-east orientation, a series of smaller channels parallel to the deep channel.
Deformed unit D24	Unit D24 has a sheet-like geometry with a horizontal to undulating base. The unit has a thickness of up to 45 m. The unit shows evidence for deformation in form of folded reflectors, dipping thrust-faults and transparent seismic facies.
Unit U30	Unit U30 is present in two shallow and broad valleys. The unit reaches a thickness up to 33 m. The distribution of Unit U30 is associated with the distribution of Unit U35 and deformed Unit D24. Internally, the unit is horizontally stratified with medium to high amplitude, closely spaced parallel reflectors. Locally acoustically transparent or with internal channels.
Unit U31	Unit U31 is a channelised unit, which forms wide meandering channel system with tributary channels. A maximum thickness is up to 119 m. Internally, unit is acoustically chaotic or locally contains low to high amplitude stratification parallel to the base of the channel.
Unit U35	Unit U35 forms two shallow and wide valleys/depressions with an east-west orientation. Internally, Unit U35 has a complex acoustic character from locally stratified, acoustically transparent to chaotic. The chaotic intervals comprise discontinuities high amplitude reflectors with sharp to transitional terminations. Complexities include also internal erosion surfaces and inclined reflectors.
Unit U70	Unit U70 forms the infill of deep glacial valleys with a north-east to south-west orientation. The base often lies deeper than the maximum penetration of the

fUGRO

	2D-UUHR seismic data (i.e., approximately 200 m below MSL). Two seismic facies are observed. The lower part of the valley-fill is acoustically chaotic to transparent, whereas towards the top the valley-fill is stratified. Internal horizon H69 is interpreted in some of the valleys of Unit U70.
Unit U75	Unit U75 is locally present in the west-central part of the site. It has a seismically complex character. It has a thickness of up to 31 m. Internally, Unit U75 has a complex seismic character. The internal seismic character, including acoustically transparent intervals, stratified (inclined reflectors) intervals and internal erosion surfaces.
Unit U90	Unit U90 is present throughout most of the site, except in the north and where it is cut out by valleys of Unit U70. It has a thickness of up to 87 m. Internally, Unit U90 has a complex seismic character, interpreted to comprise early to middle Pleistocene fluvial deposits.
BSU (Base Seismic Unit)	The BSU is present throughout most of the site except where it is eroded by channels of Unit U70. This unit is stratified and is interpreted to comprise Miocene marine and deltaic deposits.

FUGRO

Document Arrangement

Document Number	Document Title
F176286-REP-MOB-001	Mobilisation Report
F176286-REP-OPS-001	Operations Report
F176286-REP-GEOP-001	**Geophysical Survey Report (WPA scope)**
F176286-REP-MAG-001	Magnetometer Box Survey Report (WPB scope)

Contents

Appendices

Figures in the Main Text

Tables in the Main Text

Abbreviations

AI	Artificial intelligence
ALARP	As low as reasonably practicable
BEK	Danish Råstofbekendtgørelsen
BSF	Below seafloor
BSU	Base seismic unit
CM	Central meridian
COG	Centre of gravity
CRP	Central reference point
CUBE	Combined Uncertainty and Bathymetric Estimator
DGPS	Differential global positioning system
DTM	Digital terrain model
DTU	Technical University of Denmark
EGN	Empirical gain normalisation
ENC	Electronic navigational charts
EPSG	European Petroleum Survey Group
ETRS	European Terrestrial Reference System
GEOP	Geophysical
GEUS	Danish Geologiske (Geological) UnderSøgelse (Survey)
GIS	Geographic information system
GNSS	Global navigation satellite system
OWF	Offshore Wind Farm
HF	High frequency
HIPS	Hydrographic Information Processing System
HV	High voltage
HVF	HIPS vessel file
IHO	International Hydrographic
KDE	Kernel density estimation
LF	Low frequency
MAG	Magnetometer
MBES	Multibeam echosounder
MCS	Multi-channel seismic
MIG	Migrated
MMO	Man-made object
ML	Machine learning
MLSS	Multi-level stacked sparker
MOB	Mobilisation
MRU	Motion reference unit

MSL	Mean Sea Level
MSS	Mean sea surface
MVP	Moving velocity profile
NE	North-east
NW	North-west
OCR	Offshore Client Representative
OPS	Operations
OWF	Offshore Wind Farm
PEP	Project execution plan
PSD	Particle-size distribution
QC	Quality control
QHD	Qinhuangdao
REP	Report
SBP	Sub-bottom profiler
SE	South-east
SEG	Society of Exploration Geophysicists
SIPS	Sonar Information Processing System
SSS	Side scan sonar
SVP	Sound velocity probe
SVS	Sound velocity sensor
SW	South-west
TPU	Total propagated uncertainty
TQ	Technical query
TSG	Template Survey Geodatabase
TVU/THU	Total vertical uncertainty / total horizontal uncertainty
UUHR	Ultra Ultra high resolution
USBL	Ultra short baseline
UTM	Universal Transverse Mercator
UXO	Unexploded ordnance
WPA	Work package A

1. Introduction

1.1 General

Energinet Eltransmission A/S (Energinet) is developing a new offshore wind farm and energy island in the Danish Sector of the North Sea. This report details the results of the geophysical survey covering the North Sea OWF Zone West (Lot 2) site.

The project survey site, henceforth referred to as 'the OWF Zone West site' and 'the site', is located offshore Denmark approximately 59 km west of Thorsminde and covers an area of approximately 534 km². The site was divided into 18 survey blocks. Figure 1.1 and Figure 1.2 present the location of the site and the survey blocks respectively.

The OWF Zone East (Lot 1) and OWF Zone West (Lot 2) sites are referred on figures and charts as 3GW Project Area.

Guidelines on the use of this report are provided in Appendix A.
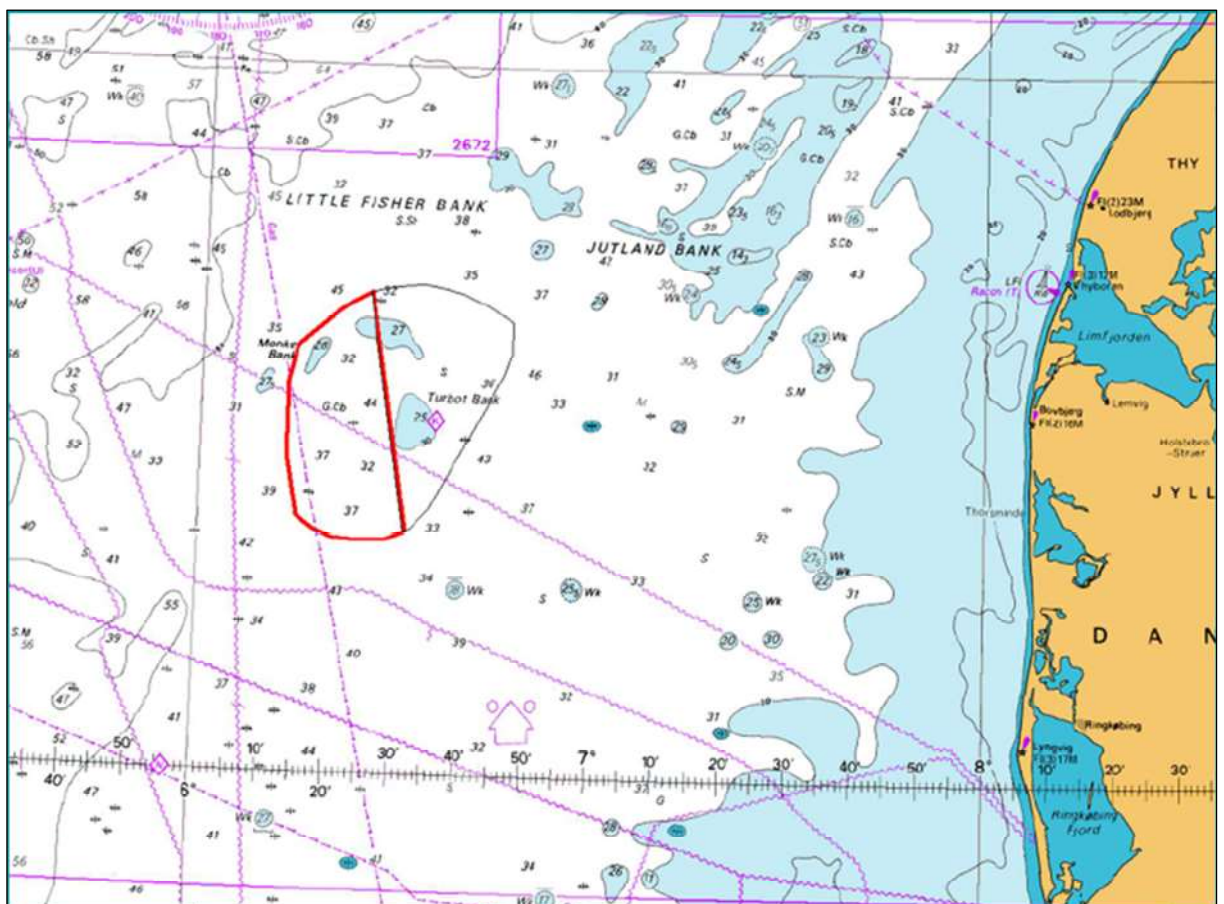
Figure 1.1: Location of the OWF Zone West (red outline) and OWF Zone East (grey outline) sites. Both sites together represent 3GW Project Area.
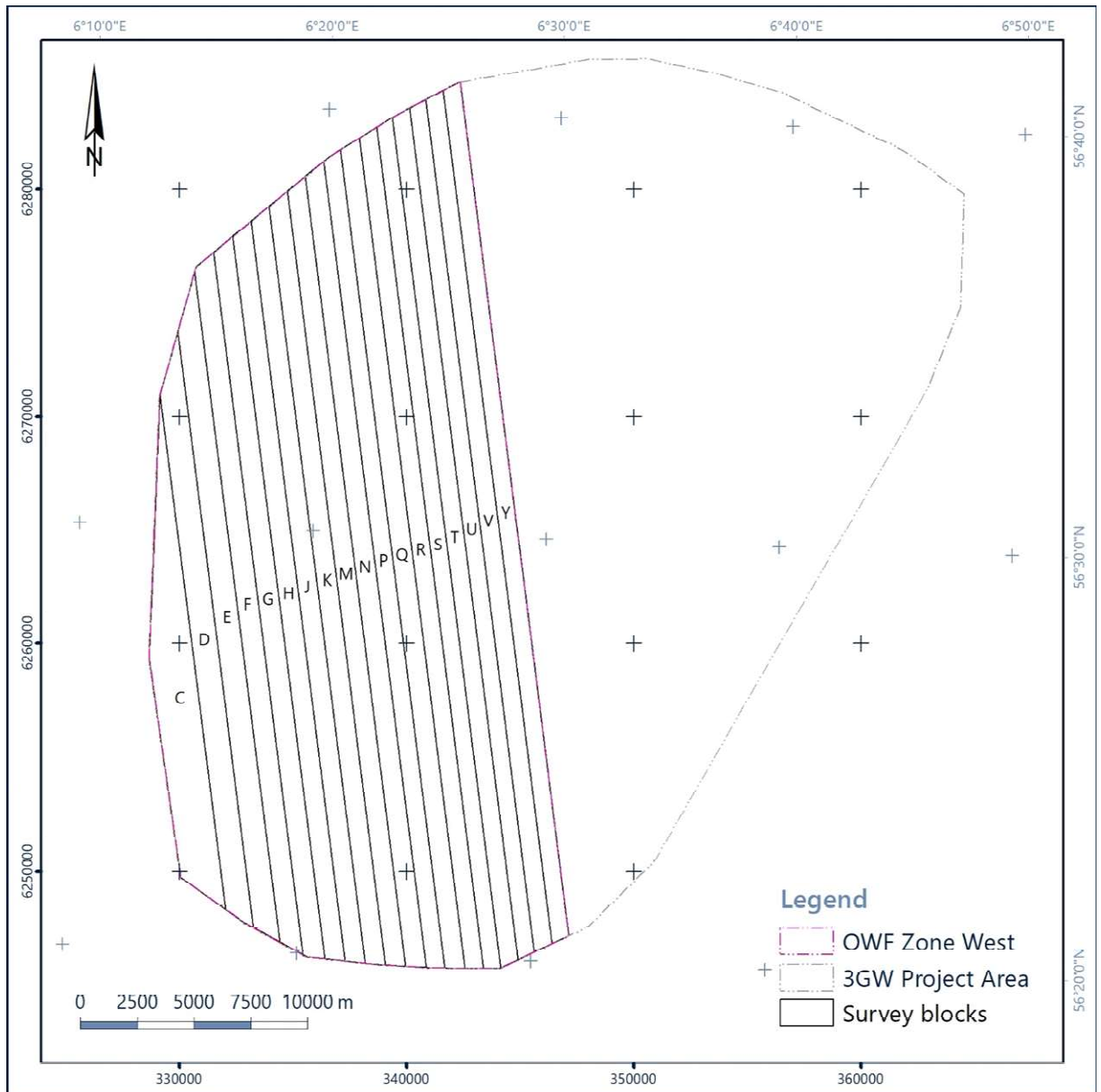
Figure 1.2: Survey blocks within the OWF Zone West site.

1.2 Survey Aims and Overview

The following sub-sections provide details about the main survey requirements and the scope of work for the Client's Work Package A (WPA); the Energinet Denmark North Sea OWF Zone West (Lot 2) Geophysical Survey.

1.2.1 Survey Aims

The aim of the offshore geophysical survey is to map the bathymetry, the static and dynamic elements of the seafloor and the sub-seafloor geological soil layers to at least 100 m below seafloor (BSF).

The acquired data will be used as the basis for:

- Initial marine archaeological site assessment;
- Planning of environmental investigations;

- Planning of initial geotechnical investigations;
- Decision of foundation concept and preliminary foundation design;
- Assessment of subsea inter-array cable burial design;
- Assessment of installation conditions for foundations and subsea cables;
- Site information enclosed in the tender for the offshore wind farm concession.

To achieve these objectives Fugro:
- Acquired accurate site-wide bathymetric data in order to determine water depths, topography, gradients etc. using multibeam echosounder (MBES);
- Acquired site-wide, high-resolution side scan sonar (SSS) data to map natural and anthropogenic seafloor hazards, for example the presence and location of boulders, mobile and sedentary seabed sediments, infrastructure, wrecks and debris items that may impact future survey and construction planning;
- Acquired single magnetometer data across the area (along the planned survey lines) to identify ferrous objects, surface geology, chartered and unchartered wrecks and infrastructure in support of the ALARP principle of UXO risk mitigation prior to sediment grab samples and geotechnical operations;
- Acquired high-resolution sub-bottom profiler (SBP) data to determine the shallow sub-surface soil conditions, boulders and shallow geological features that will influence site selection and foundation design;
- Acquired multichannel 2D-UUHR (ultra ultra high resolution) seismic data with penetration to 100 m BSF to determine deeper sub-seafloor soil conditions that may influence foundation design below the effective penetration of the SBP.

1.2.2 Survey Overview

A summary of the main survey requirements for the geophysical survey operations is presented in Table 1.1. To supplement Energinet requirements further details of Fugro methods are provided where relevant.

Table 1.1: Survey requirements overview – geophysical survey operations (Work Package A).

Equipment Method	Energinet Requirement	Fugro Method
Vessels	Suitable research/survey vessel	Fugro Pioneer
Line Spacing	Line plan to accommodate all the requirements	- Geophysical lines were run at 62.5 m spacing; - Every 250 m lines and 1 km cross lines were run with 2D-UUHR.
Survey Priority	Not specified	Refer to F176286-PEP-005 04 Ops Plan for full details.
Max Vessel Speed	Maximum of 4.0 knots (±10%)	
Surface Positioning	- Two independent systems available; - Dynamic heading accuracy of ± 0.2° or better; - Static heading accuracy of ± 0.05° or better; - Horizontal uncertainty of the vessel of ± 0.5m or better.	

Equipment Method	Energinet Requirement	Fugro Method
USBL	+/-2 m accuracy for data acquired from towed sensors	Fugro was able to repeatedly achieve +/-1m accuracy for USBL calibration and +/-2 m accuracy for data acquired from towed sensors. i.e. a processed target accuracy of +/-2 m.
2D-UUHR	- Minimum penetration: 100 m, dependent on geology; - Fundamental frequency between 1 kHz and 3 kHz; - Vertical resolution better than 0.3 m; - Fire rate ≥ 2 pulses/second; - Variable energy levels between 100 J and 1000 J; - A suitable multi-channel and multi-element hydrophone streamer (e.g. 48 channels @ 3.125 m) with depth control plus depth measurement for continuously monitoring and recording of streamer depth.	- Fugro Multi-level Stacked Sparker (MLSS): - Fugro MLSS power supply (900 J); 3 array MLSS: 360 tips corresponding to 900 J; 70 m HV cable; - Sea ground cable. 96-channel streamer: - Geometrics Geo Eel digital streamer; 96 channels at 1 m group interval; 1.4 m flat tow; - Head buoy and Tail buoy; - Tension control with 3 x Fugro adaptive drogues; - CNT-2 recorder; - Record length of 220 ms; - Sampling interval of 0.125 ms; - Recording format: SEG-D. - Sparker and streamer positioning: - Fugro PBP v1.0 on Fugro MLSS; - Fugro PBP v1.0 on Head buoy and Tail buoy.
Multibeam Echo sounder/Backscatter	100% coverage; - Equal distance mode; - Motion compensated; 0.25 m x 0.25 m bin size / 16 x pings per 1.0 m x 1.0 m (for accepted exceptions refer to TQ-012); - THU is <0.5 m; - TVU is compliant with IHO Special Order; - Grid standard deviation (95% confidence interval) is less than 0.2 m.	
Parametric SBP	- High-frequency single channel sub-bottom profiler system; - Minimum penetration: 10 m, dependent on geology; - Vertical resolution: better than 0.3 m.	- Transmit and receive frequency: 8 kHz to 12 kHz (adjustable); - Compensated for vessel motion; - Infill required for data gaps > 20 m.
Side Scan Sonar	- Minimum target size insonification of 0.5 m along the shortest axis; - Dual channel system operating at both HF and LF; 200% coverage including nadir;	Infill required where USBL gaps of >10 s

Equipment Method	Energinet Requirement	Fugro Method
	■ Altitude to be set to 8-12% of range; ■ Survey speed to be a maximum of 4.0 knots (±10%).	
Magnetometer	■ 5 m maximum altitude; ■ Magnetometer measurement sensitivity: 0.01 nT; ■ Magnetometer sampling frequency: 1 – 20 Hz (selectable); ■ Maximum noise level: 2 nT.	■ Magnetometer sampling frequency: 10 Hz; ■ Lateral blanking distance 5 m; ■ Infill required where USBL gaps of more than 10 s or altitude out of spec for more than 10 m (for accepted exceptions refer to TQ-014).
SVP	The speed of sound in water shall be measured in the survey area at suitable time intervals.	■ The Vertical Sound Velocity Profiles undertaken with a resolution of 0.1 m/s and an accuracy of ±0.15 m/s; ■ The Vertical Sound Velocity Profiles able to measure within the range 1,350-1,600 m/s.

Grab Sampling	■ Precise positioning of the grab sample location (not more than 5 m from the designated position);
	■ Accuracy of the positioning better than 2 m;
	■ Safe storage of the sample (at least 3 kg – refer to TQ-013) for onshore delivery with proper labelling
		■ Day or Dual Van Veen Grab Sampler;
		■ Proper and clear communication with vessel navigators and survey personnel
		■ Safe Winch operation and deployment of the grab
		■ Monitoring of the tension of the winch wire
		■ Upon recovery of the soil sample:
		  • Visual Analysis of the sample
		  • Sample photograph

1.3 Geodetic Parameters

The project geodetic and projection parameters are summarised in Table 1.2.

Table 1.2: Project geodetic and projection parameters.

Project Global Positioning System Geodetic Parameters	
Datum	ETRS89
EPSG code	25832
Semi major axis	6 378 137.000 m
Semi minor axis	6 356 752.314 m
Inverse flattening	298.257222101
Project Projection Parameters	
Grid Projection	Universal Transverse Mercator, Northern Hemisphere
UTM Zone	32 N
Central Meridian	009° 00' 00.000" East
Latitude of Origin	00° 00' 00.000" North
False Easting	500 000 m
False Northing	0 m

Project Global Positioning System Geodetic Parameters	
Scale Factor at Central Meridian	0.9996
Units	Metres

1.4   Vertical Datum

The vertical datum for North Sea OWF Zone West (Lot 2) was reduced to Mean Sea Level (MSL) utilising the DTU21 MSL Tide Model as a vertical offshore reference frame supplied by the Technical University of Denmark (DTU).

2. Mobilisation and Operations

The data was acquired using the survey vessel Fugro Pioneer.

Fugro Pioneer mobilisation and calibrations for survey operations were undertaken between 14 and 31 May 2021 in the port of IJmuiden, the Netherlands, at an offshore calibration site during the transit to the survey area and completed on site (see report number F176286-REP-MOB-001).

Operations on the Fugro Pioneer occurred between 24 May and 19 October 2021. Details are provided in report F176286-REP-OPS-001.

3.   Vessel Details and Instrument Spread

3.1   Vessel Details Fugro Pioneer

The Fugro Pioneer (Figure 3.1) is a 53 m vessel built at Damen Shipyards in 2014. Being purpose designed for the demanding environments in which Fugro's coastal fleet operate, the Fugro Pioneer has excellent weather capabilities and is an ideal platform for 2D-UUHR and geophysical surveys.

The Fugro Pioneer is equipped for 24-hour operations with space for a maximum of 31 persons.

Figure 3.1: Fugro Pioneer

3.2   Instrument Spread Fugro Pioneer

The equipment used for the survey is presented in Table 3.1.

Table 3.1: Instrument Spread Fugro Pioneer

Requirement	Equipment
Primary GNSS	Fugro StarPack GNSS receiver with StarFix.G2+ corrections
Secondary GNSS	Fugro StarPack GNSS receiver with StarFix.G2+ corrections
MRU and heading sensor	IXSEA Hydrins, IXBLUE Octans
USBL	Kongsberg HiPAP 501 with C-Node beacons
Multibeam echosounder	Dual Head Kongsberg EM2040
Side scan sonar	Edgetech 4200 (300/600 kHz) Edgetech 4200 (100/600 kHz)

Requirement	Equipment
Magnetometer	Geometrics G-882 fitted with a depth sensor and altimeter, towed piggy-backed behind the side scan sonar fish
Parametric sub-bottom profiler	Innomar Medium SES-2000
Sound velocity probe	2x SAIV CTD
Sound velocity sensor	1x Valeport Mini SVS installed near MBES head with 1x spare 1x Moving Velocity Profile (MVP)
Tidal heights	Fugro StarPack GNSS receiver with Starfix.G2+ corrections
2D-UUHR Source	Fugro Multi-Level Stacked Sparker (360 tips)
2D-UUHR Receiver	Geometrics Geo Eel 96 channel hydrophone streamer
Grab sampler	0.1 m2 Dual Van Veen grab 0.1 m2 Day grab as back-up

For full details of the Fugro Pioneer including weather limitations, vessel offsets and field procedures refer to Fugro Operations report F176286-REP-OPS-001.

4.   Results

4.1   Regional Geological Setting

The Danish Sector of the North Sea was influenced by the Eridanos River system from the Cenozoic to Middle Pleistocene. The Eridanos River flowed through what is now the Baltic Sea towards the west through what is now Denmark into the North Sea (Figure 4.1). Cenozoic deposits are expected to comprise coarsening upward deltaic successions of clay and sand. Over time, the depo-centre of the Eridanos River system shifted westward and during the Early to Middle Pleistocene, fluvial sediments were deposited (Figure 4.1).

During the Pleistocene, the site was under the influence of a series of glaciations separated by interglacial periods (Figure 4.2). This resulted in a complex stratigraphic architecture. The pre-Pleistocene and Early Pleistocene sediments were glacio-tectonically deformed during the glaciations (Huuse and Lykke-Andersen, 2000a; Larsen and Andersen, 2005).

During the Elsterian and Saalian glacial periods, the ice sheet covered the site completely. The action of the ice sheet eroded glacial valleys, which cut up to 350 m into older deposits. The complex infill of these valleys comprises sand, clay and locally till (Huuse and Lykke-Andersen, 2000b; COWI, 2021; Kirkham et al., 2021). Deposits of the Saalian glacial landscape ('Bakkeøer') are preserved in Jutland and in the Danish Sector of the North Sea. These deposits comprise sediments deposited in periglacial and subglacial environments (Larsen and Andersen, 2005; GEUS and Orbicon, 2010; Ramboll, 2021).

Interglacial deposits are locally preserved and consist of Holsteinian and Eemian marine sand and clay (Jensen et al., 2008; Larsen and Andersen, 2005; GEUS and Orbicon, 2010; Ramboll, 2021).

During the Weichselian glacial period, the southern margin of the ice-sheet was located approximately in the northern part of the study area (Huuse and Lykke-Andersen, 2000b). As a result, in the north of the site, till and glacio-tectonic deformation, whereas in the south of the site outwash plain deposits may be expected (GEUS and Orbicon, 2010; Ramboll, 2021).

In the late Weichselian to early Holocene, after the end of the last glacial maximum, marine transgression commenced and deposition in fluvial and estuarine environments prevailed in at the site (Leth, 1996; Larsen and Andersen, 2005; Jensen et al., 2008).

During the Holocene, the site was inundated by the North Sea and marine sands were deposited (Leth, 1996; GEUS and Orbicon, 2010; Ramboll, 2021).

Figure 4.3 gives an overview of the expected stratigraphy at the site (GEUS and Orbicon, 2010; Ramboll, 2021).
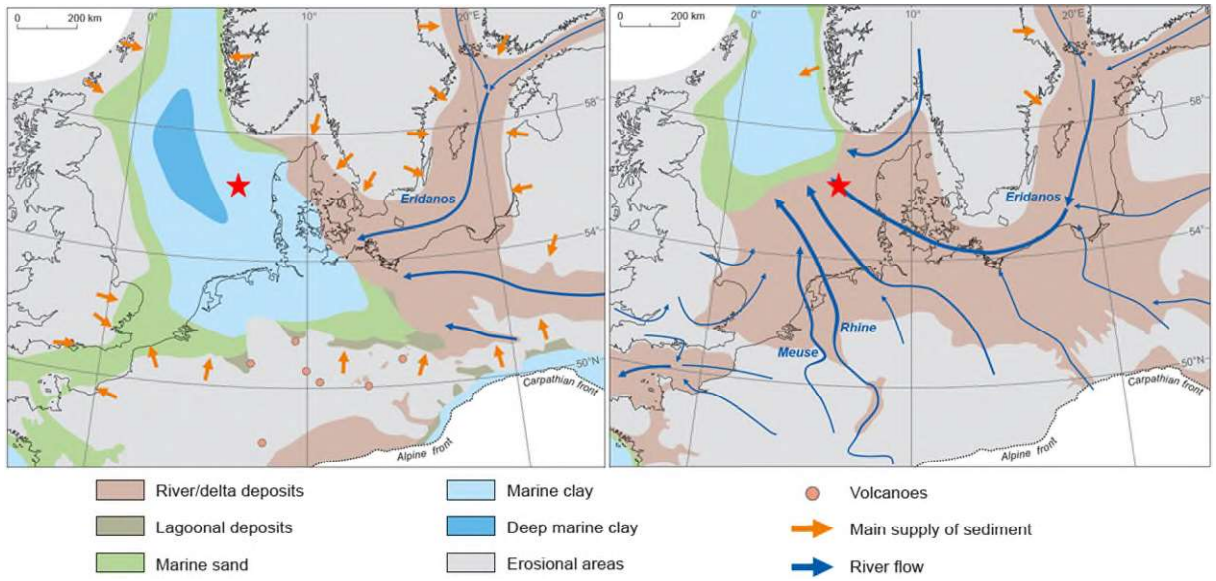
Figure 4.1: Miocene palaeogeography - left image and Early to Middle Pleistocene palaeogeography - right image (after Gibbard and Lewin, 2016). The site location is marked with a red star
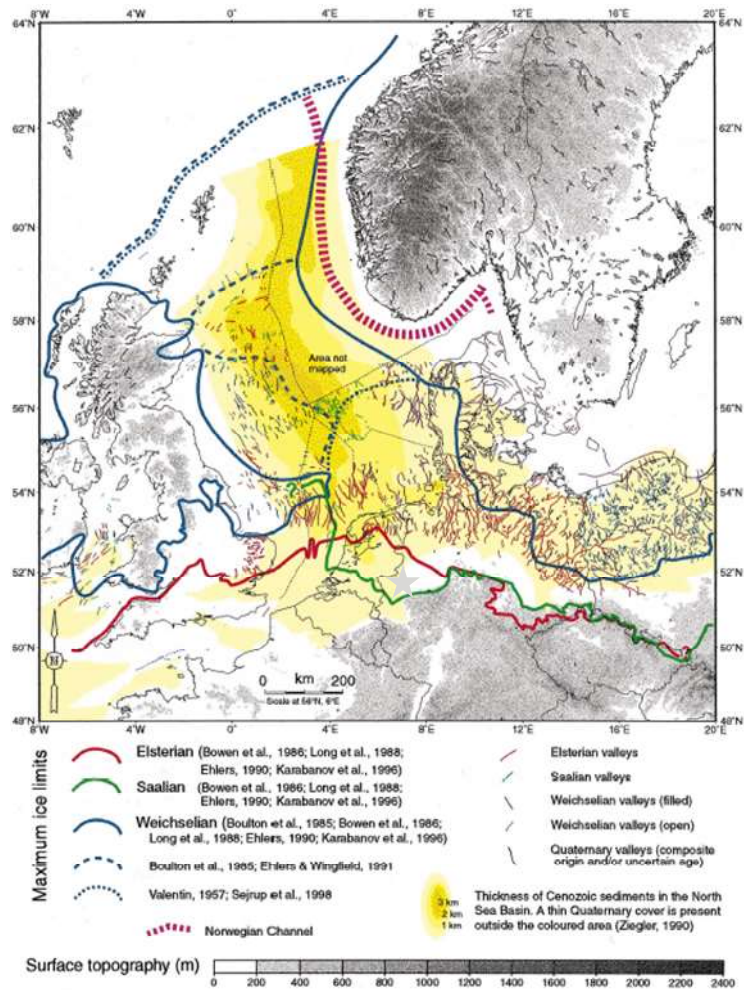
Figure 4.2: Ice sheet extent and location of tunnel valleys of the three main glaciations (after Huuse and Lykke-Andersen, 2000b).

Geological event | Depositional Environment | Chronostratigraphy

Geological event:
- Jutland coastal stream intensifies
- The opening of the English Channel
- Transgression
- Regression
- Yonger Yoldia transgression
- Weichselian Glaciation
- Eemian Sea
- Sallian/Elsterian Glaciation(s)

Depositional Environment:
- Jyske Rev Sand (Open marine) / Coastal deposits
- Hiatus (dry land)
- Meltwater silt/sand / Glacial till
- Meltwater sand
- Marine Eem
- Older glaciale deposits / Channel infill
- Pre-Quaternary

Chronostratigraphy (Years BP (x1000)):
- Holocene: Late Holocene — 2, — 4, — 6; Mid Holocene — 12, — 10; Early Holocene — 12
- Pleistocene: Weichsel — 18, — 24; Eem >130; Saale/Elsterian
- (Plioc.)/Miocene/Cretaceous

Figure 4.3: Expected stratigraphy at the site (after GEUS and Orbicon, 2010; Ramboll, 2021).

4.2 Seafloor Conditions

4.2.1 Bathymetry

An overview of the bathymetry within the OWF Zone West site is shown in Figure 4.4 and charts provided in a separate PDF file (see Appendix B). Seafloor gradient is illustrated in Figure 4.5.

In the OWF Zone West site water depths range from 29.2 m to 49.7 m MSL. The minimum water depth was observed in the north-eastern part of the site (Figure 4.6) and the maximum depth was recorded in the north central part of the site (Figure 4.7).

The bathymetry across the site is dominated by the presence of dynamic morphology with mobile bedforms represented by sand waves, large ripples and ripples. Sand waves were predominantly observed within the shallowest part of the site in the north-east, where they are often superimposed by large ripples. The shallowest part of the site is characterised by very low number of boulders in comparison to the rest of the site. General orientation of the features observed within the site is SW-NE. Detailed description of the features identified within the site is presented in section 4.2.2.

The OWF Zone West site is characterised by gentle seafloor slopes, on average between approximately 0° and 5°. Seafloor gradients locally exceed 10°, in areas of seafloor scour, slopes and potential areas of debris.
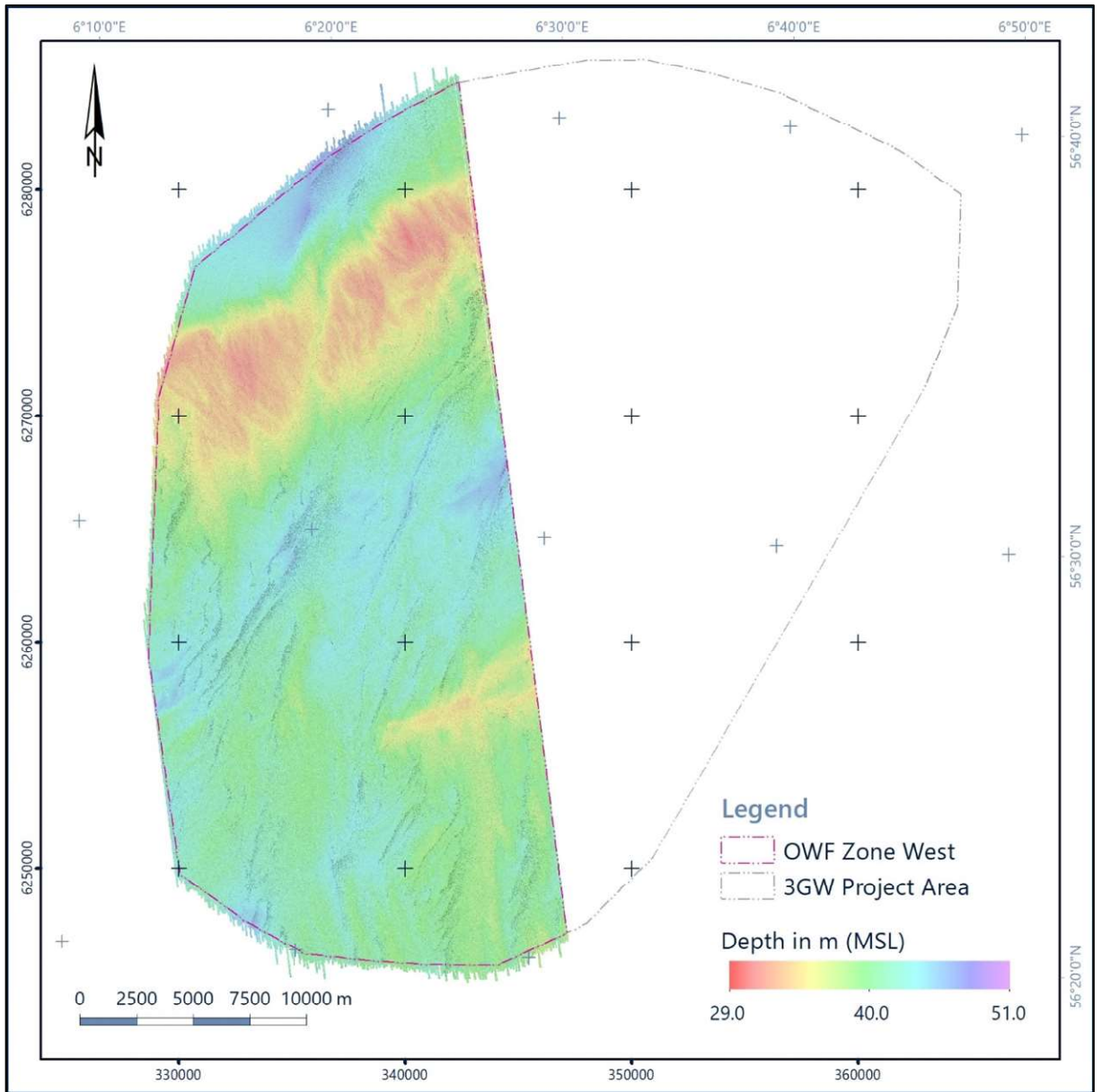
Figure 4.4: Bathymetry overview of the OWF Zone West site.
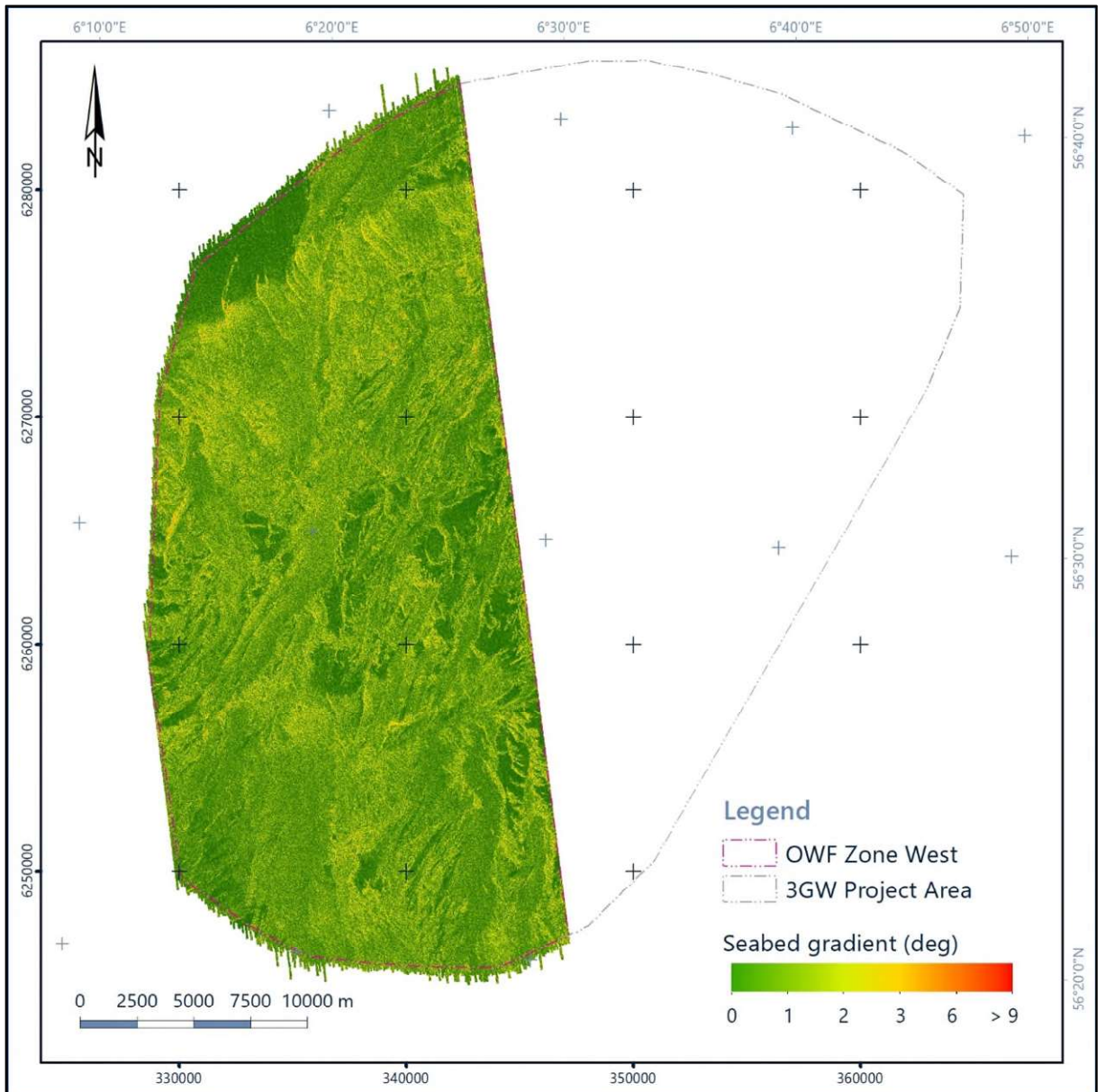
Figure 4.5: Seafloor gradient overview in the OWF Zone West site.
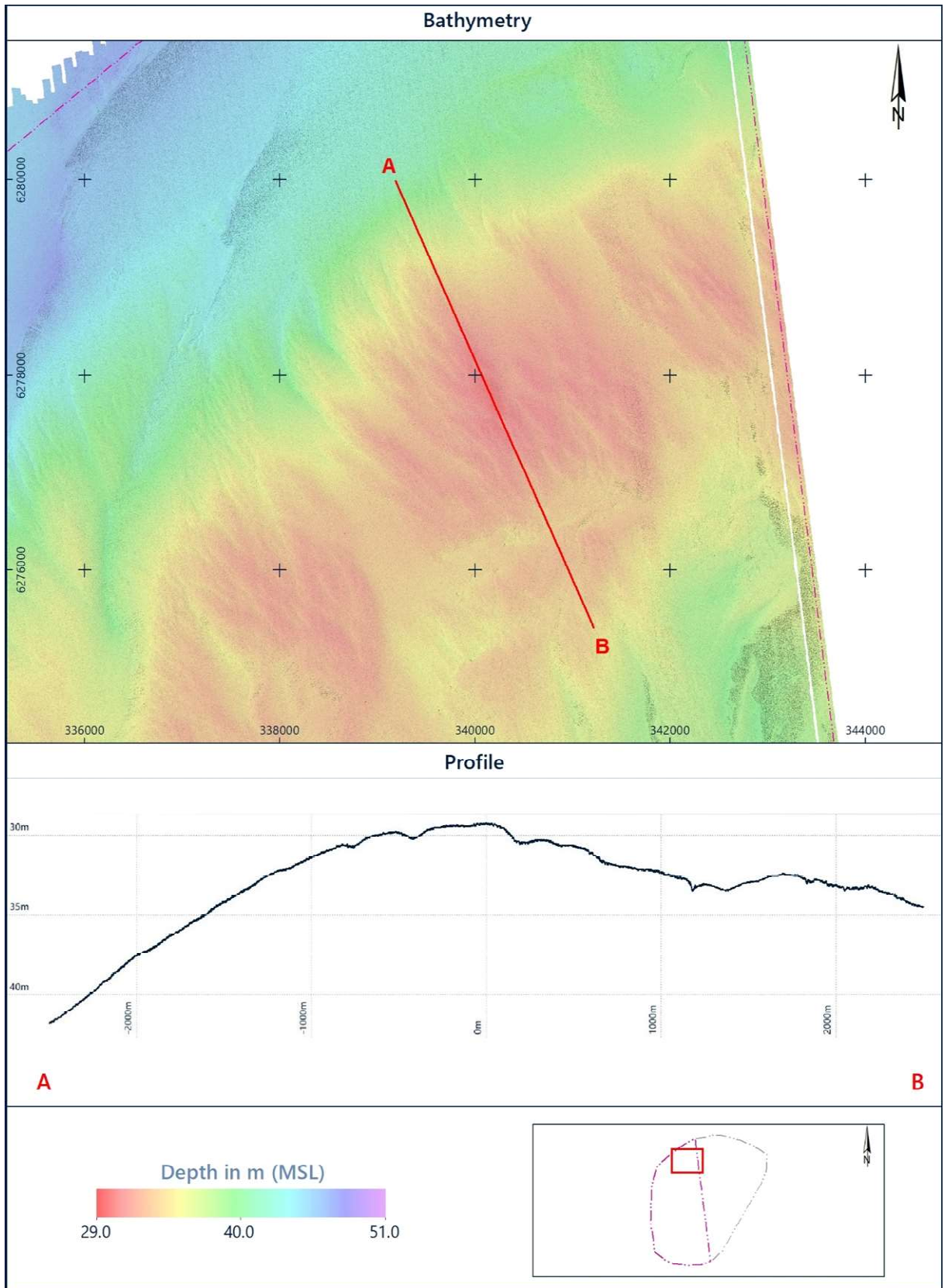
Figure 4.6: Profile crossing the shallowest area in the OWF Zone West site.
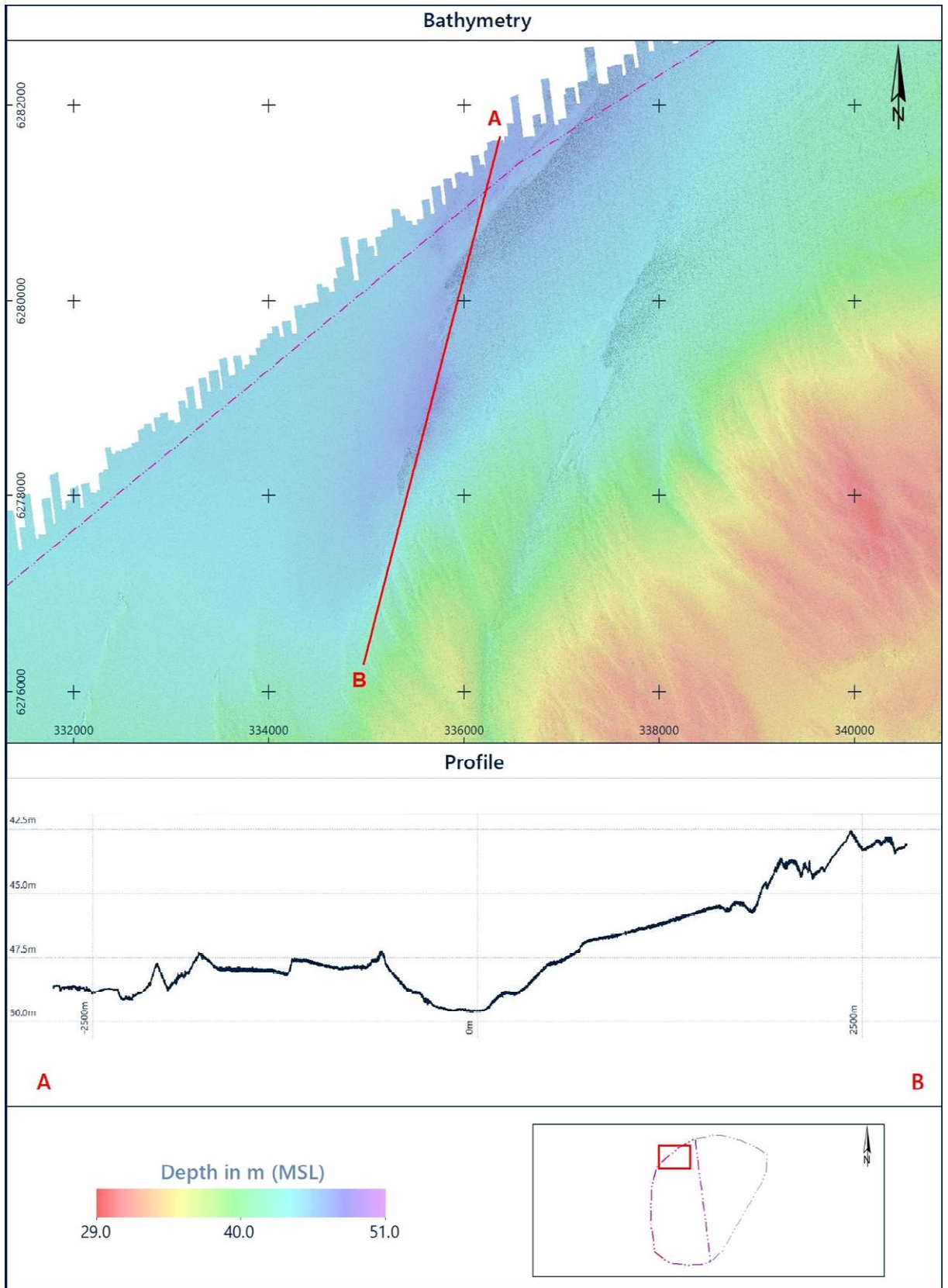
Figure 4.7: Profile crossing the deepest area in the OWF Zone West site.

4.2.2 Seafloor Morphology

Various morphological features of different dimensions were identified at the seafloor. These morphological features are a result of the interplay of variable (sub-seafloor) geological conditions and past and present hydrodynamic conditions (e.g., tides, currents) under the influence of changes in sea level.

Seafloor morphology interpretation was based on the combination of MBES (including gradient), backscatter, SSS and SBP datasets. The data analysis was carried out using acoustic characteristics such as overall pattern, roughness, reflectivity, and backscatter strength. Seafloor sediment interpretation was also taken into consideration when defining the feature boundaries, i.e. no sand waves were interpreted within the till/diamicton areas.

The following natural morphological features were identified in the OWF Zone West site:

- Sand waves;
- Large ripples;
- Ripples;
- Areas of high-density boulders (boulder field);
- Areas of numerous boulders (boulder field);
- Possible pingo remnants or potential sites of archaeological interest;
- Ridges;
- Possible biogenic features.

Additionally, the following morphological features of anthropogenic origin were identified:

- Rock dumps;
- Trawl marks areas.

An overview of the seafloor morphology is shown in **Error! Reference source not found.** and Figure 4.9. Localised features (i.e. possible pingo remnants, ridges and possible biogenic features) are not included in the figures due to their small size and large scale used to create the overview images. All the identified morphological features are presented in charts provided in a separate PDF file (see Appendix B).

The acoustic characteristics of the natural types of morphology identified are summarised in Table 4.1, while the anthropogenic types of morphology identified are summarised in Table 4.2.

Table 4.1: Acoustic characteristics of the natural morphological features identified in the OWF Zone West site.

Backscatter Image	MBES Image	SSS Image	Acoustic Description	Morphological Interpretation
			Low reflectivity	Sand waves
			High reflectivity	Ripples
			Medium reflectivity	Large ripples
			Medium reflectivity	Area of high-density boulders (boulder field)
			Medium reflectivity	Area of numerous boulders (boulder field)
			Low reflectivity	Possible pingo remnant
			Medium reflectivity	Ridge
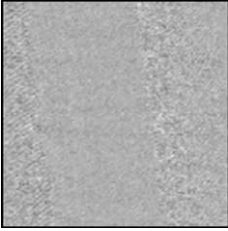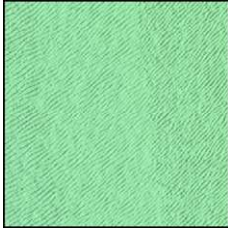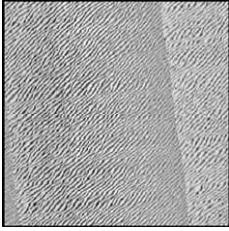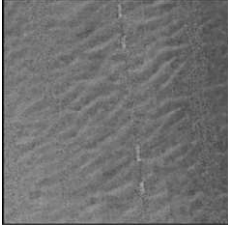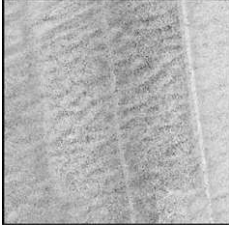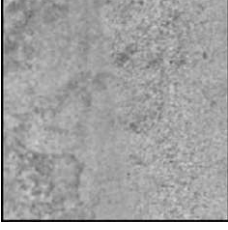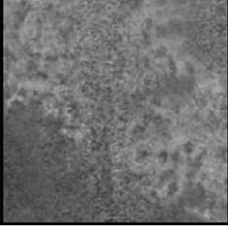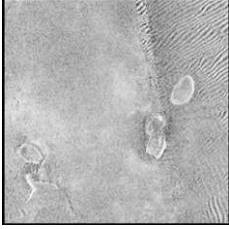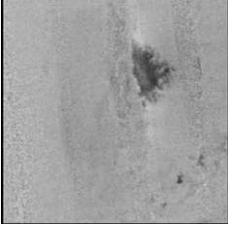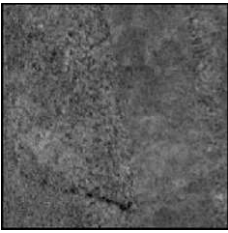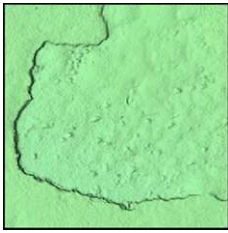
Backscatter Image	MBES Image	SSS Image	Acoustic Description	Morphological Interpretation
			Low reflectivity	Possible biogenic feature

Table 4.2: Acoustic characteristics of the anthropogenic morphological features identified in the OWF Zone West site.
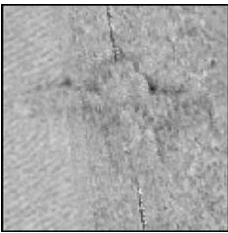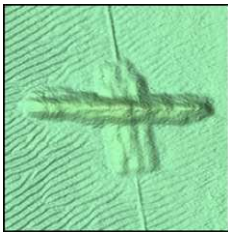
Backscatter Image	MBES Image	SSS Image	Acoustic Description	Morphological Interpretation
			Medium reflectivity	Rock dump
			Medium reflectivity	Area of trawl marks
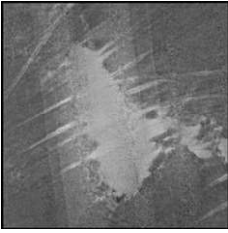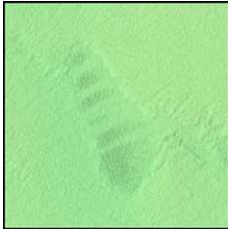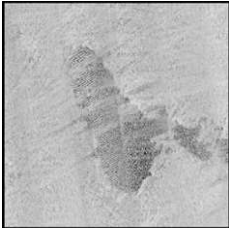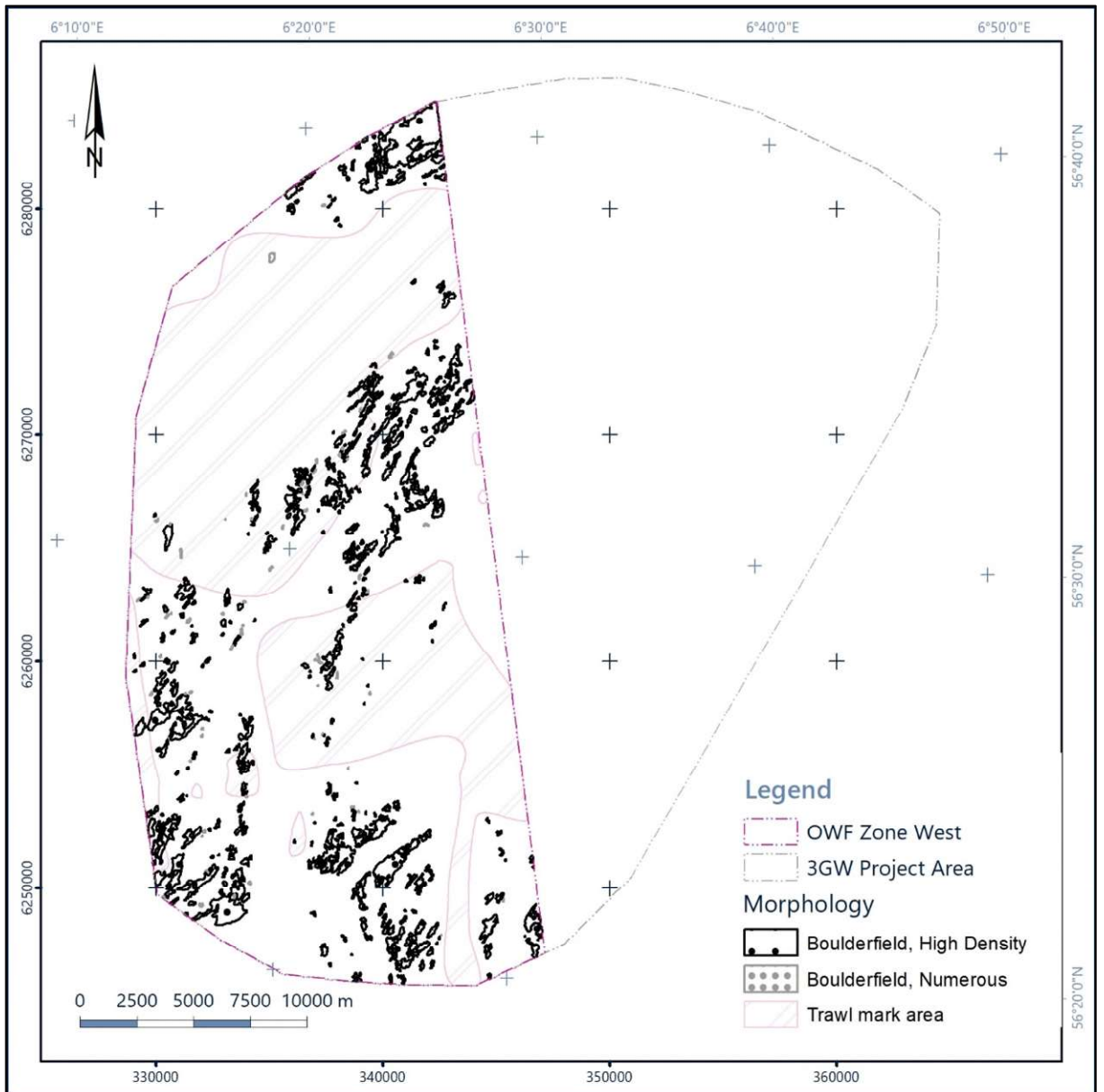
Figure 4.8: Overview of the selected morphological features in the OWF Zone West site. Localised features (i.e. possible pingo remnants, ridges and possible biogenic features) are not included.
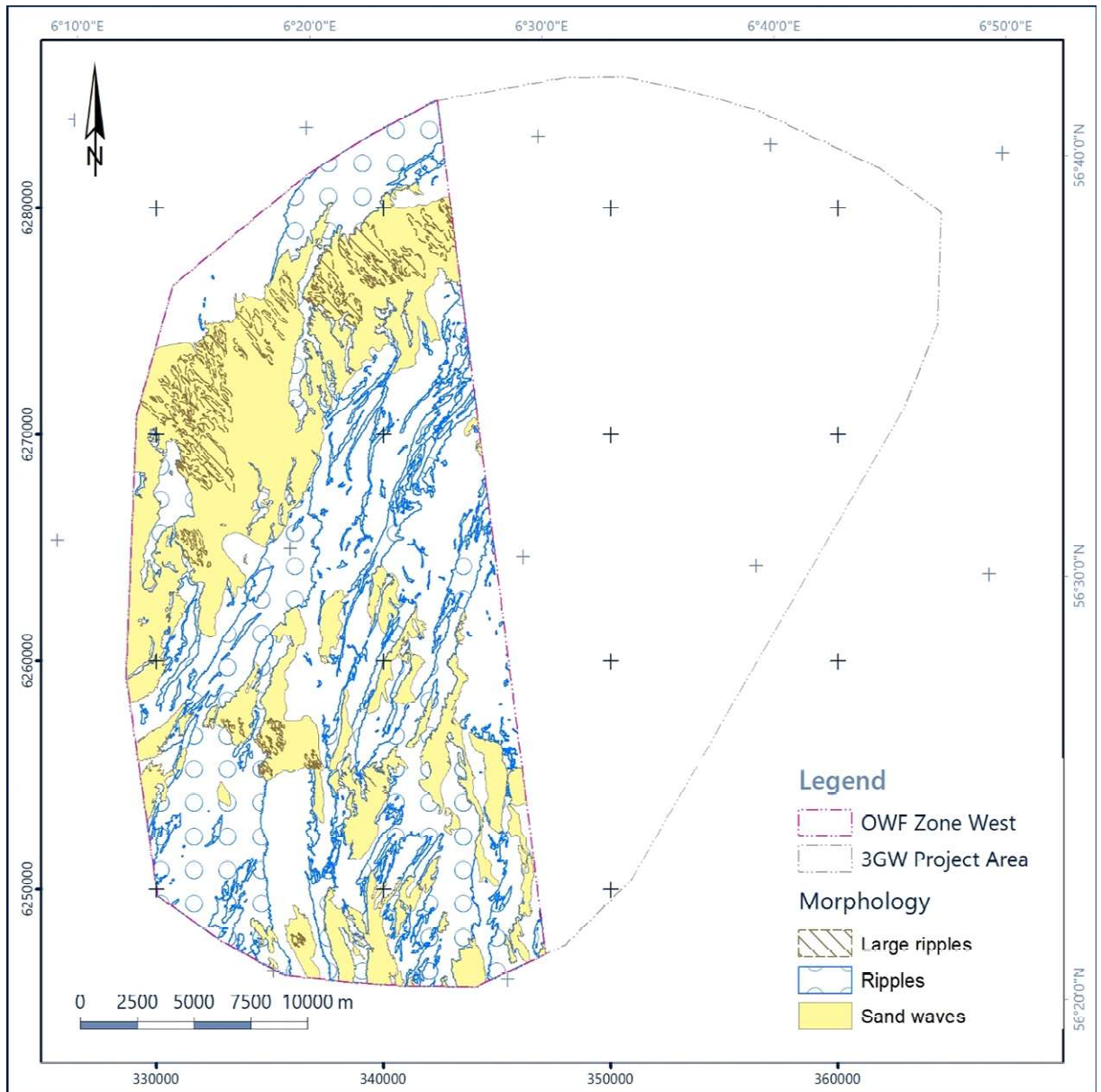
Figure 4.9: Overview of the morphological features (bedforms) in the OWF Zone West site.

4.2.2.1 Bedforms

The OWF Zone West site is exposed to tidal currents, and thereby characterized by significant sediment transport. Sand waves, often superimposed by ripples and large ripples, were observed across the site, predominantly where the Holocene sediments are very thick. The wavelength of these sand waves ranges from 200 m to a maximum of 400 m, with an average height of 4 m. Those bedforms are described as sand waves following the classification presented in Table 4.3, although it would be more correct to classify those as large sand waves. During the survey there was no evidence of mobility of these large bedforms, therefore it is possible to assume that they are relatively stable (Figure 4.10).

Table 4.3: Bedform classification applied to the features observed in the OWF Zone West site.

Bedform	Dimensions
Ripples	<u>Wavelength</u> < 5 m <u>Height</u> < 0.01 m to 0.1 m
Large Ripples	<u>Wavelength</u> 5 m to 15 m <u>Height</u> 0.1 m to 1 m
Mega Ripples	<u>Wavelength</u> 15 m to 50 m <u>Height</u> 1 m to 3 m
Sand Waves	<u>Wavelength</u> 50 m to 200 m <u>Height</u> 3 m to 5 m
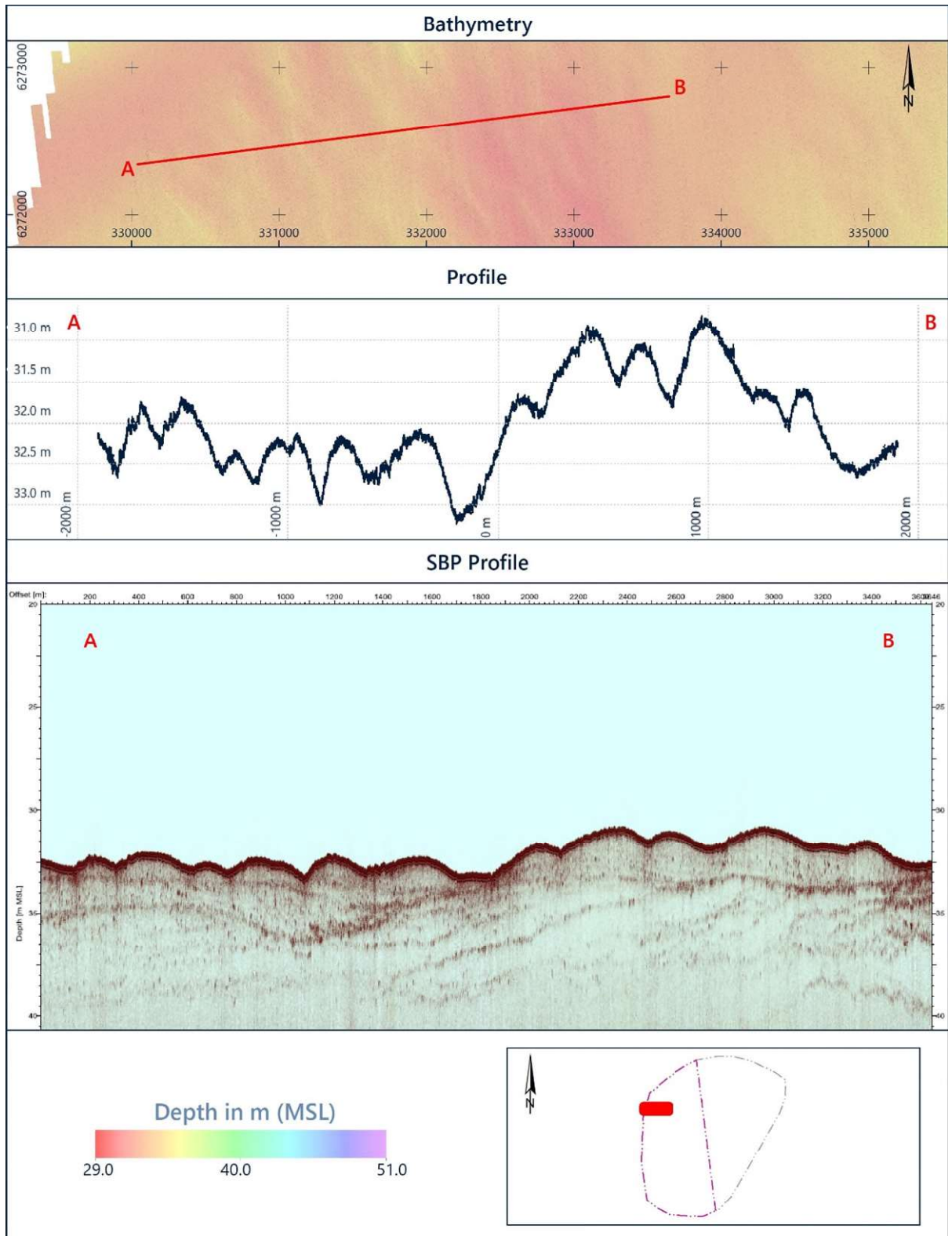
Figure 4.10: Example of sand waves observed in the OWF Zone West site.

Most of the sand waves (Figure 4.10) described are superimposed by large ripples (Figure 4.11). The large ripples are mostly found in the northern area and have wavelengths ranging from 6 m to 15 m and height varying between 0.15 m and 0.40 m. Their crests are generally oriented in SW-NE direction.
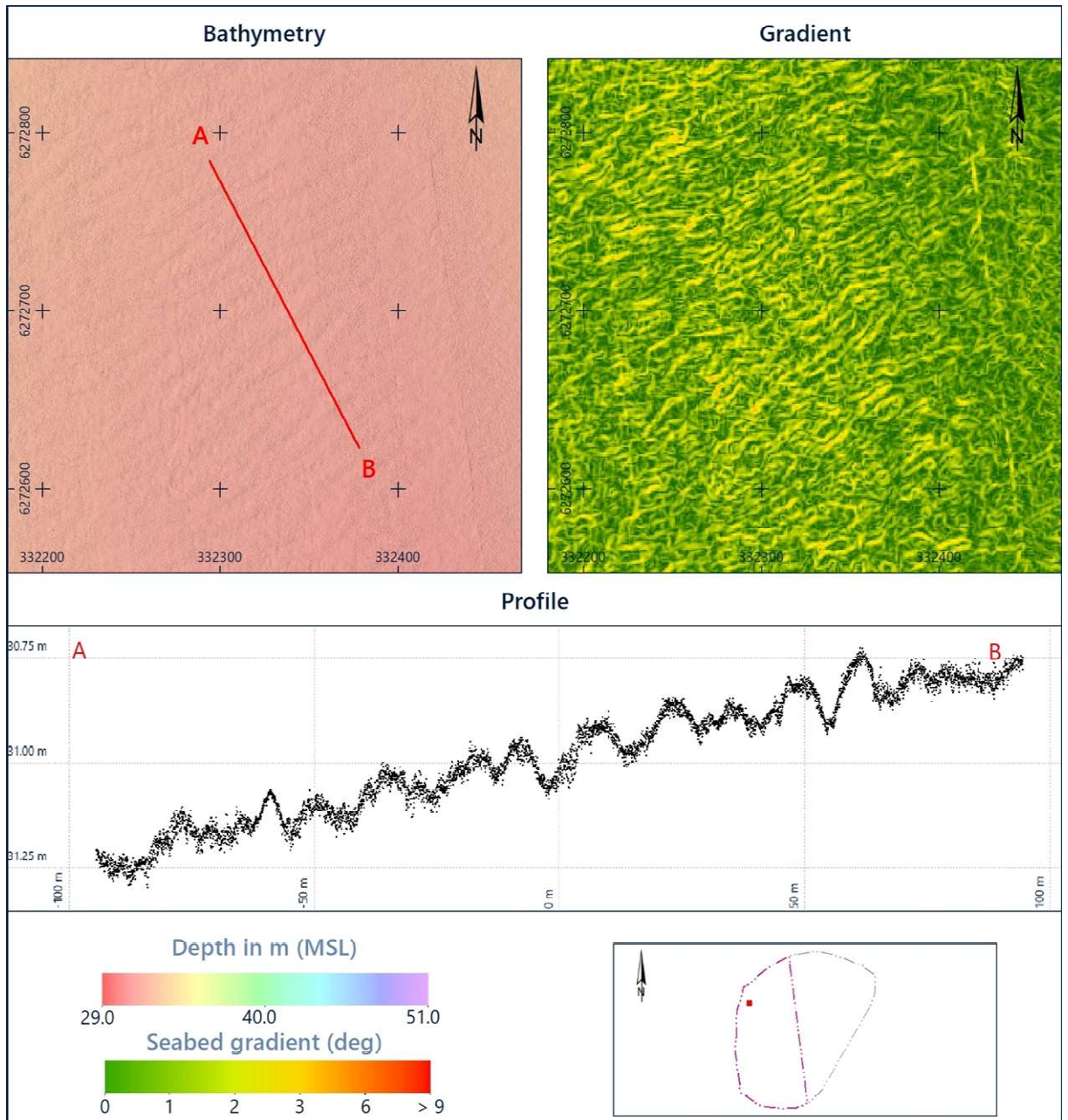
Figure 4.11: Example of large ripples superimposed on sand waves in the OWF Zone West site.

The ripples were found within the gravel and coarse sand and sand, which sometimes fill the pre-existing depressions. The average wavelength is approximately 2 m, while the average height is approximately 0.10 m (Figure 4.12).
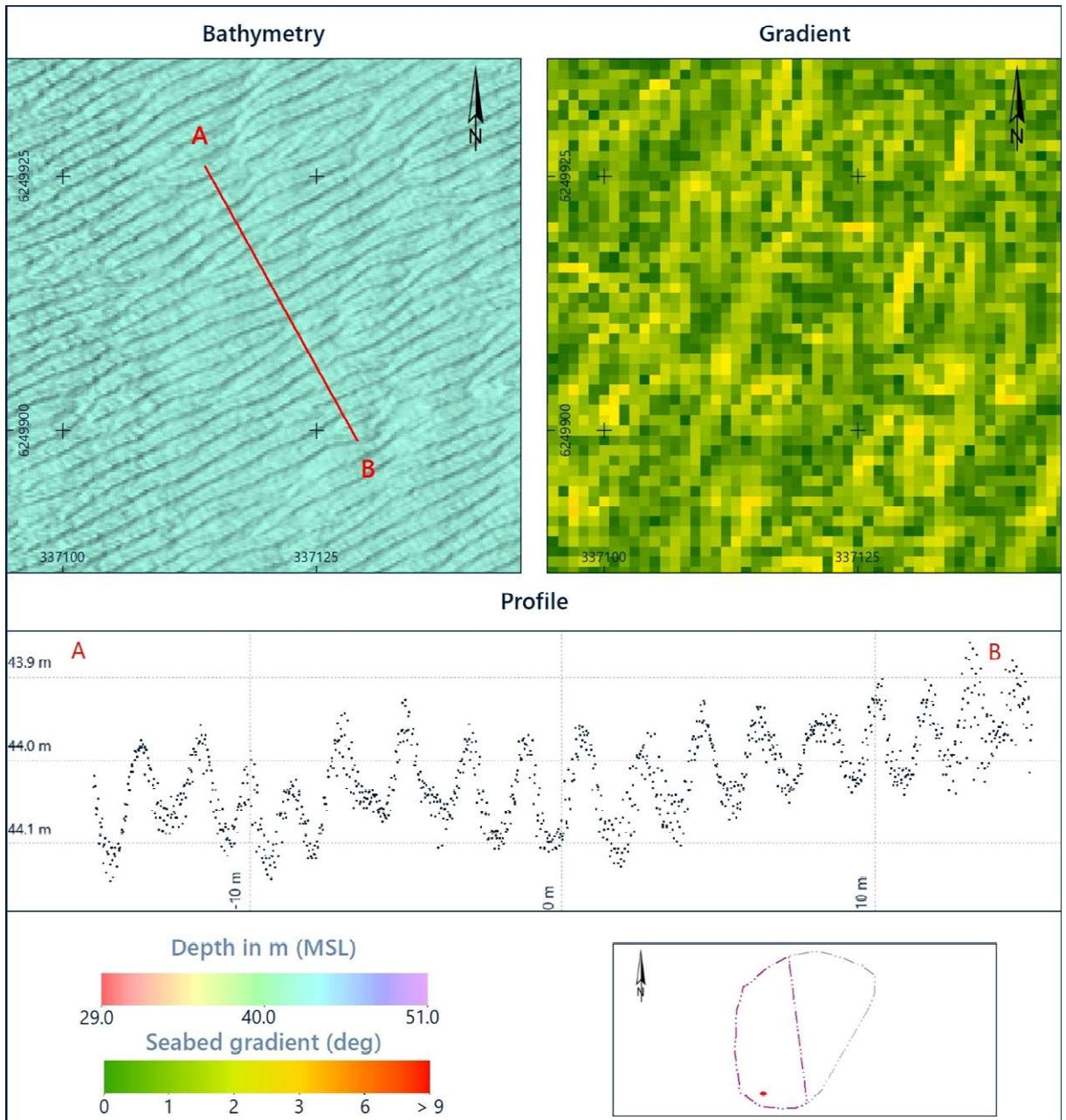
Figure 4.12: Example of ripples observed in the OWF Zone West site.

4.2.2.2 Boulder Fields

Where the boulder density reached at least 40 boulders in a seafloor area measuring 100 m x 100 m, these areas were defined as boulder fields. Two types of boulder fields are present within the site as specified in Table 4.4.

Table 4.4: Boulder field types identified in the OWF Zone West site.

Boulder Field Types	Number of Boulders within 100 m x 100 m Area
Type 1: Intermediate boulder density	40 - 80
Type 2: High boulder density	> 80
No minimum size requirement, all boulders count towards the minimum boulder amount to determine boulder fields.	

Most of the targets observed in SSS and MBES datasets are interpreted as boulders (refer to section 4.2.5.1). The boulders are spread evenly across the entire site except in the parts where Unit U10 is thicker than in the surrounding areas (Figure 4.13). See section 4.3.1.11 for more details.
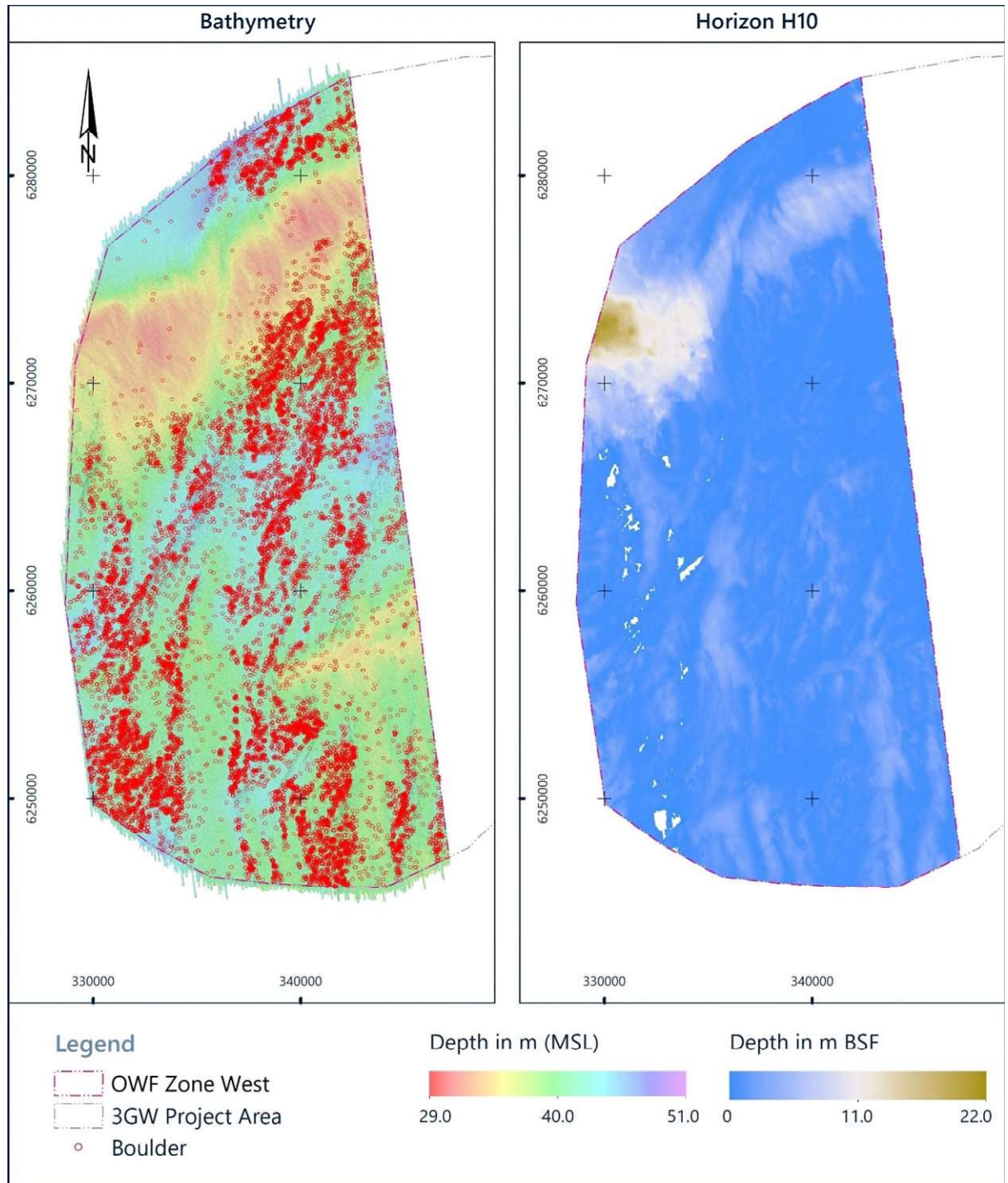
Figure 4.13: Boulder distribution in the OWF West Zone site compared with the thickness of Unit U10.

An example of high-density boulder field is shown in Figure 4.14, while an example of intermediate density boulder field is shown in Figure 4.15.
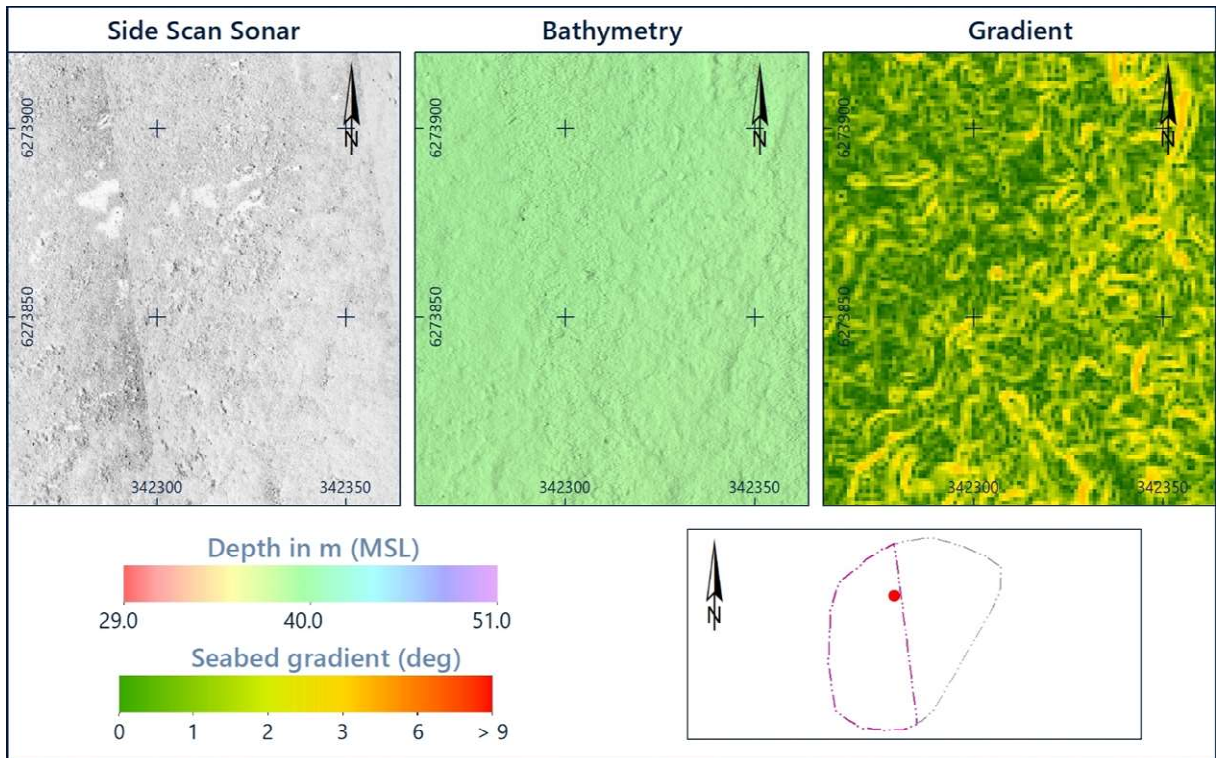
Figure 4.14: Example of high-density boulder field in the OWF Zone West site.
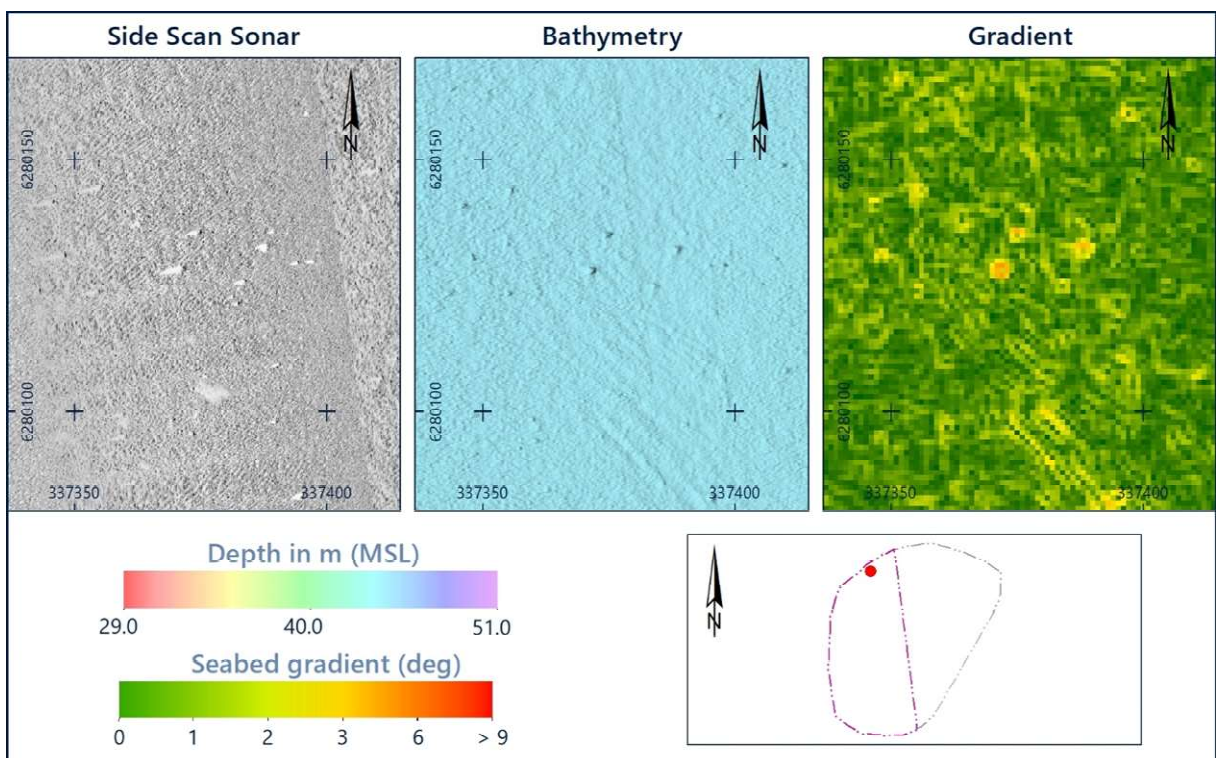
Figure 4.15: Example of intermediate density boulder field in the OWF Zone West site.

4.2.2.3 Possible Pingo Remnants or Potential Sites of Archaeological Interest

Four (4) semi-circular features (possible pingo remnants or potential sites of archaeological interest) were found. These features have all different dimensions, the diameter goes from 10 m to 40 m, while the height varies from 0.2 m to 0.5 m. See Figure 4.16 and Figure 4.17 for more details.
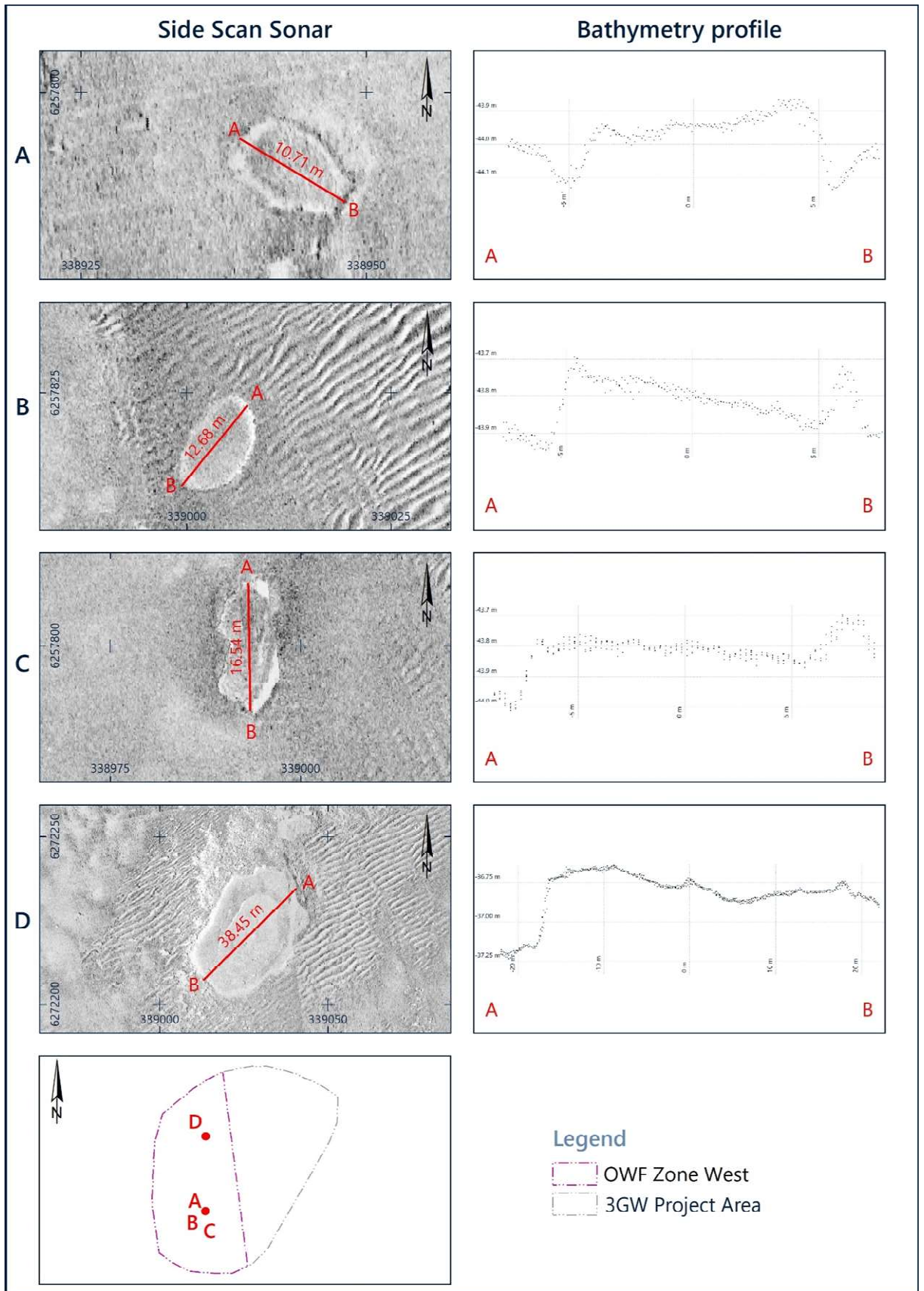
Figure 4.16: Example of the possible pingo remnants or potential sites of archaeological interest.
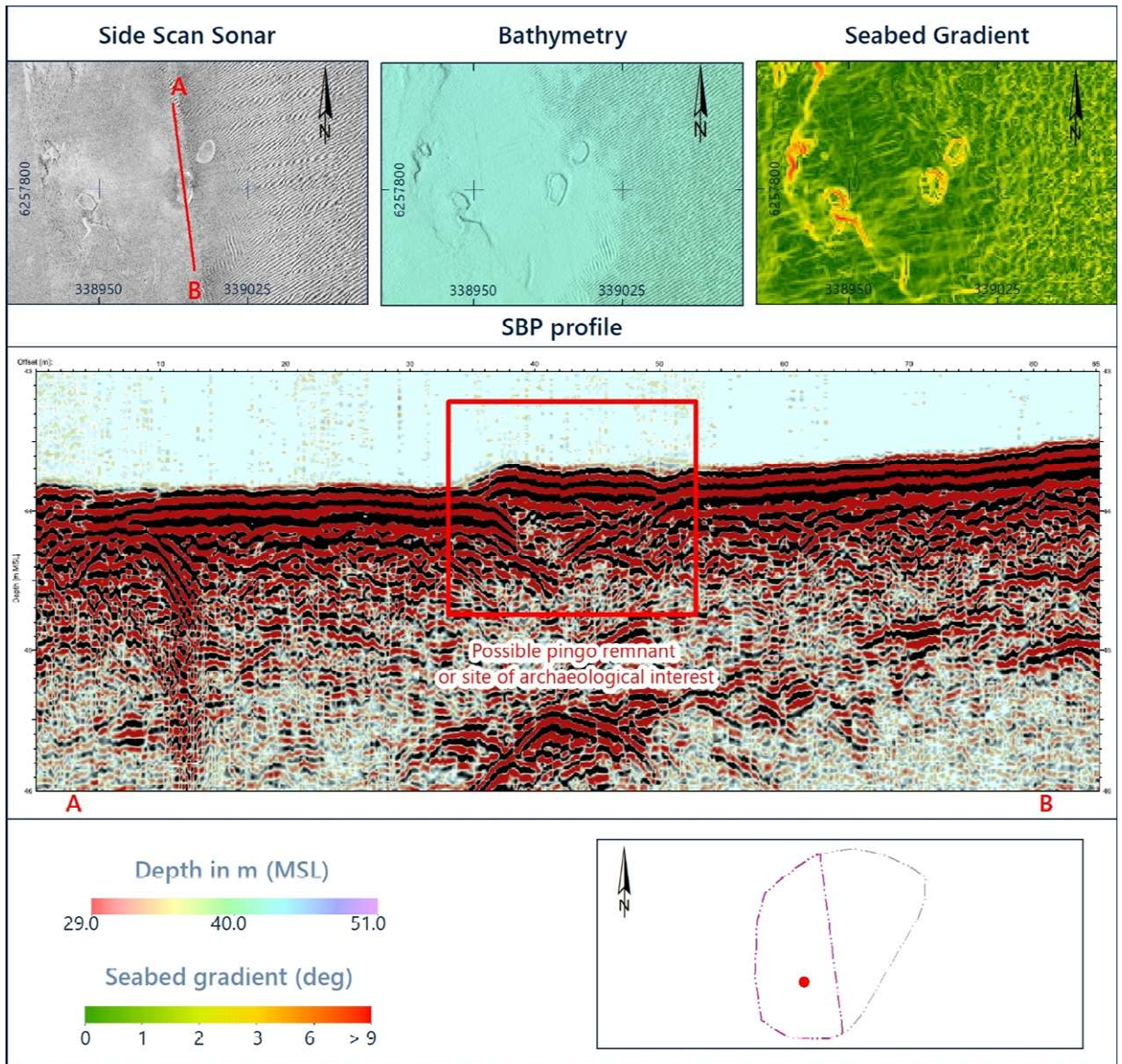
Figure 4.17: Example of possible pingo remnant or potential site of archaeological interest visible in the SBP data.

4.2.2.4 Ridges

In the OWF West Zone site, isolated topographical highs of elongated shapes were classified as ridges. These ridges exhibit relatively high gradient and are predominantly associated with till/diamicton and gravel and coarse sand sediments. Ridges were mostly observed in the northern and central parts of the site and are characterised by varying dimensions. Refer to Figure 4.18 for an example.
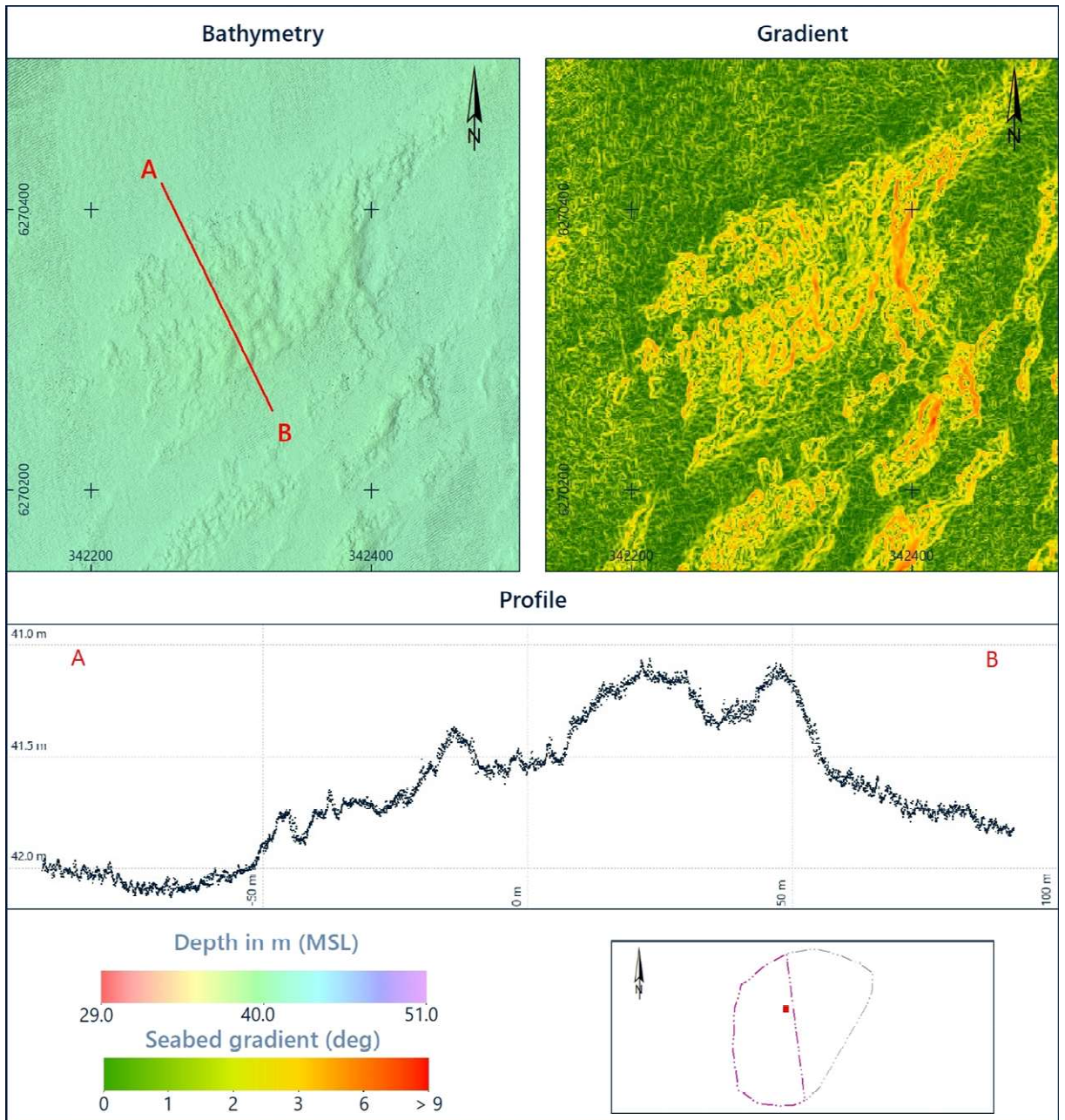
Figure 4.18: Example of a ridge observed in the OWF West Zone site.

4.2.2.5 Possible Biogenic Areas

Possible biogenic areas were observed and mapped for the purpose of further environmental investigation. The water depths where they were found range approximately from 35.0 m to 45.0 m MSL. These features are very similar in shape to boulders but are characterised by very low reflectivity strength as seen on SSS data. All possible biogenic areas were observed in proximity to steep slopes, predominantly, where muddy sand sediment type is present (Figure 4.19).
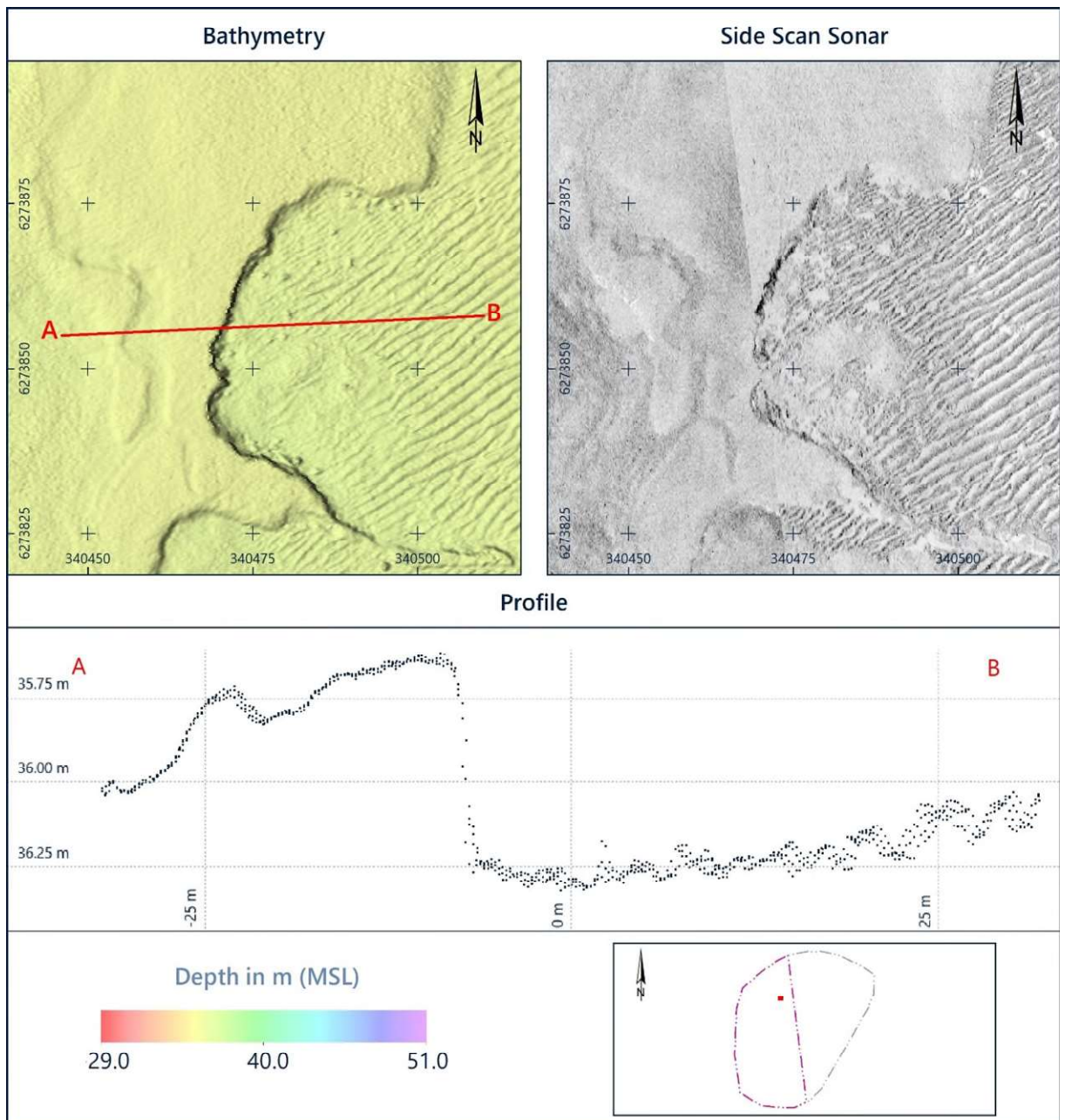
Figure 4.19: Example of a possible biogenic area in the OWF West Zone site.

4.2.2.6   Trawl Marks

Most of the site shows evidence of extensive fishing activity. Numerous well-preserved trawl marks of various orientations were observed in the SSS, backscatter and MBES data. The density of trawl scars is lower in the south-western part of the site compared to the density observed elsewhere. An example on how the fishing activity is disturbing the sediment distribution is shown in Figure 4.20.
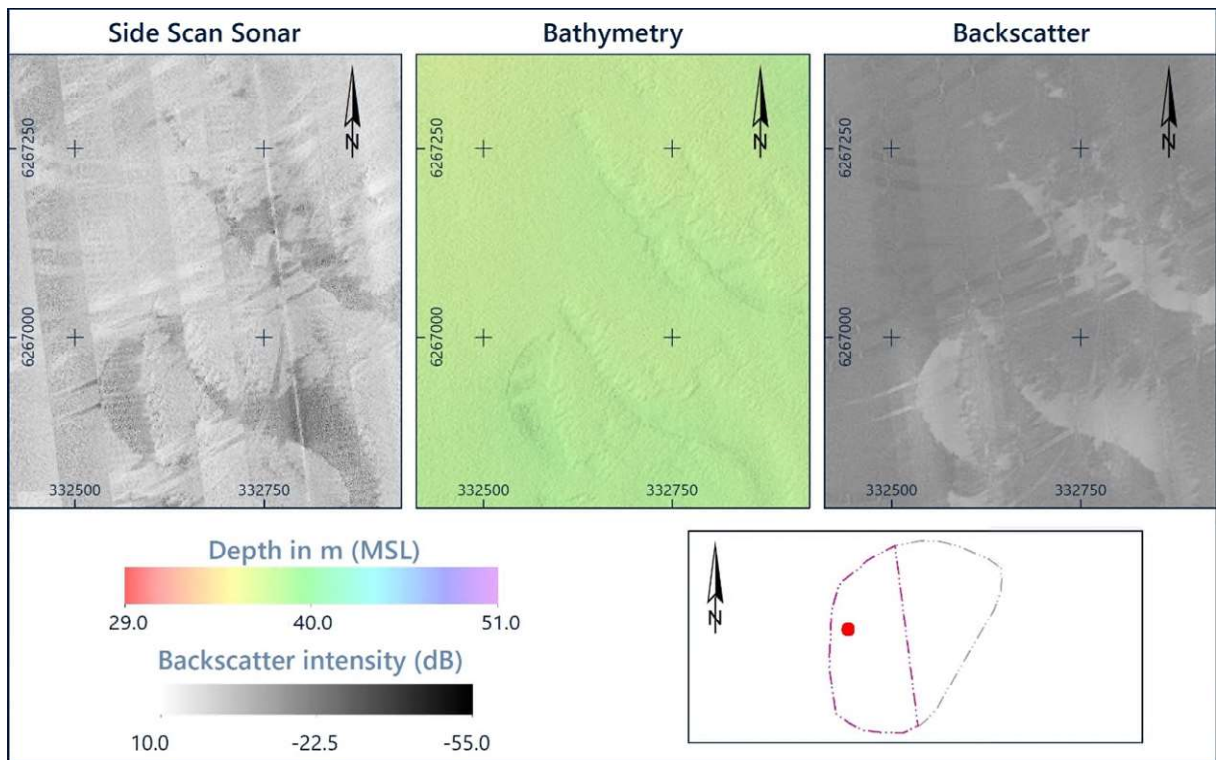
Figure 4.20: Example of an area with trawl marks in the OWF West Zone site.

4.2.3 Substrate Type

An overview of the substrate type interpretation and classification is shown in Figure 4.21 and presented in the charts provided in a separate PDF file (see Appendix B).

Substrate type interpretation and classification were based on the results of the grab sample laboratory analysis (PSD), cross-correlated with backscatter intensity and supported by SSS dataset. The boulder density map derived from the automatic boulder picking tool was used to aid the interpretation. The substrate type classification follows the Danish Råstofbekendtgørelsen (BEK no. 1680 of 17/12/2018, Phase IB).

As the Danish Råstofbekendtgørelsen (BEK no. 1680 of 17/12/2018, Phase IB) presents no quantitative ranges for classification, the interpretation remains very subjective. To remove the subjectiveness of the interpretation process Fugro applied the following ranges:

- Samples containing ≥65% of sand were classified as:
  - 1b – Sand, solid sandy bottom;
- Samples containing <65% sand were classified as:
  - 1a – Sand, silty, soft bottom, when % silt > % clay;
  - 1c – Clay bottom, when % clay > % silt;
- Samples containing gravel smaller than 20 mm in size were classified as:
  - 2a – Sand, gravel and pebbles – few larger stones;
- Samples containing gravel larger than 20 mm but smaller than 10 cm were classified as:
  - 2a/2b – Sand, gravel and pebbles – few larger stones/ Sand, gravel and pebbles – seabed cover of larger stones 1% to 10%;
- Samples containing stones, for which PSD results are not available, were classified as:

- 3 – Sand, gravel, and pebbles – seabed cover of larger stones 10% to 25%.

The data analysis was carried out using acoustic characteristics such as overall pattern, roughness, reflectivity, and backscatter strength. An overview of the backscatter data is presented in Figure 4.22.

The substrate type polygon boundaries were derived from seafloor sediment interpretation. Several polygons were grouped and adjusted where necessary based on the grab sample analysis following the classification specified above. An overview of the grab samples results is presented in Figure 4.23.

The substrate types identified within the site are as follows:

- 1a – silty soft bottom; comprising mainly mud and sandy mud and muddy sand;
- 1b – solid sandy bottom; comprising mainly gravel and coarse sand, muddy sand, and sand;
- 2a – Sand, gravel and pebbles – few larger stones;
- 2b – Sand, gravel and pebbles – seabed cover of larger stones 1% to 10%;
- 3 – Sand, gravel and pebbles – seabed cover of larger stones 10% to 25%.

Table 4.5 presents a few examples of cross-correlation between the grab samples and backscatter reflectivity.

Table 4.5: Cross-correlation between the grab samples and backscatter reflectivity.
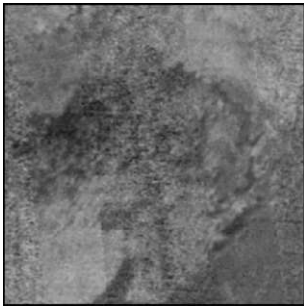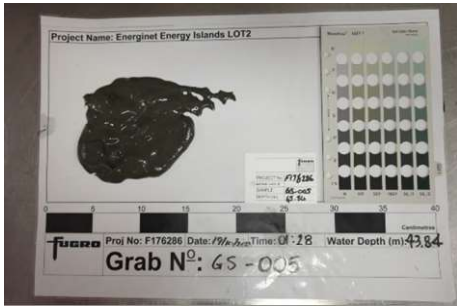
Backscatter Image	Grab Sample Image	Acoustic Description	Grab Sample Description
		Low reflectivity	1a - Sand, silty, soft bottom
		High reflectivity	1b - Sand, solid sandy bottom
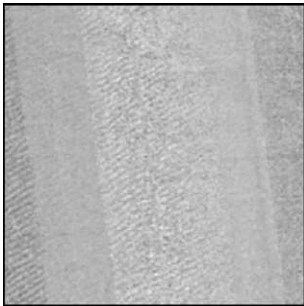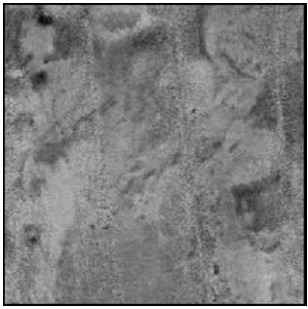
Backscatter Image	Grab Sample Image	Acoustic Description	Grab Sample Description
		Low to high reflectivity	2a – Sand, gravel and pebbles – few larger stones
		Medium to high reflectivity	2b – Sand, gravel and pebbles – seabed cover of larger stones 1% to 10%
		Medium to high reflectivity	3 – Sand, gravel and pebbles – seabed cover of larger stones 10% to 25%
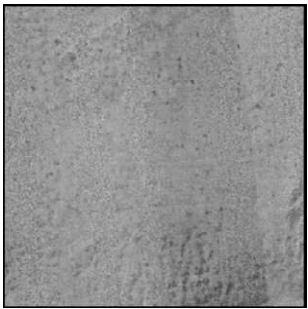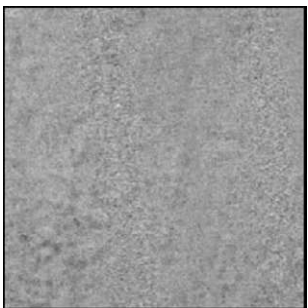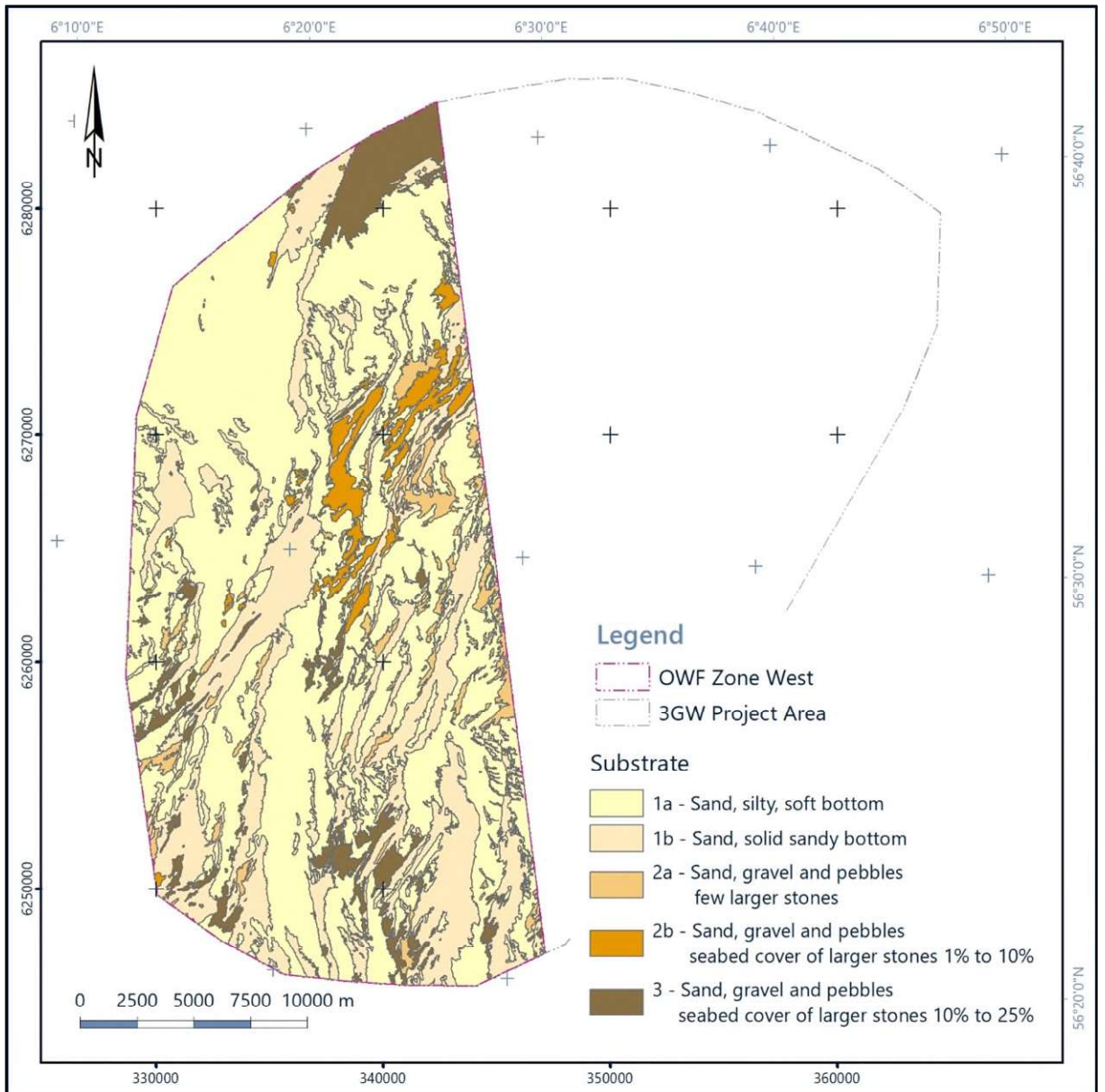
Figure 4.21: Overview of the substrate types in the OWF Zone West site.
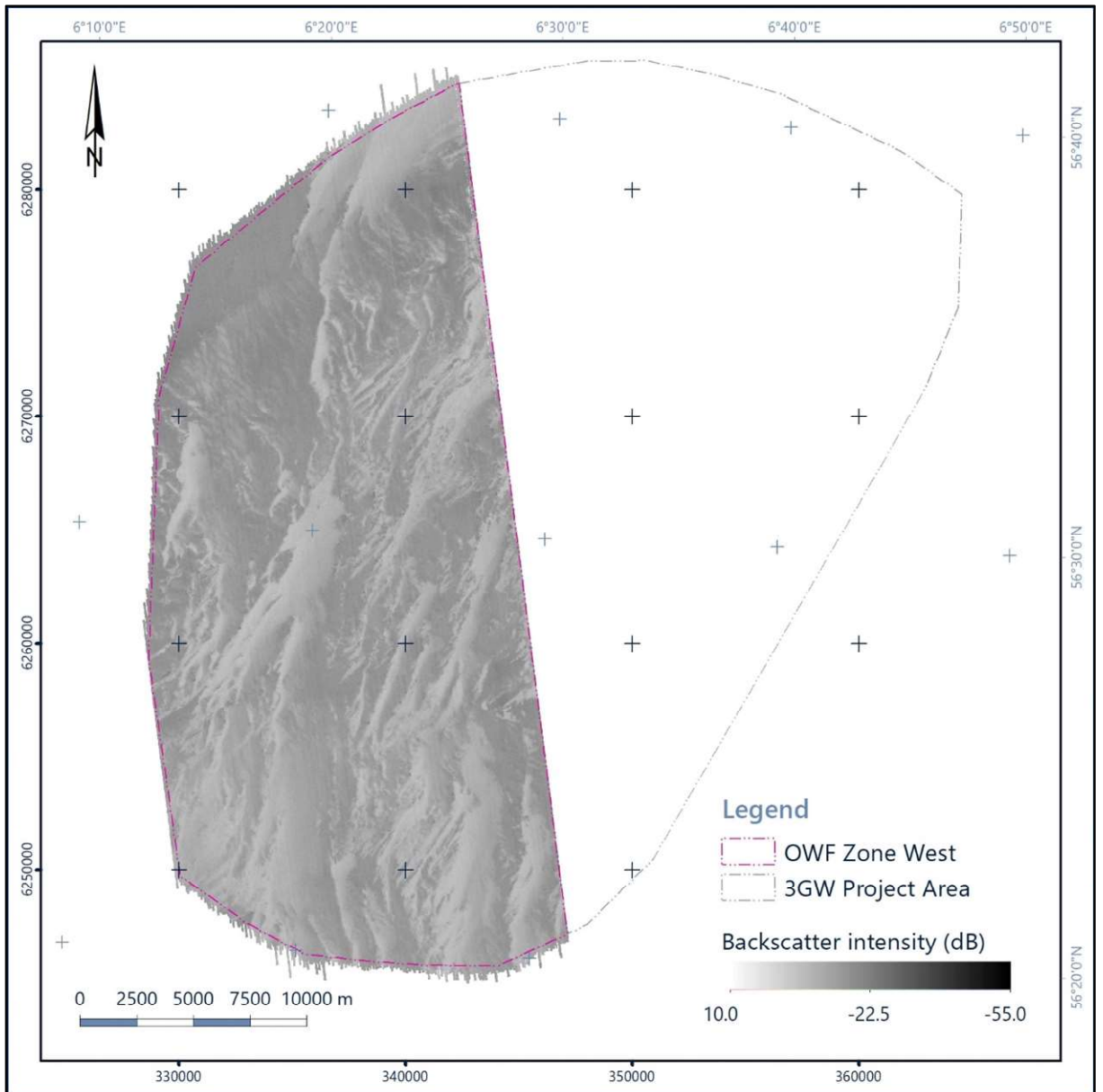
Figure 4.22: Overview of the backscatter data in the OWF Zone West site.
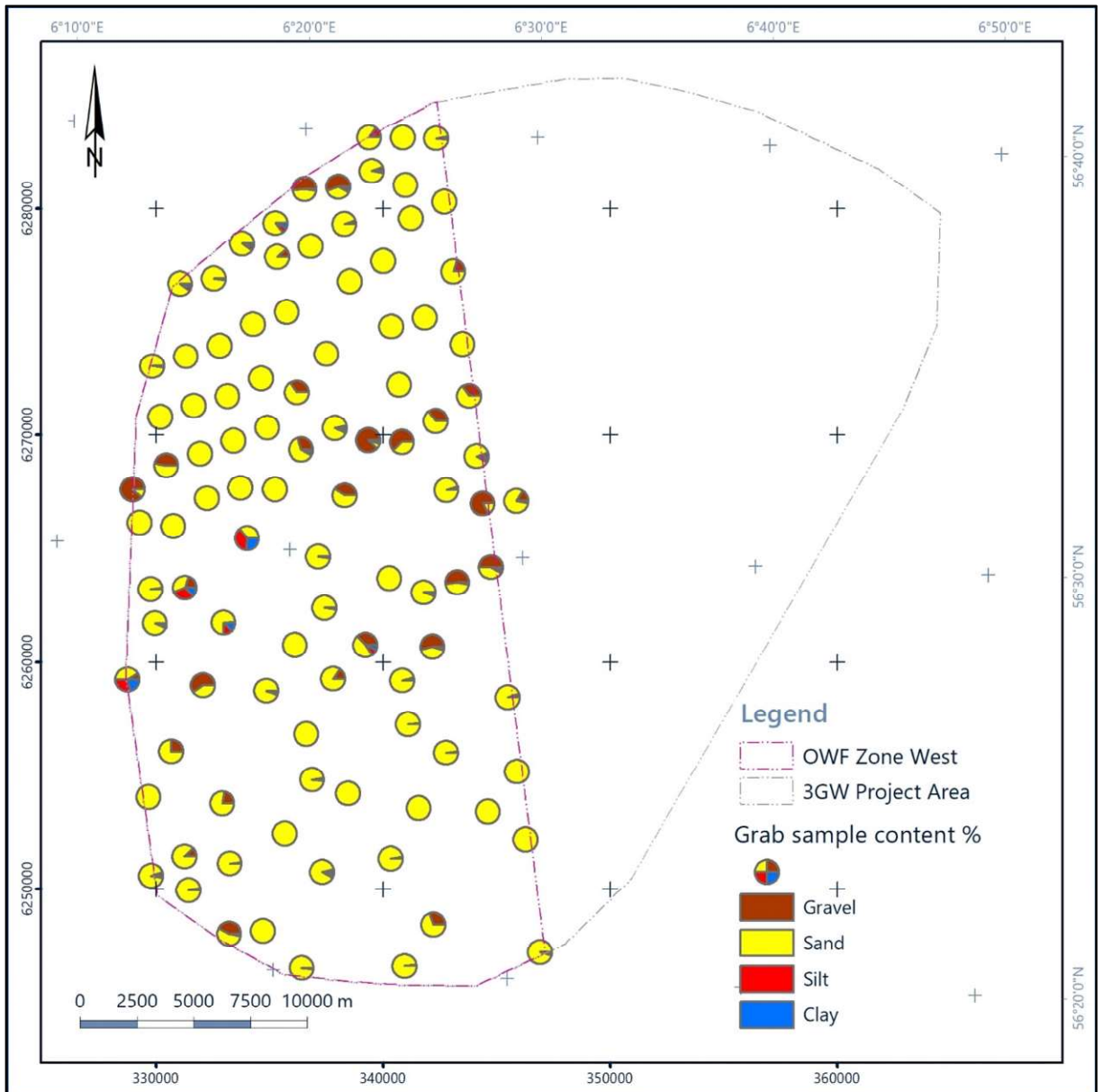
Figure 4.23: Overview of the grab samples collected in the OWF Zone West site.

4.2.4 Seafloor Sediments

An overview of the seafloor sediment interpretation and classification is shown in Figure 4.24 and presented in the charts provided in a separate PDF file (see Appendix B).

Seafloor sediment interpretation and classification were based on a combination of SSS, MBES and backscatter datasets and correlated with the sub-surface geology interpreted in the SBP data. The data analysis was carried out using acoustic characteristics such as overall pattern, roughness, reflectivity, and backscatter strength.

In addition, seafloor sediment interpretation incorporated soil description of grab samples following the onshore laboratory analysis. The grab sample soil descriptions are based on Danish standard (Larsen et al., 1995) and GEUS terminology was used to define mapped sediment classes. Detailed laboratory analyses of the collected grab samples are supplied as a part of the final deliverables.

An overview of the backscatter data is presented in Figure 4.22, followed by an overview of the grab sampling results shown in Figure 4.23.

The seafloor sediments identified in the OWF Zone West site comprise the following:

- Mud and sandy mud;
- Muddy sand;
- Sand;
- Gravel and coarse sand;
- Till/diamicton.

The acoustic characteristics of the identified sediment types are summarised in Table 4.6.

Table 4.6: Acoustic characteristics of the sediment types identified in the OWF Zone West site.

Backscatter Image	MBES Image	SSS Image	Acoustic Characteristics	Geological Interpretation
			Low to very low reflectivity	Mud and sandy mud
			Medium to low reflectivity	Muddy sand
			High reflectivity	Sand
			High reflectivity	Gravel and coarse sand
			High reflectivity	Till/diamicton
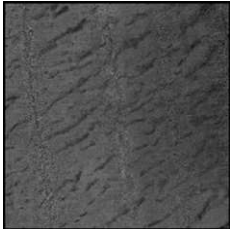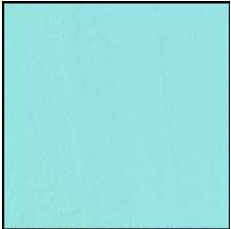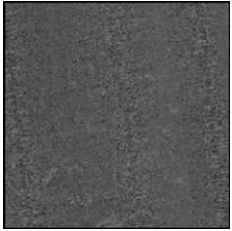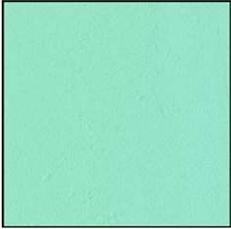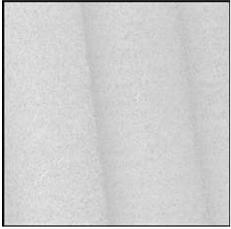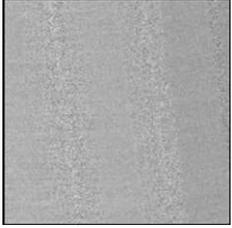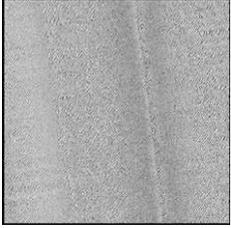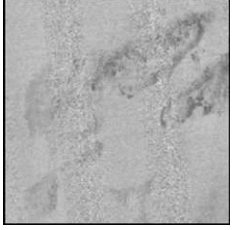
The dominant sediment type within the site is sand, with areas of higher component of finer sediment defined as muddy sand and mud and sandy mud. Areas of gravel and coarse sand were identified where the Holocene unit is relatively thin.

The till/diamicton corresponds to areas where Unit U30 is exposed at or close to the seafloor. It is interpreted that Unit U30 was deposited in a (glacio-) marine or (glacio-) lacustrine depositional environment (section 4.3.1.8). In glacio-marine and glacio-lacustrine deposits ice-rafted debris may be present. The till/diamicton refers to a poorly sorted sediment containing a wide range of grain sizes as observed in the SSS dataset (and not to the depositional environment). Figure 4.25 shows an example of the cross-correlation between the till/diamicton and the distribution of Unit U30.
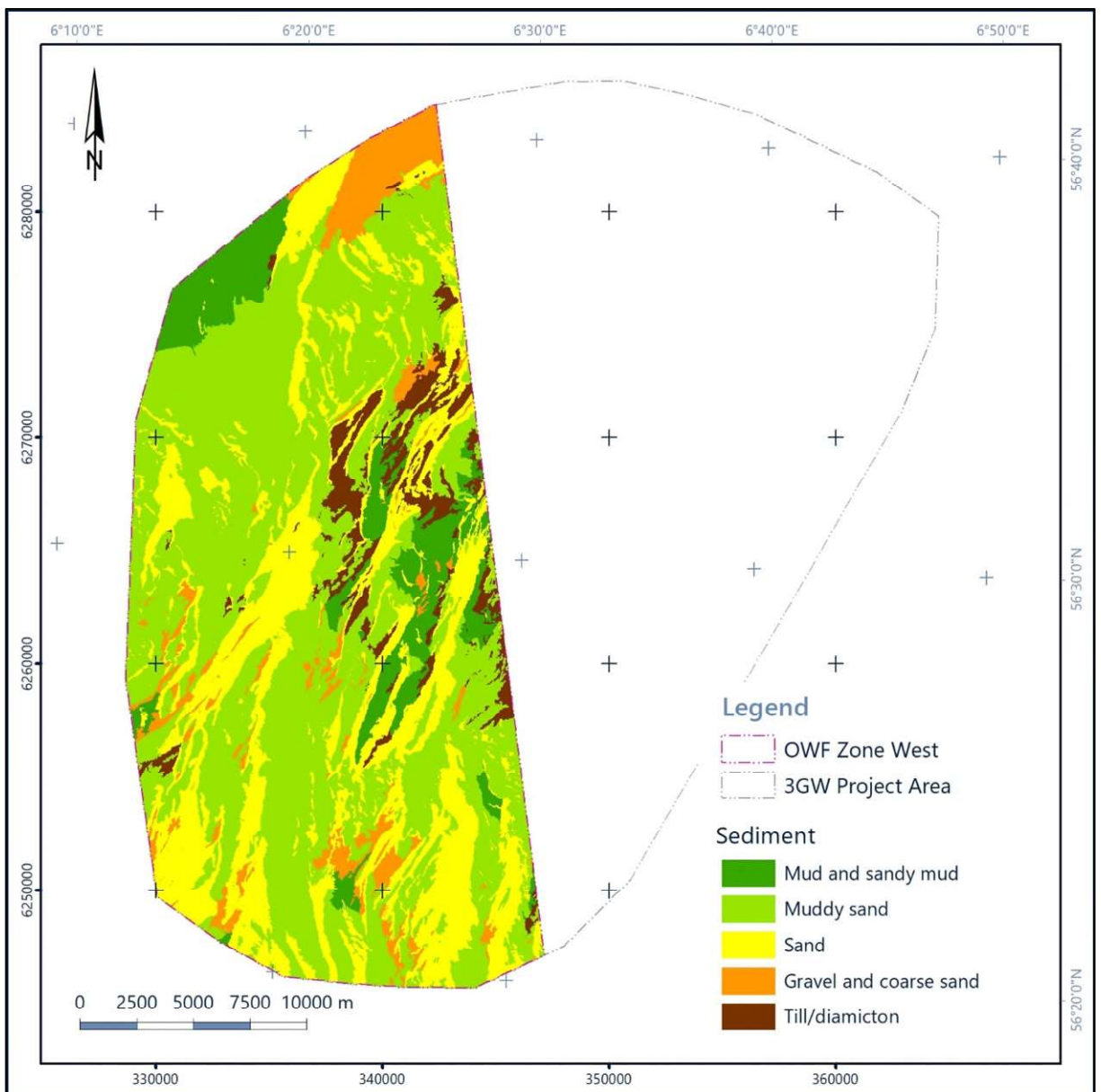
Figure 4.24: Overview of the seafloor sediment interpretation in the OWF Zone West site.
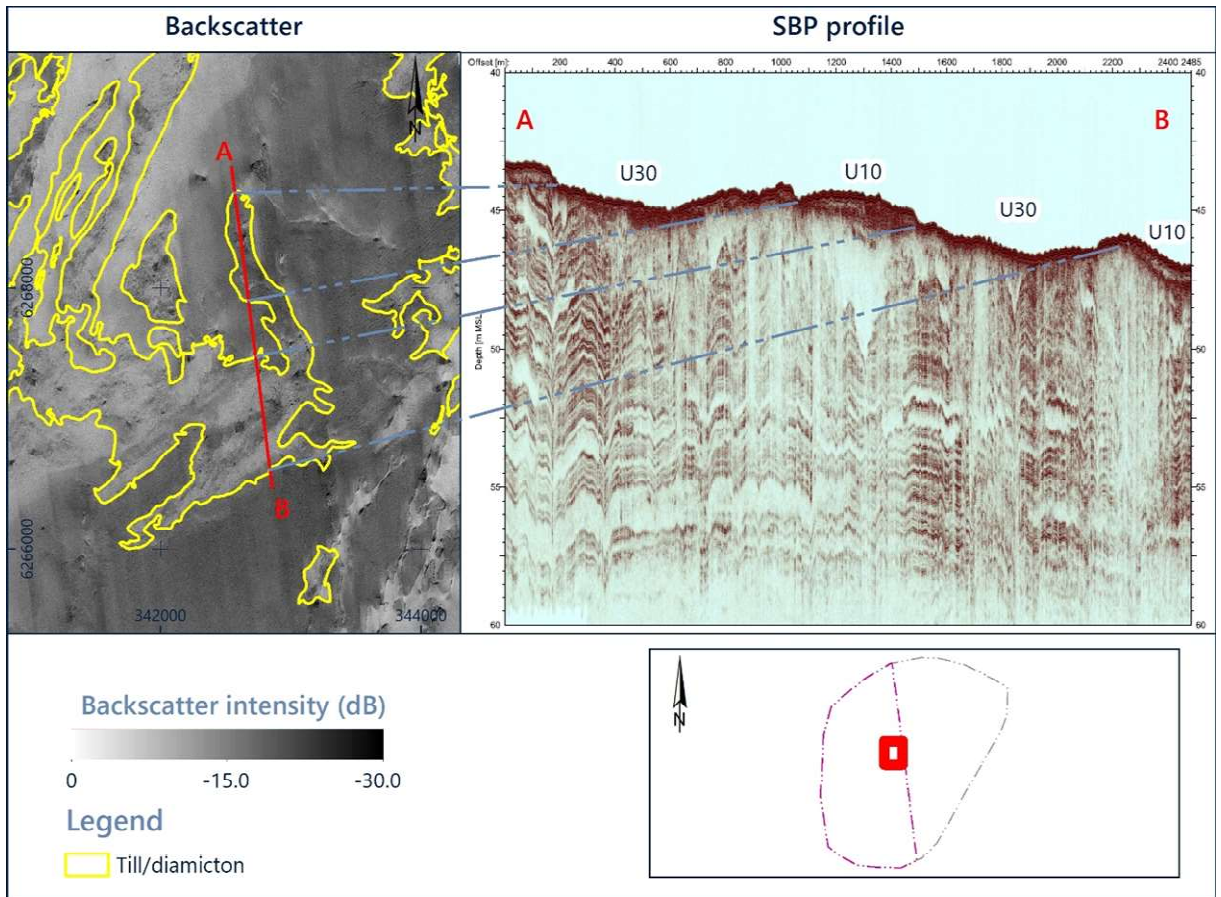
Figure 4.25: Example of the cross correlation between the till/diamicton and Unit H30 at/close to seafloor.

4.2.5   Seafloor Features and Targets

Seafloor features and targets were identified in the SSS, MBES and MAG data, and cross-correlated where possible. The identified targets are shown on charts provided in a separate PDF file (see Appendix B).

Table 4.7 summarises the quantities of targets picked.

Table 4.7: Summary of seafloor targets identified in the OWF Zone West site.

Sensor	Target Classification	Quantity
SSS	Boulder	18412
	Debris/Suspected debris	111
	Isolated depression/Pockmark	6
	Pipeline	45
	Seabed mound	14
	Unidentified	6
	Wreck	2
MAG	Linear feature	348
	Unidentified	2797

A total of 18596 targets measuring at least 1.0 m in any dimension were identified. Out of 18596 targets, 15222 were observed in both the SSS and MBES datasets.

Details of all the identified SSS targets are presented in the target list supplied in the GIS database as part of the final deliverables and catalogues including SSS images (Appendix C). An overview of the SSS targets is presented in charts provided in a separate PDF file (see Appendix B).

Boulders

Most of the identified targets observed in the SSS and MBES datasets were boulders of varying dimensions. Boulders were observed throughout the site except for the shallowest area (up to approximately 35 m water depth) stretching from SW to NE in the northern part of the site. Boulder density is also lower across another, slightly smaller, shallow area (up to approximately 38 m water depth) in the south-eastern part of the site (Figure 4.13).

Figure 4.26 presents a data example of a boulder picked in the OWF Zone West site (EA_H_SSS_00170: L=2.66 m, W=0.60 m, H=0.40 m).
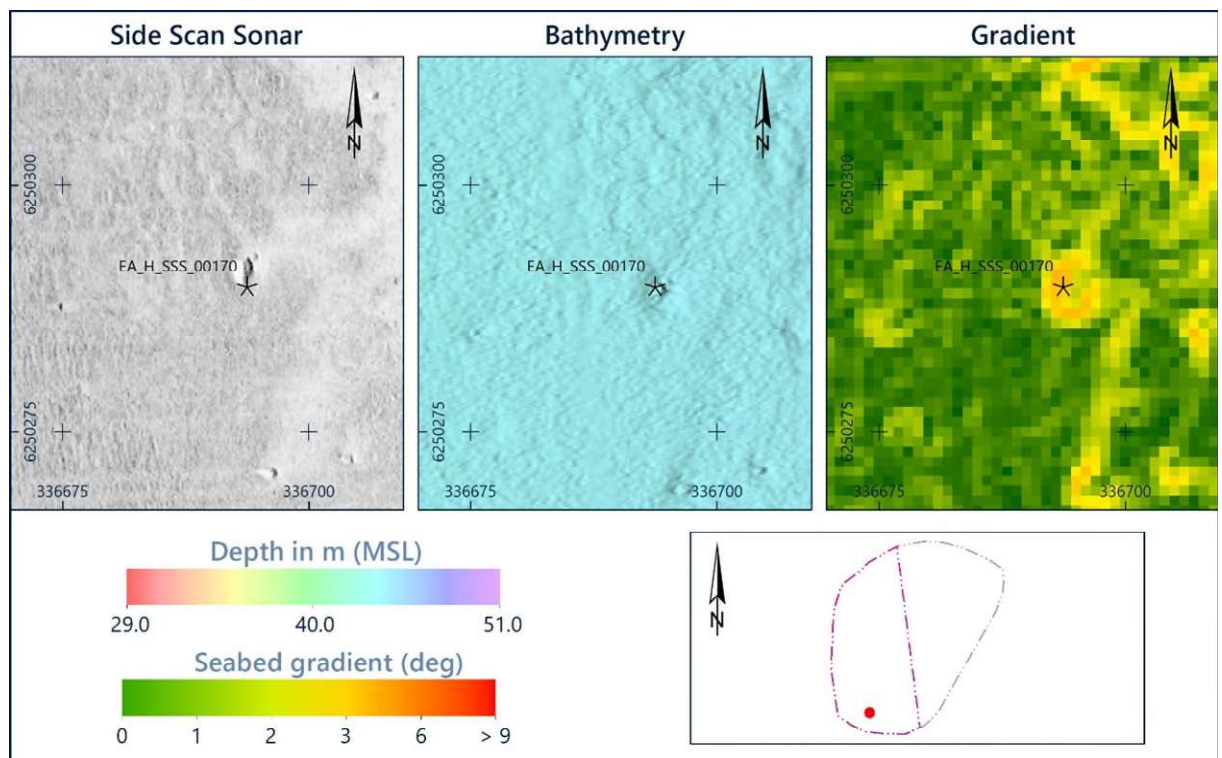
Figure 4.26: Example of a boulder observed in the OWF Zone West site.

The areas where the boulder density reached at least 40 boulders in a seafloor area measuring 100 m x 100 m were defined as boulder fields. Two types of boulder fields are present within the site as specified in Table 4.4.

Boulder fields were mapped following two methodologies – manual and automatic, which are described in detail in section 5. The results of both methods were cross-checked. The

observed differences are attributed to the fact that manual interpretation is subjective to interpreter's experience and approach, while the automatic method provides consistent result, which is limited by the data quality and type of seabed within the surveyed area.

Manually defined polygons mark boulder fields without subdividing them into two types. The subdivision was made based on the automatic results. The comparison is presented in Figure 4.27 and Figure 4.28.
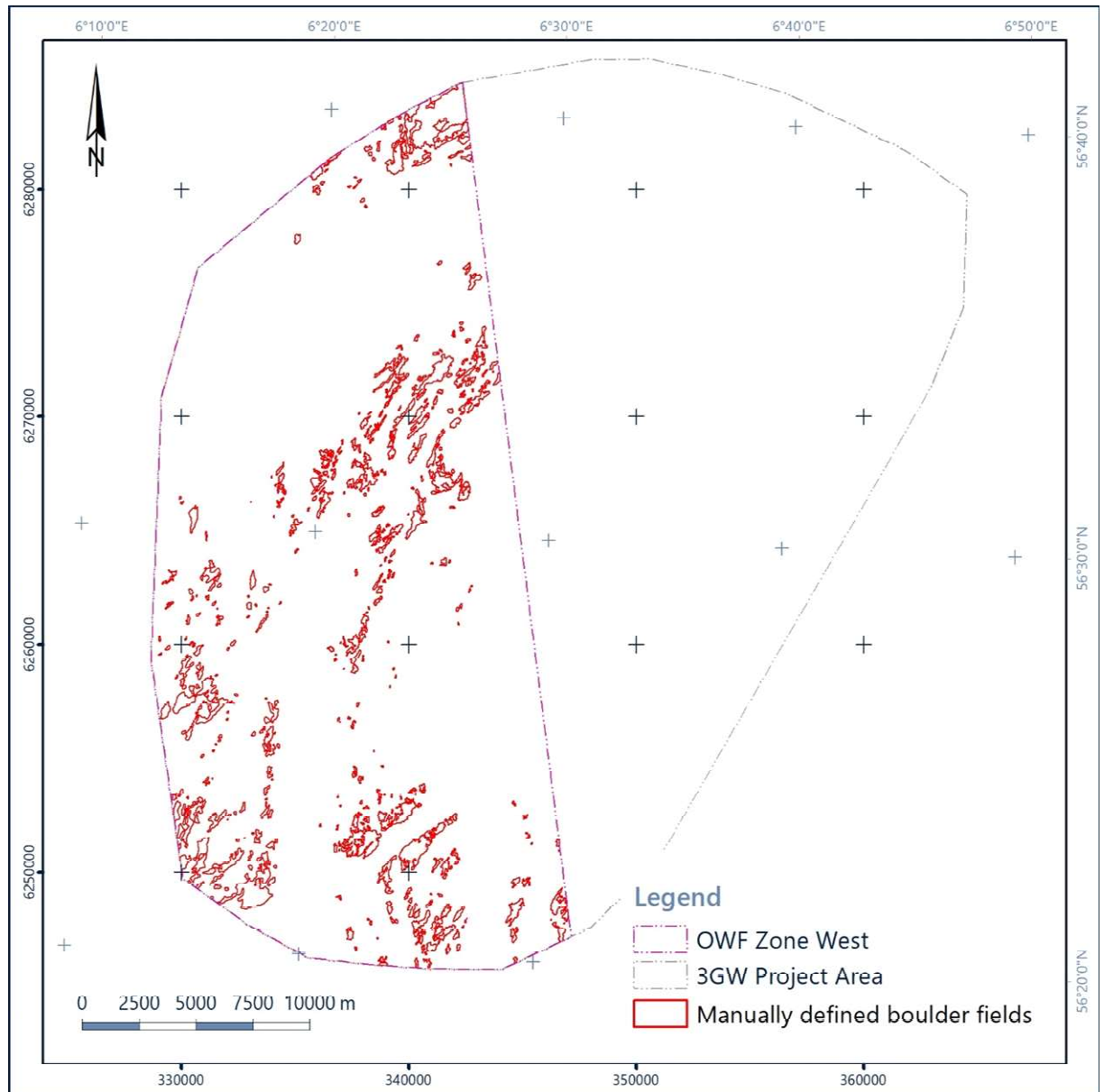
Figure 4.27: Manually defined boulder polygons in the OWF Zone West site.
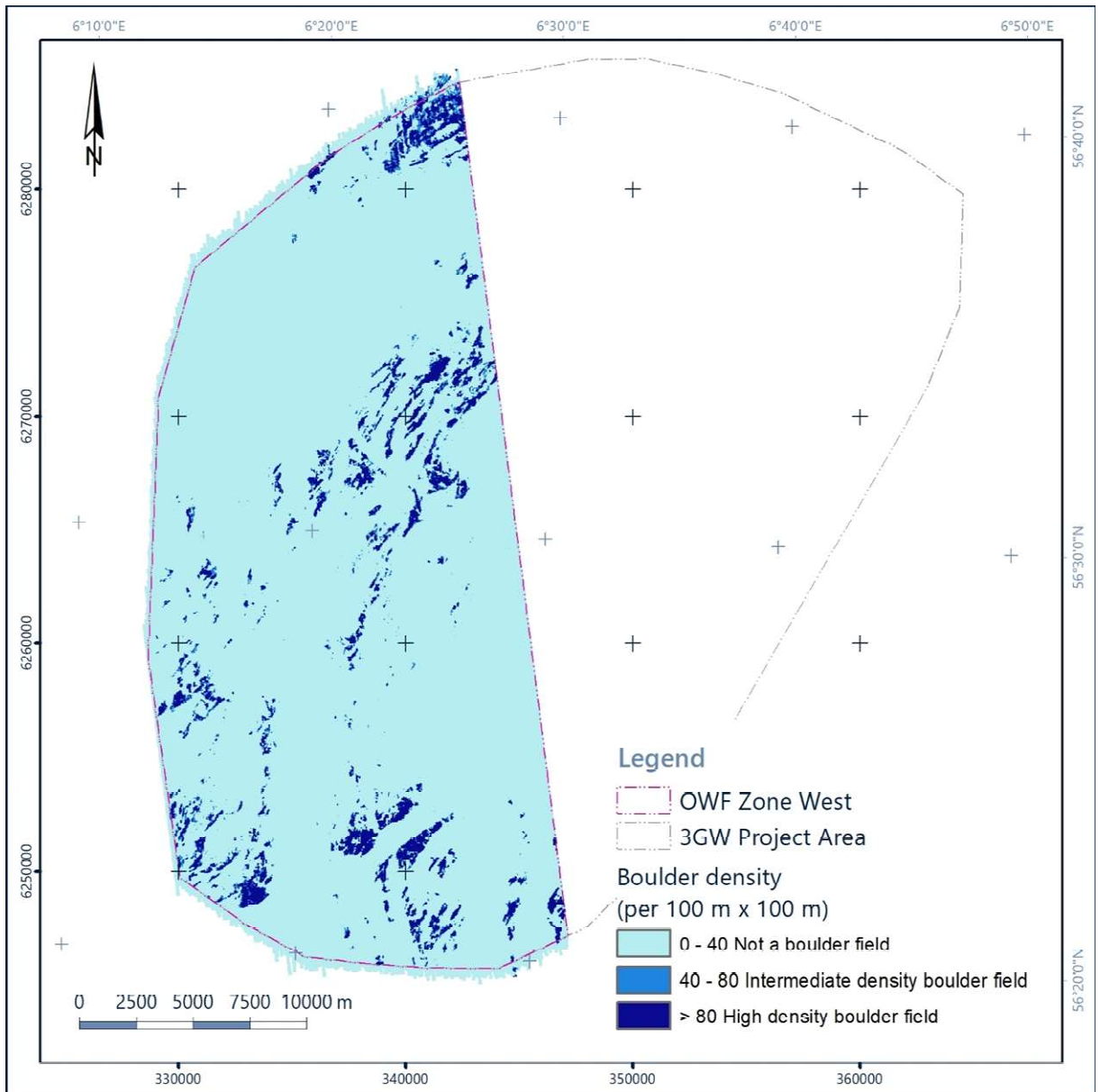
Figure 4.28: Boulder density map in the OWF Zone West site derived from automatic boulder picking tool.

Suspected Debris

Suspected debris was the second most numerous target type identified. Items interpreted as potential debris are generally characterised by more angular or elongated shape and relatively high reflectivity compared to the targets described as boulders. It should be noted that certain ambiguity of the interpretation is to be expected and some of the targets interpreted as debris may in fact be of geological origin.

Figure 4.29 presents a data example of debris (EA_Y_SSS_00345: L=5.02 m, W=0.69 m, H=0.98 m).
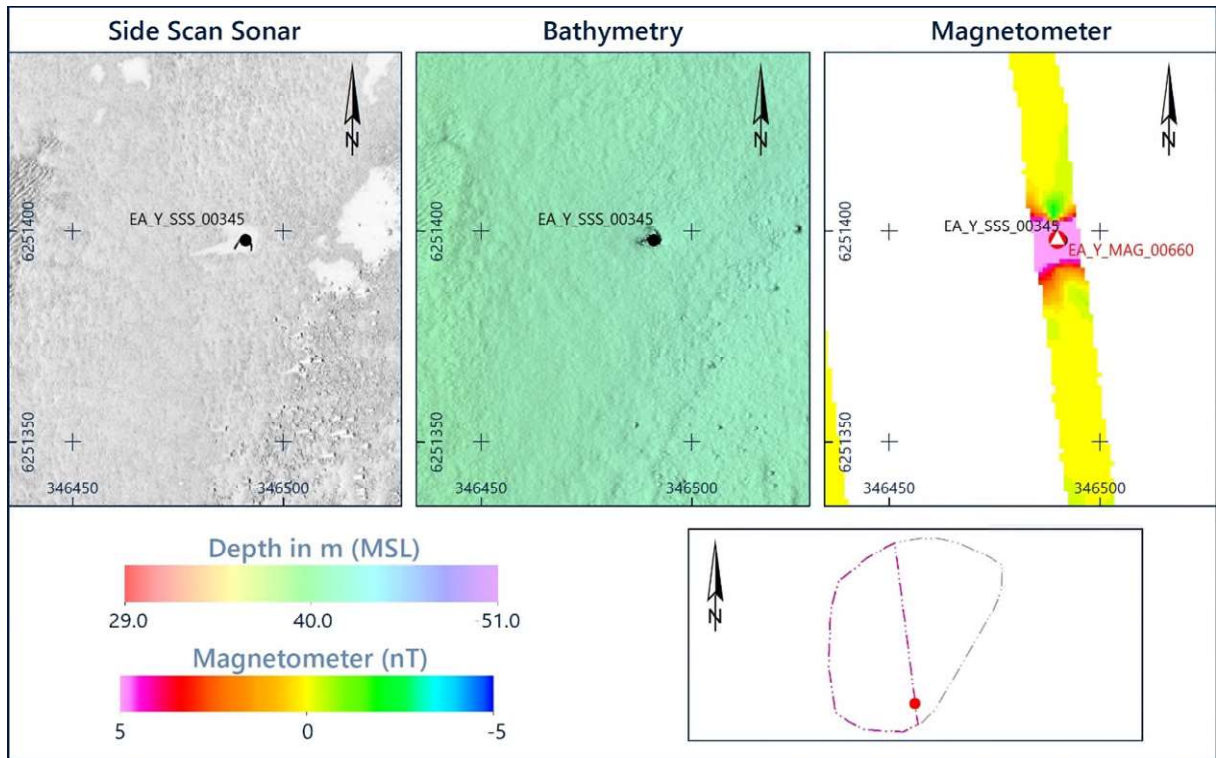
Figure 4.29: Example of debris observed in the OWF Zone West site.

Seabed Mounds

Fourteen (14) targets were identified as seabed mounds. The SSS reflectivity of the seabed mounds is medium to low which can indicate geological origin.

Figure 4.30 presents a data example of a seabed mound (EA_H_SSS_00245: L=3.79 m, W=1.74 m, H=0.56 m).
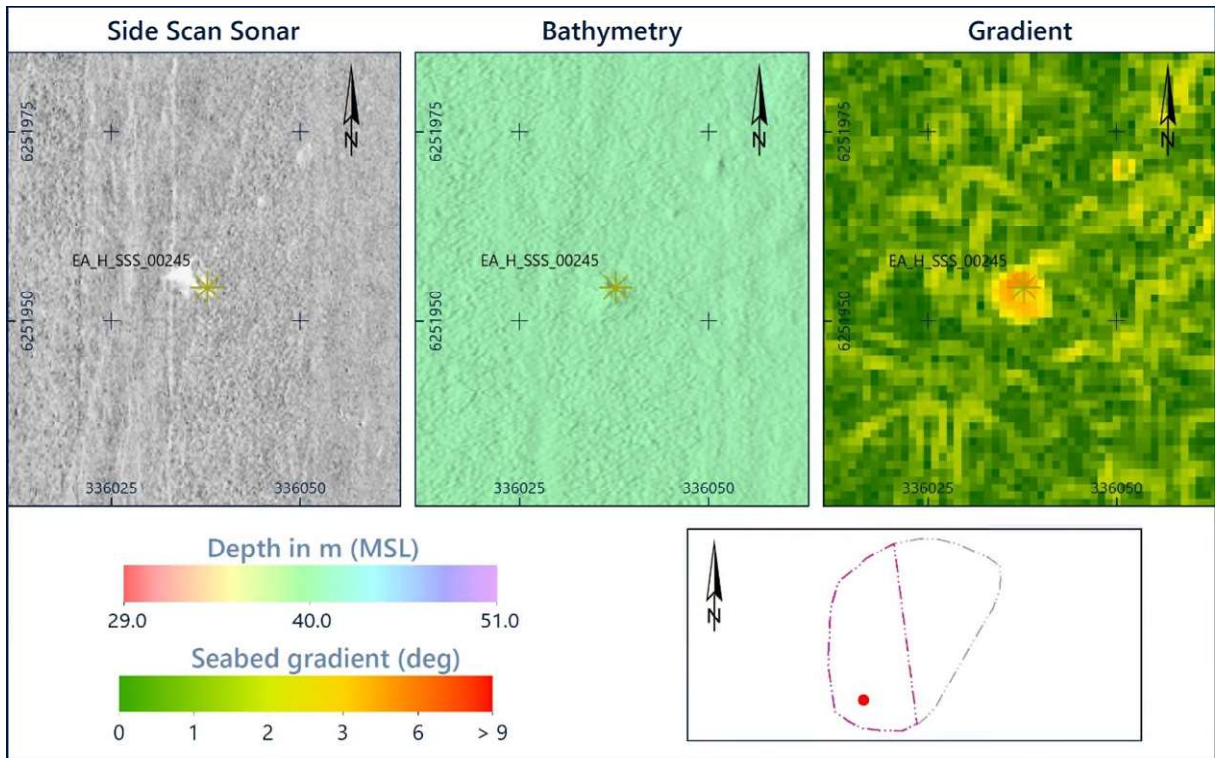
Figure 4.30: Example of a seabed mound observed in the OWF Zone West site.

Depressions

Six (6) SSS targets were classified as isolated depressions. These depressions measure approximately 0.5 m to 2 m in diameter, while their depths do not exceed 0.1 m below the surrounding seafloor. Some of these targets had no observed shadow and their dimensions were subsequently marked with 'non-measurable height'. For these targets the height column lists 0 m.

Figure 4.31 presents a data example of a depression (EA_H_SSS_00278: L=1.68 m, W=1.49 m).
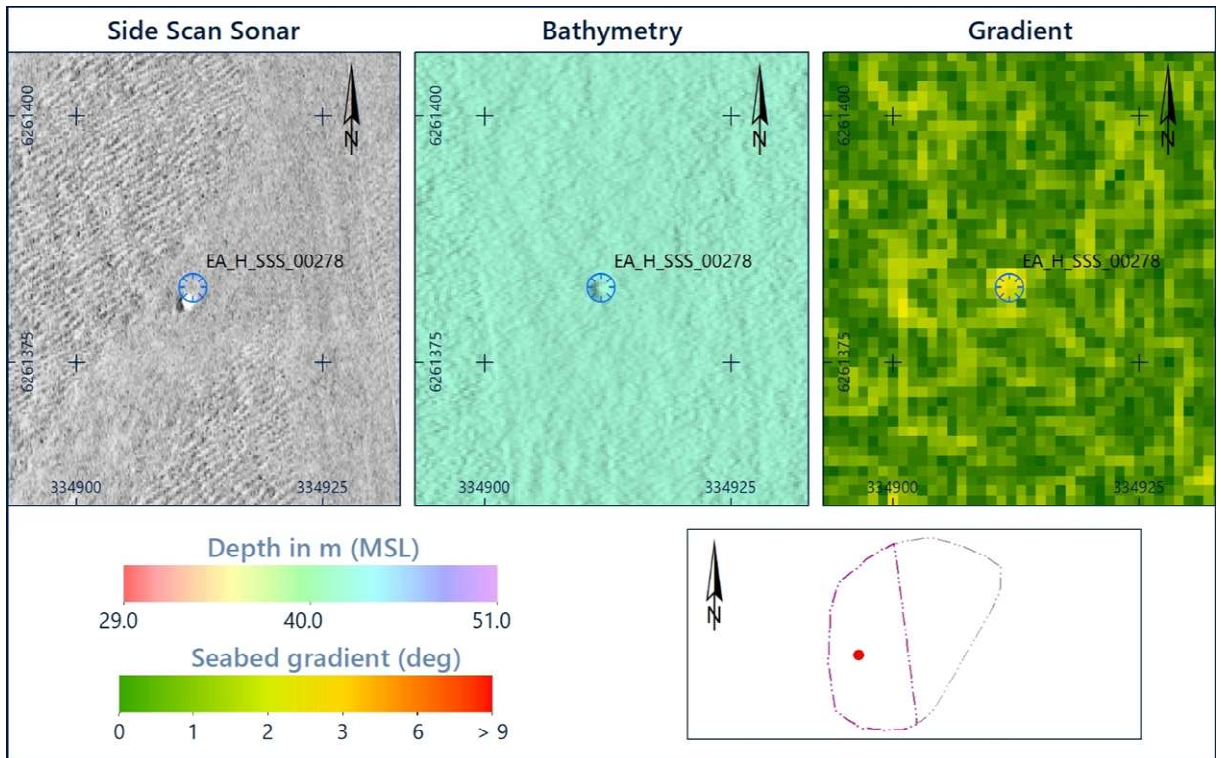
Figure 4.31: Example of an isolated depression observed in the OWF Zone West site.

Wrecks

Two (2) possible shipwrecks were identified within the site. The Fallwind wreck was identified in Block R at 45.81 m water depth (EA_R_SSS_00580). This wreck is approximately 73.43 m long and 20.61 m wide.

Based on the observed debris and the ENC chart, another possible wreck was identified in Block P (EA_P_SSS_00591). The dimensions of this target are approximately 31.49 m by 11.85 m, and the local water depth is 45.8 m. The details and coordinates of the targets are presented in Table 4.8.

Table 4.8: Possible wrecks in the OWF Zone West site.

Block	Target	Details	Easting	Northing
P	EA_P_SSS_00591	Possible Wreck (91D - ENC Database)	337224.95	6279528.76
R	EA_R_SSS_00580	Fallwind Wreck	340612.44	6263664.83
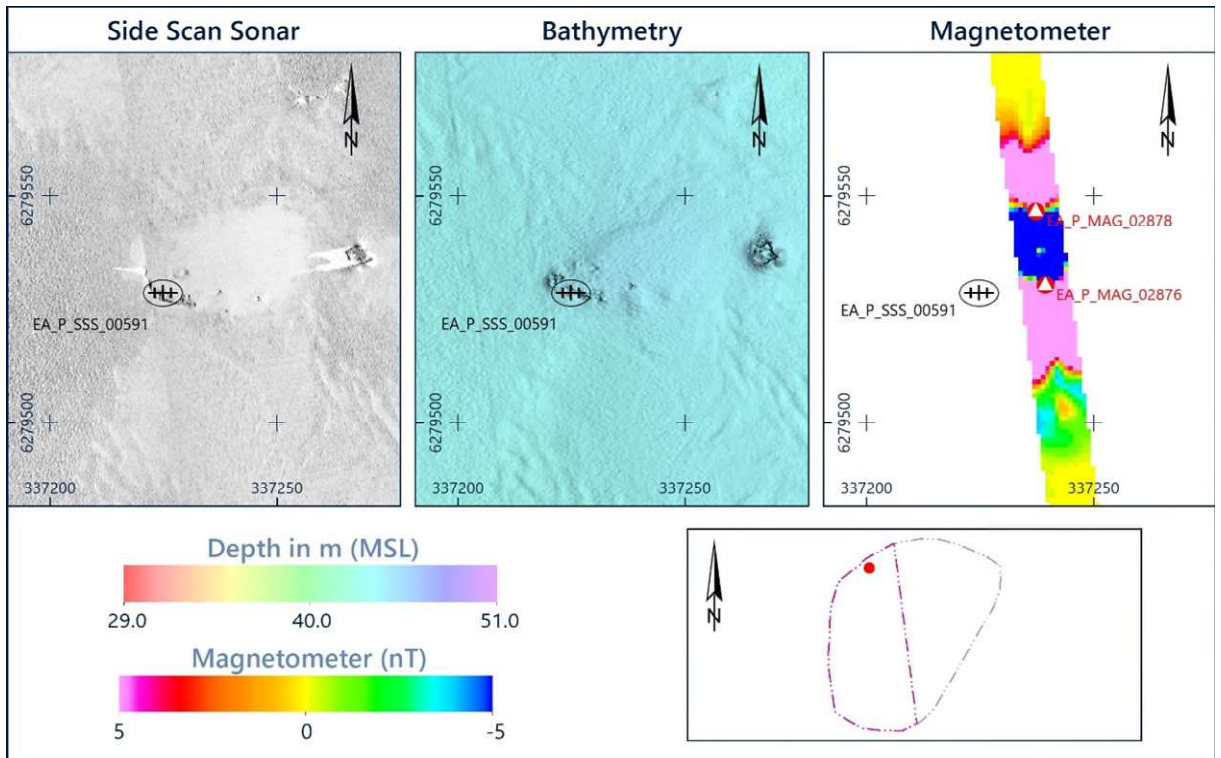
Figure 4.32: Data example of the possible wreck (EA_P_SSS_00591) in Block P of the OWF Zone West site.
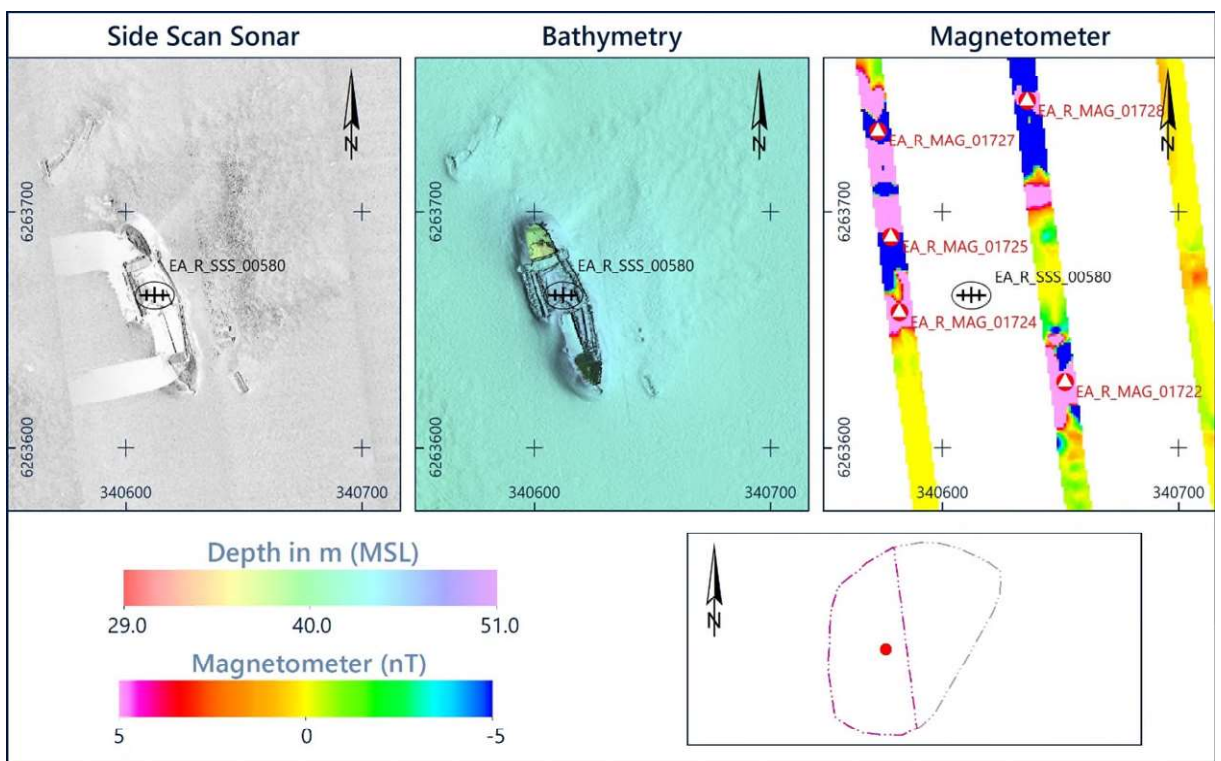
Figure 4.33: Data example of the Fallwind wreck (EA_R_SSS_00580) in Block R of the OWF Zone West site.

Pipelines and cables

One (1) pipeline and two (2) cables were identified within the site. The pipeline, identified as the Europipe II gas pipeline, runs N-S across Block D and E and was observed in the SSS, MAG, MBES and SBP sensors. Forty-five (45) sections of exposed pipeline were identified, with a total length of approximately 20 km.

The cables were identified as the cables Havfrue/AEC-2 and TAT14 Segment K. Both cables cross the site (OWF East and OWF West Zones) in a NW-SE direction. The cables were identified from the MAG sensor and could not be observed in the SSS and SBP data. Rock dumps were observed at the crossings of the cables and the Europipe II pipeline. Table 4.9 provides details of the pipeline found in the site. Refer to Figure 4.34 and Figure 4.35 for data examples of the pipeline. The interpretation of the out-of-plane reflection of the pipeline is called '2DUUHR_Pipeline' in the digital deliverables.

Table 4.9: Pipeline found in the OWF Zone West site.

Block	Name	Details
D and E	Europipe II	42 Inch gas pipeline
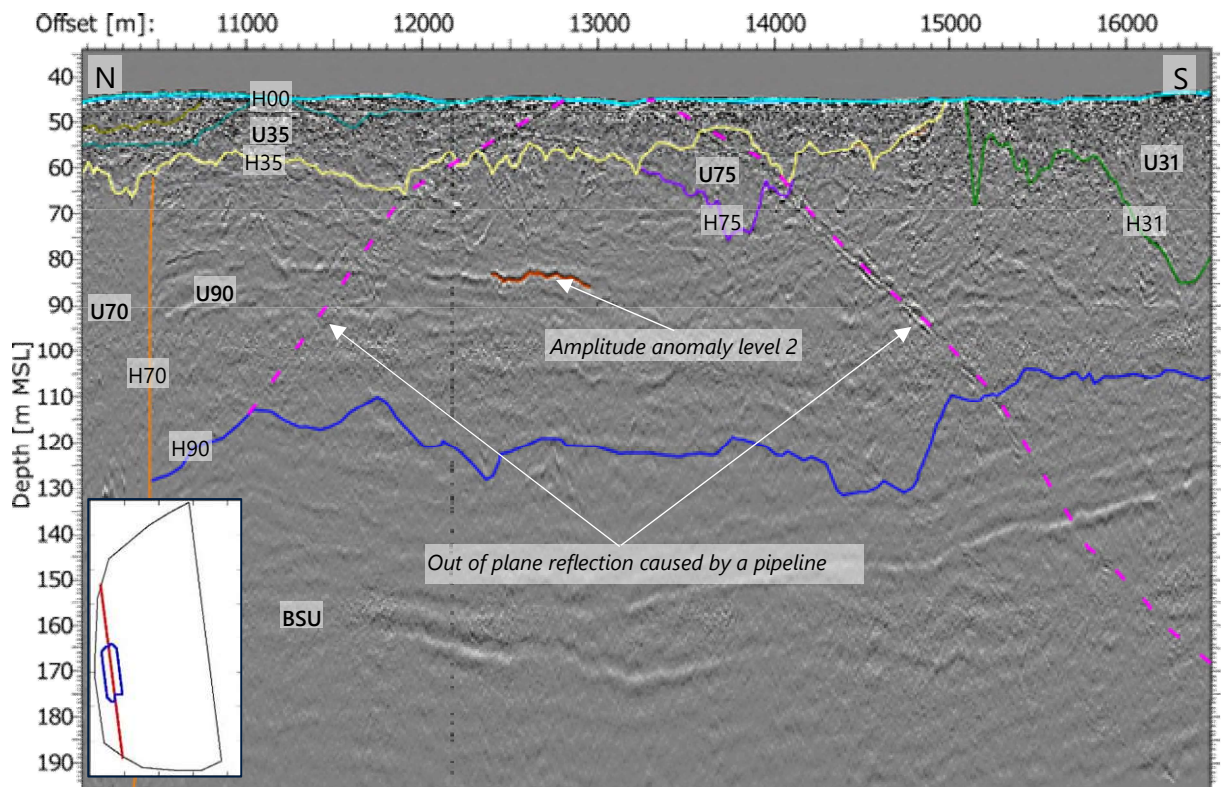
Figure 4.34: 2D-UUHR data example (line EAD2041P01.MIG) showing out-of-plane reflection of the Europipe II pipeline.
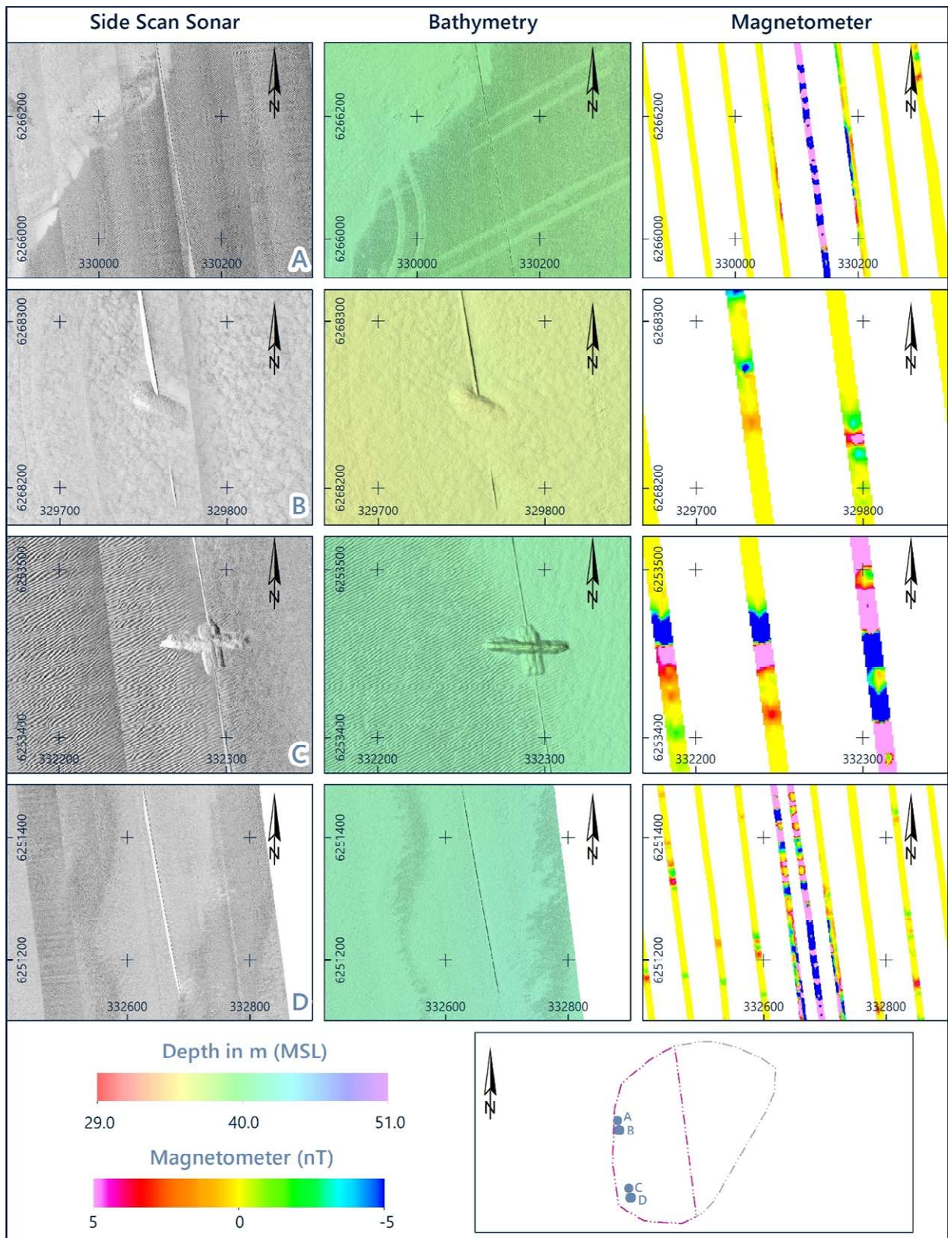
Figure 4.35: Example of exposed sections of the Europipe II pipeline and rock dumps at the crossings with the two cables.

4.2.5.2 Magnetometer Anomalies

For the purpose of target picking and data interpretation, a residual grid was created assuming a blanking distance of 5 m and cell size of 1 m. Clusters of relatively high-amplitude anomalies were observed across the entire site. Significantly fewer anomalies were

identified in the northern part of the site, where water depths are the shallowest and the Holocene deposits represented by Unit U10 are significantly thicker than in the rest of the site. Refer to Figure 4.36 for data examples of the magnetic residual grid in the site.
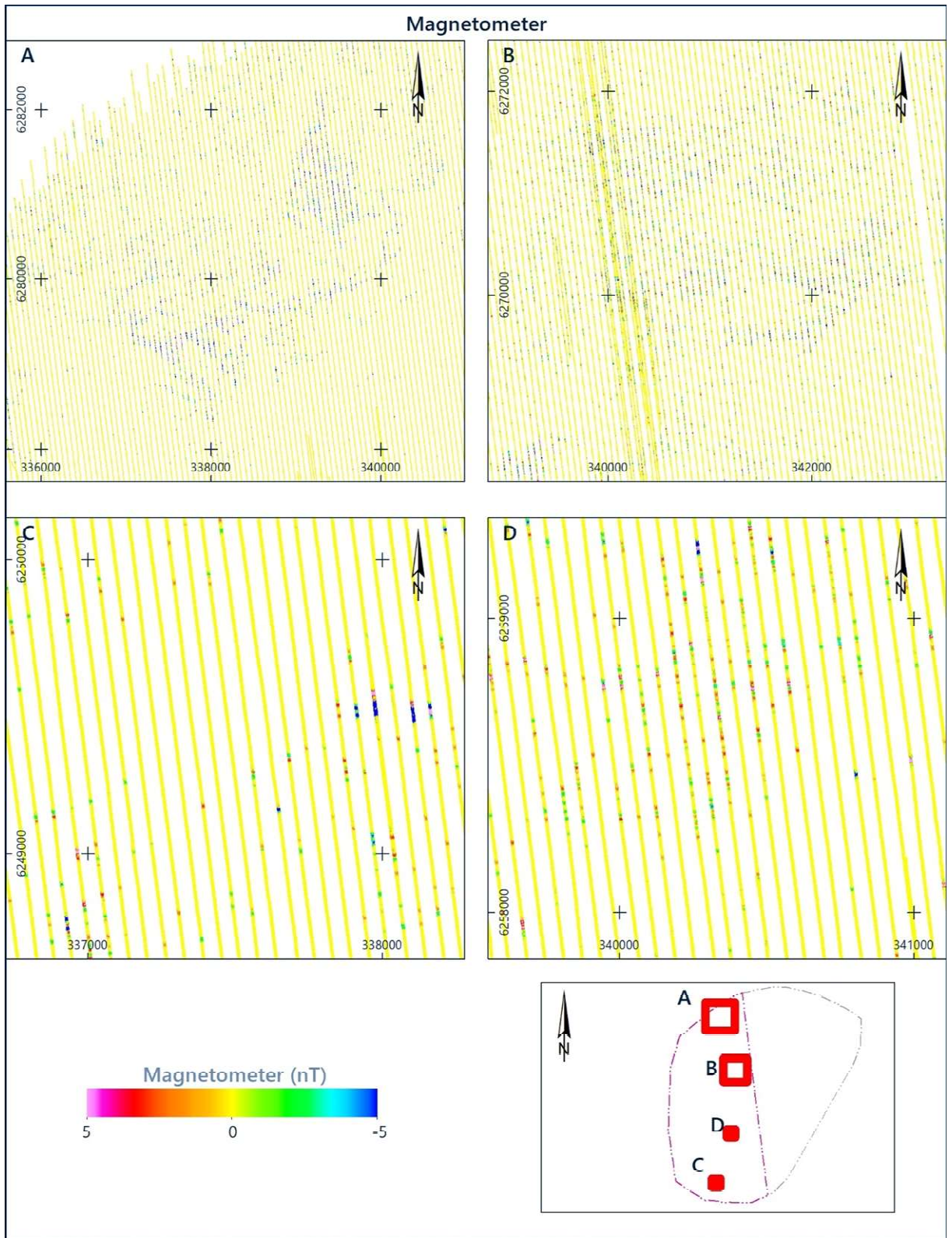
Figure 4.36: Examples of the magnetic residual grid in the OWF Zone West site.

A total of 3145 anomalies of peak to peak amplitudes ranging from 10.0 nT to 27040 nT were identified within the site. All the identified magnetic anomalies were manually measured on

the magnetic residual field profiles and classified as monopole (positive or negative), dipole or complex. Additionally, each anomaly was interpreted as non-discrete or discrete. Non-discrete anomalies are those observed very close to each other; defining the exact start and end of the anomaly is not possible (Figure 4.37).

Discrete anom alies are observed in separation from other anomalies, i.e., start and end of the anomaly is clearly defined (Figure 4.38). Both classifications were based on the single magnetometer data, which do not provide full information about the size and shape of the anomaly and should be treated as approximations.
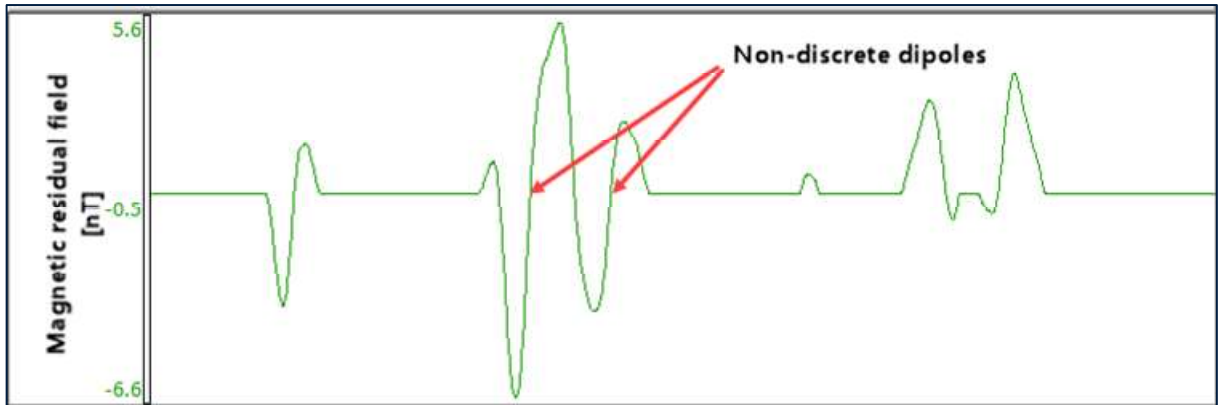
Figure 4.37: Example of two non-discrete magnetic anomalies.
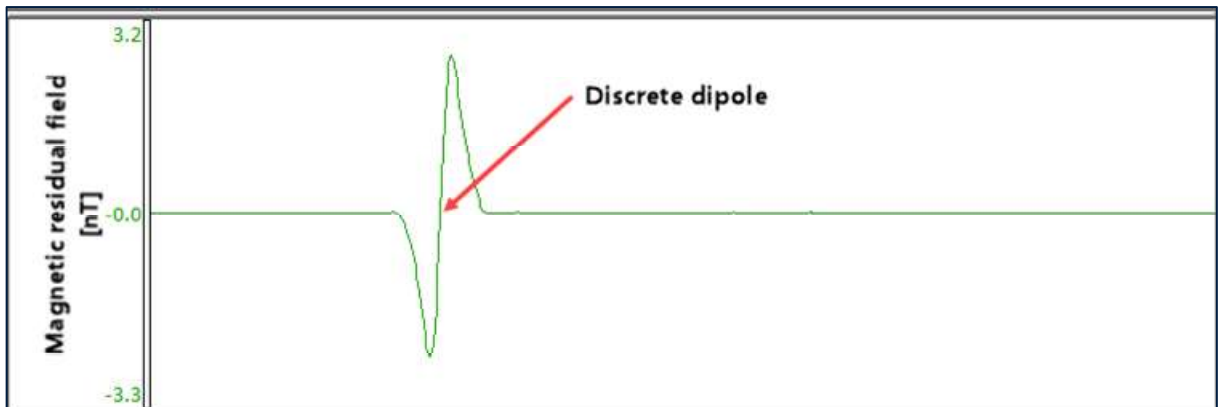
Figure 4.38: Example of a discrete magnetic anomaly.

Details of all the identified magnetometer targets are presented in the target list supplied in the GIS database as part of the final deliverables. An overview of the magnetometer targets is presented in charts provided in a separate PDF file (see Appendix B).

The magnetic residual grid shows evidence of anomalies caused by the geological conditions present across the site. Some of these anomalies can be related to buried structures. The channel-like features observed in magnetic residual field in the north of the site show certain level of correlation with the presence of horizons H10 and H20 identified on SBP and 2D-UUHR datasets. Towards the central and south-eastern part of the site some of the channels visible in magnetic data line up with horizons H20 and H31. However, due to the very complex subsurface geology present at the site no clear correlation between magnetic and seismic data was observed.

Pipelines and cables

One (1) pipeline and two (2) cables were identified within the site. The pipeline was observed to be intermittently exposed and visible in the SSS and MBES datasets. In section 4.2.5.1 Table 4.9 provides details of the pipeline found in the site. Refer to Figure 4.34 and Figure 4.35 for data examples of the pipeline.

The cables were identified as the cables Havfrue/AEC-2 and TAT14 Segment K. Both cables cross the site (OWF East and OWF West Zones) in a NW-SE direction. The cables were identified from the MAG sensor and could not be observed in the SSS and SBP data. Rock dumps were observed at the crossings of the cables and the Europipe II pipeline.

Table 4.10 summarises the cables found within the site. Figure 4.39 presents data examples of the cables.

Table 4.10: Cables found within the site.

Block	Name	Details
D to Y	Havfreu/AEC-2	Fibre-optic cable
D to Y	TAT14 Segment K	Fibre-optic cable
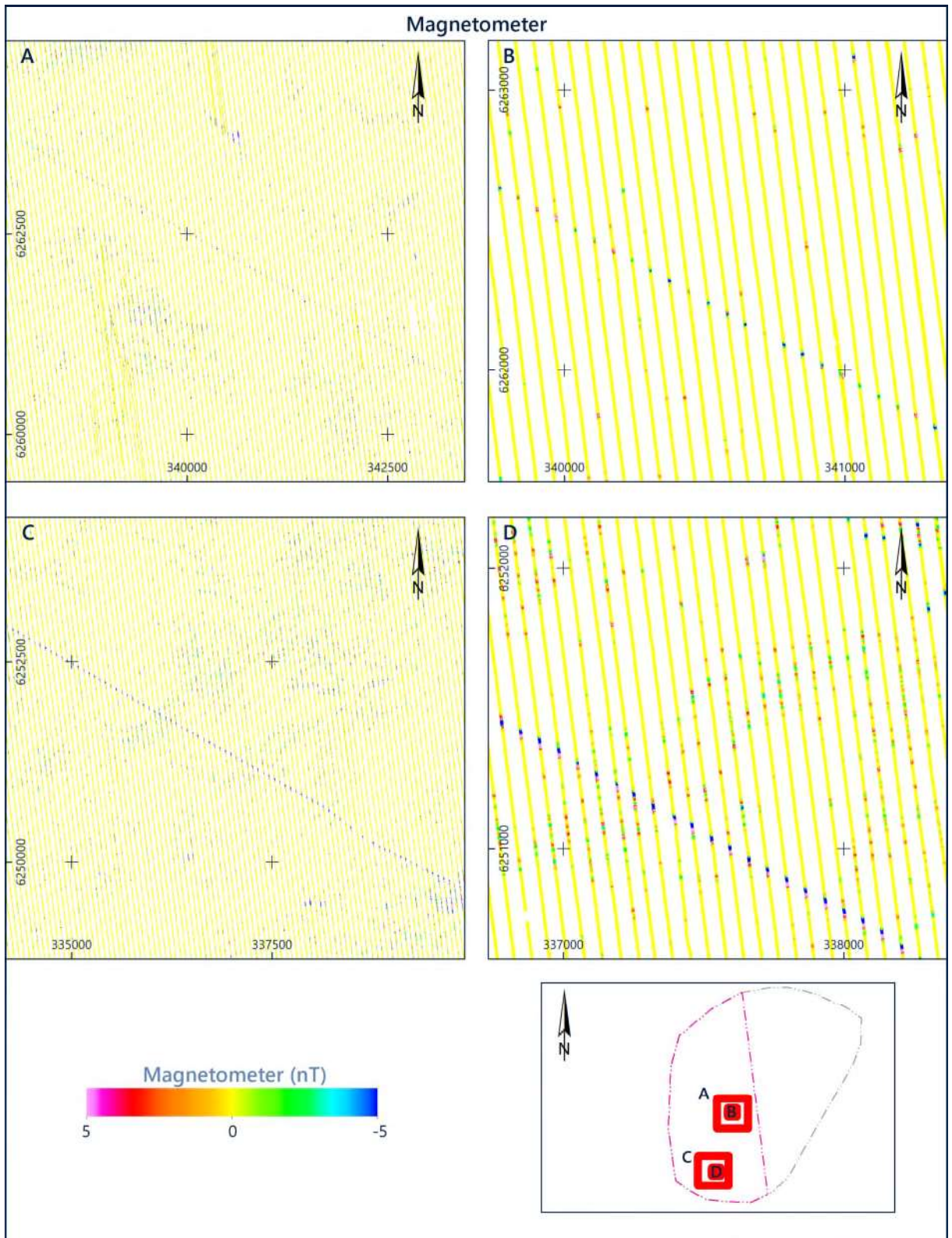
Figure 4.39: Examples of the Havfrue/AEC-2 and TAT14 Segment K cables observed on the magnetic residual grid in the site.

4.2.5.3   Target Cross-Correlation

Automatic and manual cross-correlations of all seafloor targets and MAG anomalies were performed based on the criteria presented in Table 4.11 with the following results. No SBP targets were identified within the site.

Table 4.11: Cross-correlation between targets identified on SSS, MBES and MAG datasets.

Correlated Sensors	Correlation Criteria	Total Correlated Targets
SSS and MBES	■ Manual cross-correlation ■ SSS targets observed on the MBES 0.25 m grid were moved to MBES position ■ No cross-correlation radius was used	15222
SSS and MAG	■ Automatic spatial cross-correlation followed by manual cross-correlation where relevant ■ One to one method: the nearest targets within a 2 m radius were correlated	33

In addition to the automatic spatial cross-correlation between SSS and MAG targets, both datasets were reviewed and in several cases the targets falling outside the correlation radius of 2 m were cross-correlated manually. Manual cross-correlation was carried out for targets identified as wrecks. For pipeline targets no fixed radius was assumed and the cross-correlation was based on individual interpretation of the available datasets.

The seafloor targets correlating with magnetic anomalies included boulders, debris/suspected debris, pipeline, and wrecks. Observed targets were interpreted and classified based on the SSS and MBES datasets.

Refer to Figure 4.40 and Figure 4.29 for data examples of the cross-correlated targets between SSS and MAG datasets, presenting a boulder and suspected debris, respectively. Refer to Figure 4.32 and Figure 4.33 for data examples of the cross-correlation of wrecks.
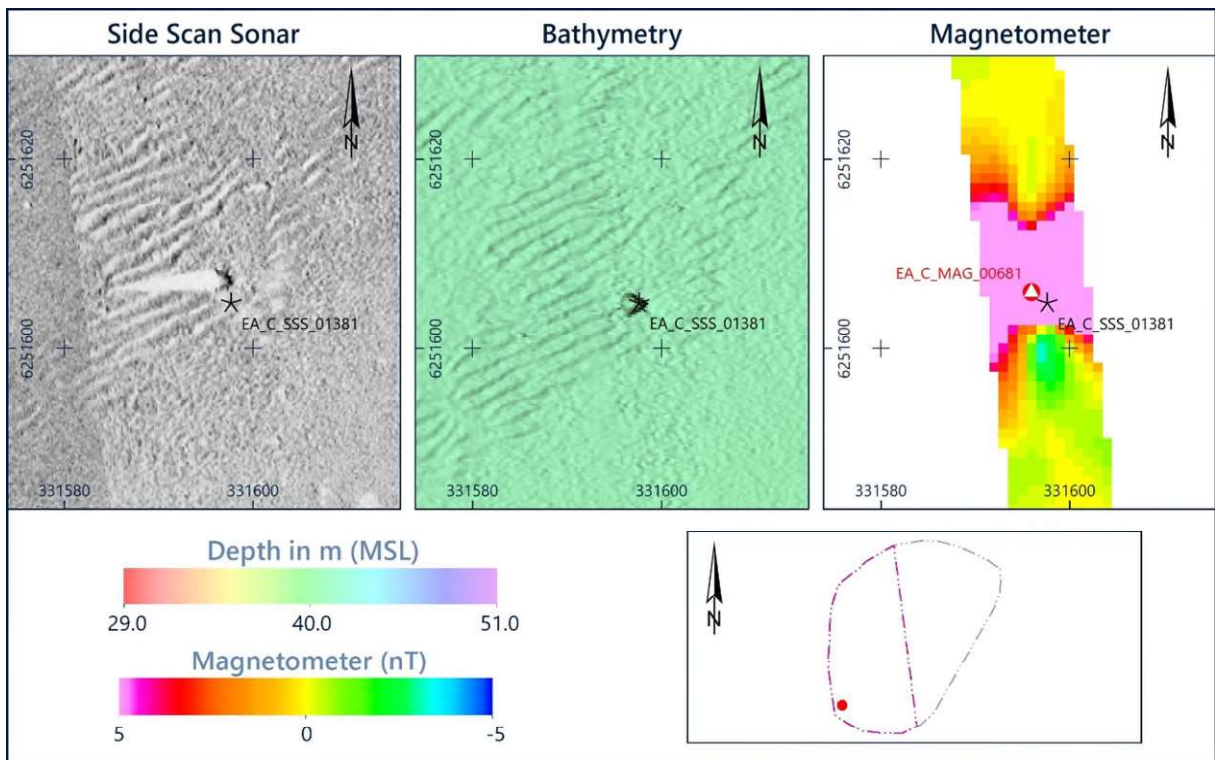
Figure 4.40: Example of the automatic target cross-correlation between the SSS targets and magnetic anomalies observed for a boulder on the site.

4.2.6   Seafloor Man-Made Objects

Several targets observed in the SSS, MAG, MBES and SBP datasets and included in respective target lists were further classified as potential man-made objects (MMOs). Each target interpreted as potential MMO was assigned a type as specified in a document provided by Energinet (Template Survey Geodatabase (TSG): Requirements to TSG).

Identified MMOs include:

- Point features classified as suspected debris (82), wreck (2) and other (4) – subset of the SSS target list;
- Linear features (64) including the pipeline and all targets of elongated shape and potentially anthropogenic origin which length exceeds 5 m identified on SSS and MBES datasets, and two (2) buried cables identified on MAG dataset – subsets of the SSS and MAG target lists;
- Two (2) rock dumps identified along the Europipe II pipeline on SSS and MBES datasets during the morphological classification.

Selected items of the observed MMOs are presented in Table 4.12 with corresponding data examples shown in Figure 4.41, Figure 4.42 and Figure 4.43. Data examples of the pipeline, cables and rock dumps are presented in section 4.2.5.

Detailed information on all the MMOs identified within the site is supplied in the GIS database as part of the final deliverables.

Table 4.12: Examples of man-made objects observed in the site.

SSS ID	Measurements* L x W x H [m]	MAG ID	Peak to Peak Amplitude* [nT]	Classification (MMO Type)
EA_M_SSS_00587	23.3 x 0.5 x 0.2	n/a	n/a	Linear debris (suspected debris)
EA_M_SSS_00386	9.3 x 5.9 x 0.4	n/a	n/a	Linear debris (suspected debris)
EA_N_SSS_00430	8.8 x 5.2 x 1.4	n/a	n/a	Cluster of debris (suspected debris)
EA_R_SSS_00754	24.5 x 1.5 x 1.0	n/a	n/a	Fishing gear (suspected debris)
Notes: *Measurements are rounded to one decimal point				
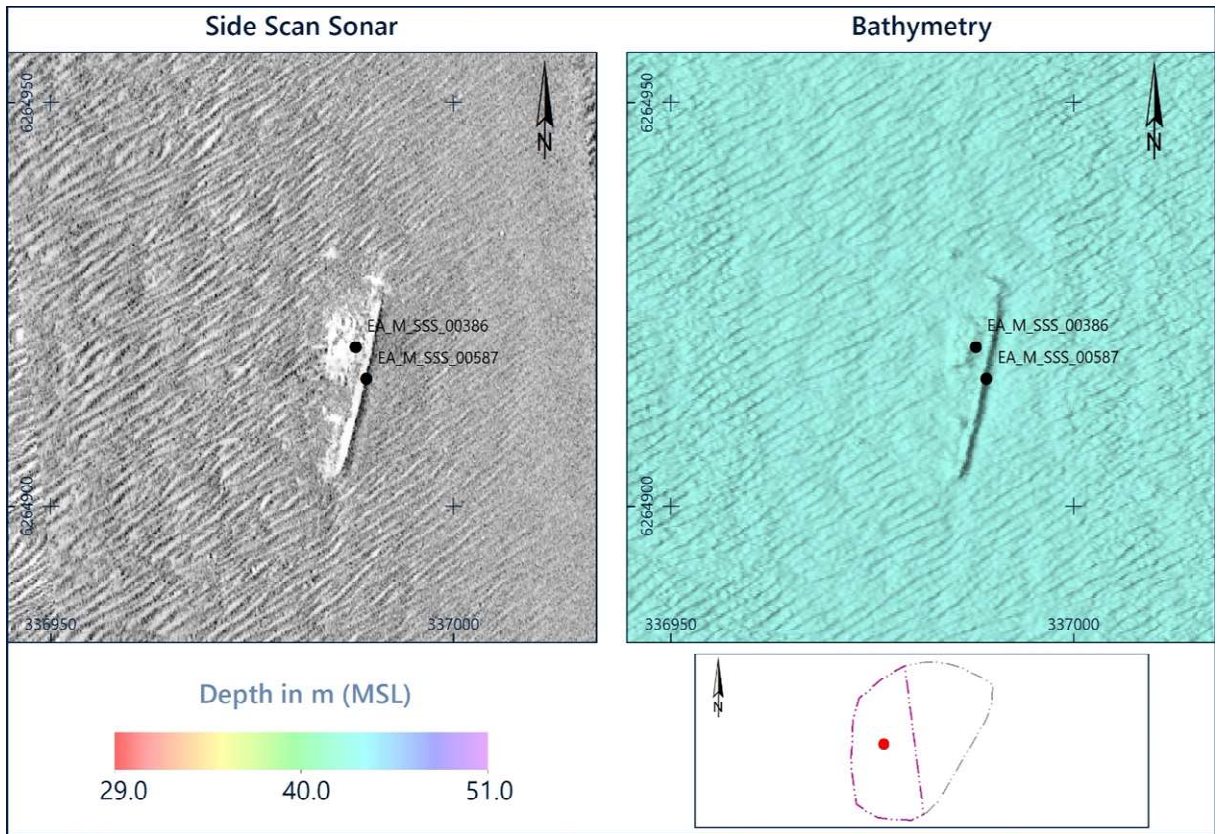
Figure 4.41: Example of potential MMO identified as a linear debris (EA_M_SSS_00368 and EA_M_SSS_00587).
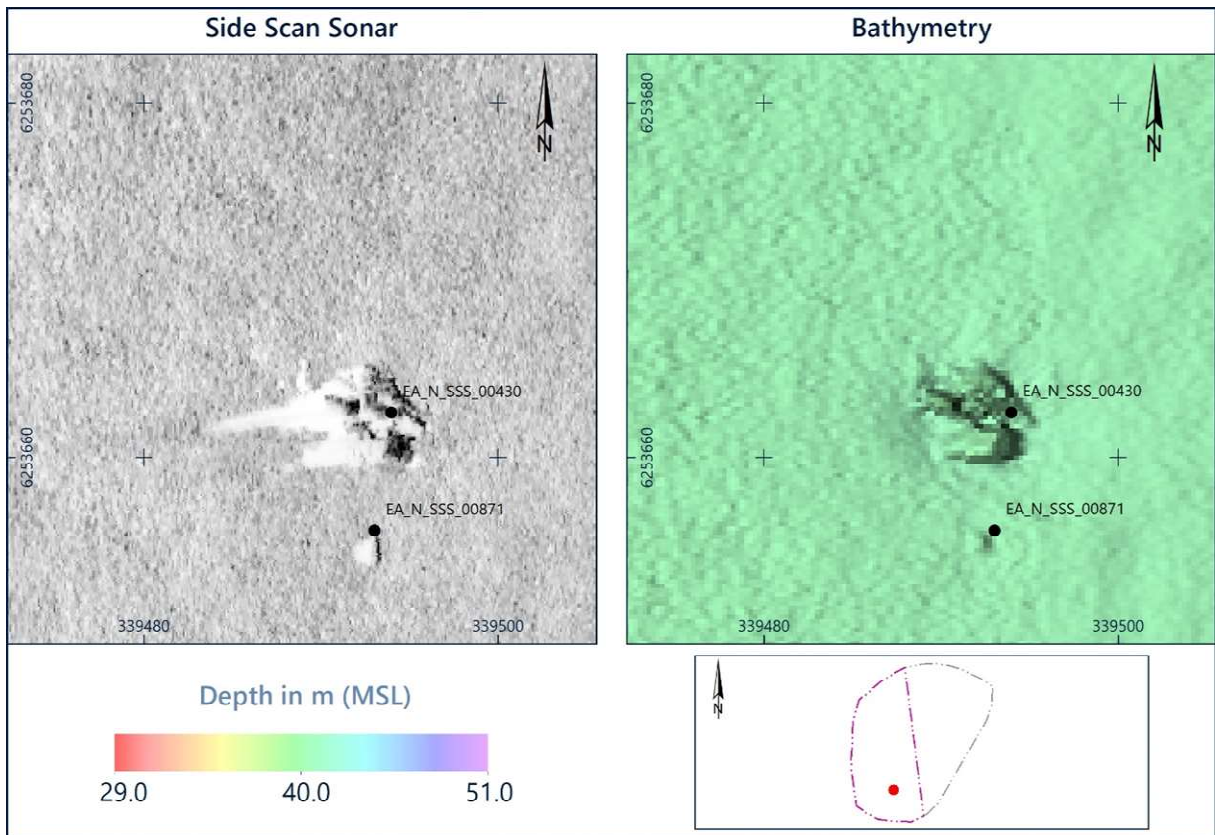
Figure 4.42: Example of potential MMO identified as a cluster of debris (EA_N_SSS_00430).
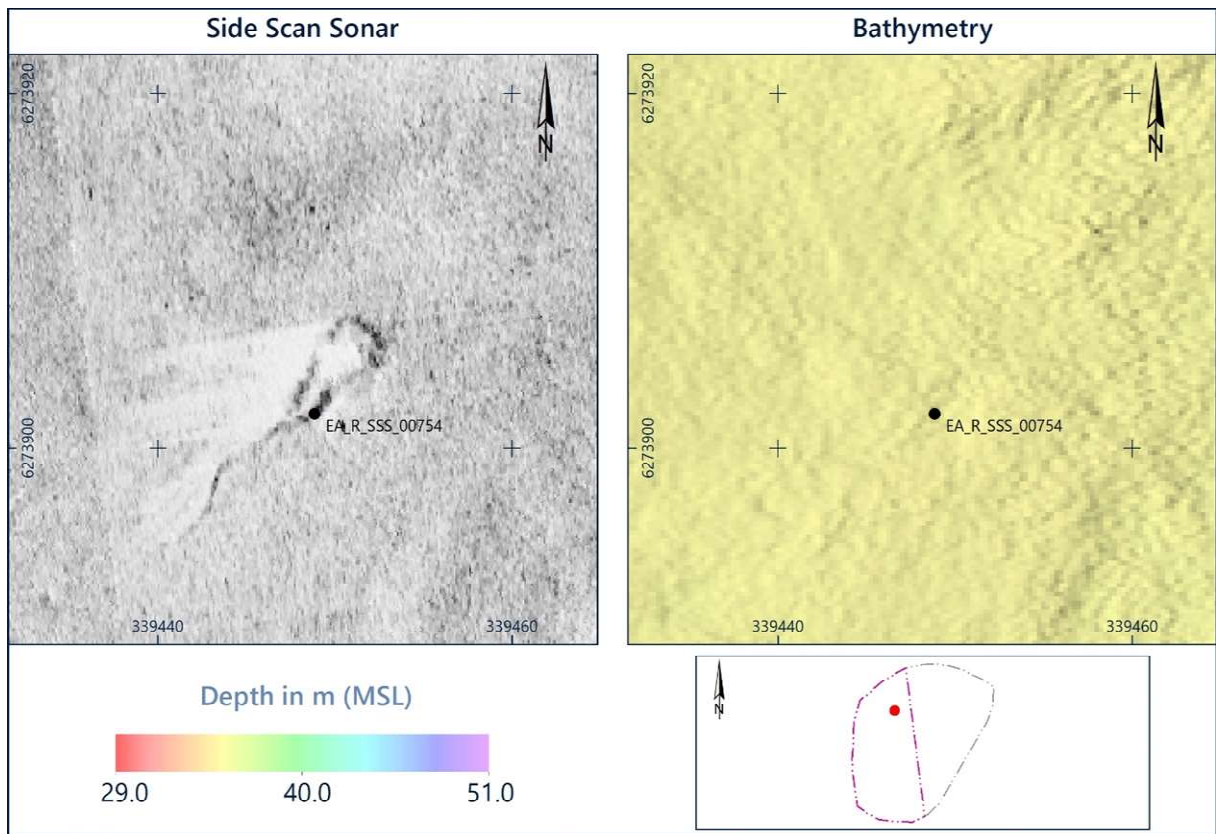
Figure 4.43: Example of potential MMO identified as suspected debris (EA_R_SSS_00754).

4.3 Sub-Seafloor Geology

4.3.1 Seismostratigraphic Units

4.3.1.1 Overview

Twelve horizons have been interpreted, which delineate ten seismostratigraphic units. Three horizons are internal horizons within a seismostratigraphic unit. The numbering of horizons and picking strategy have been aligned with the seismic interpretation of OWF Zone East (MMT, 2021).

Table 4.13 and Figure 4.44 provide an overview of the interpreted horizons and seismostratigraphic units and should be read in conjunction with the geological charts and geological profiles provided in a separate PDF file (see Appendix B).

The stratigraphic framework (depositional environment and age) is based on the character of the seismic facies and available literature for the Danish Sector of the North Sea (e.g., Larsen and Andersen, 2005; GEUS and Orbicon, 2010; Ramboll, 2021). Colour-coding of the interpreted horizons are generally based on Ramboll (2021), where applicable (Figure 4.3).

Table 4.13: Overview of the interpreted horizons and seismostratigraphic units.

Data	Unit	Horizon [Colour]		Seismic Character	Expected Lithology	Depositional Environment	Age
		Base	Internal				
SBP / 2D-UUHR	U10	H10 [light blue]	H05 [yellow] H06 [beige]	Horizontal base; acoustically transparent with point reflectors; between horizons H05 and H06 with clinoforms dipping north; below horizon H06 acoustically transparent to complex, with discontinuous and chaotic reflectors and local stratification	SAND with shells and shell fragments	Marine and coastal	Holocene
	U20	H20 [light green]	-	Channelised to planar base; various internal character: stratified with low to high amplitude reflectors parallel to the base, acoustically transparent or chaotic.	SAND and/or CLAY	Fluvial, estuarine and coastal	Late Weichselian to early Holocene
	D24	H24 [olive]	-	Horizontal and locally channelised base; shows evidence of deformation, originally stratified; folded reflectors, dipping thrust-faults, chaotic and transparent	CLAY with laminae to beds of silt and sand	(Glacio-) Marine deformed in push-moraine	Eemian to Weichselian
	U30	H30 [turquoise]	-	Horizontal base; internally stratified with parallel, closely spaced, medium to high amplitude reflectors; locally the top of the unit contains small-scale channels with seismically transparent infill.	CLAY with laminae to beds of silt and sand	Glacio-) Marine	Eemian to Weichselian
	U31	H31 [dark green]	-	Channelised base; internally acoustically chaotic, very locally stratified, with low to high amplitude reflectors parallel to the base of the channel	SAND and/or CLAY	Fluvial to estuarine	Middle to Late Pleistocene
2D-UUHR	U35	H35 [light yellow]	-	Horizontal to undulating base; internally complex from locally stratified, transparent to chaotic, with discontinuities high amplitude reflectors with sharp to transitional terminations	Silty SAND, locally gravelly	Fluvial	Middle to Late Pleistocene
	U70	H70 [orange]	H69 [red]	Channelised base (deep valleys); the lower part of the valley-fill is acoustically chaotic to transparent, towards the top the valley-fill is transparent to stratified, with reflectors parallel to the base, often wavy	SAND, CLAY and/or TILL	Glacial valley fill	Elsterian and/or Saalian
	U75	H75 [purple]	-	Horizontal base; internally complex, includes acoustically transparent intervals, stratified intervals, with inclined reflectors	SAND, with laminae of clay, locally gravelly	Fluvial	Middle to Late Pleistocene
	U90	H90 [dark blue]	-	Horizontal to undulating base; internally complex, with acoustically transparent intervals, chaotic, locally stratified intervals, with parallel horizontal to inclined reflectors	SAND with laminae to beds of clay or peat/organic clay, locally gravelly	Fluvial	Early to Middle Pleistocene
	BSU		-	Stratified with low to high amplitude reflectors, locally chaotic in the top	CLAY and SAND	Pro-delta to delta-front	Miocene
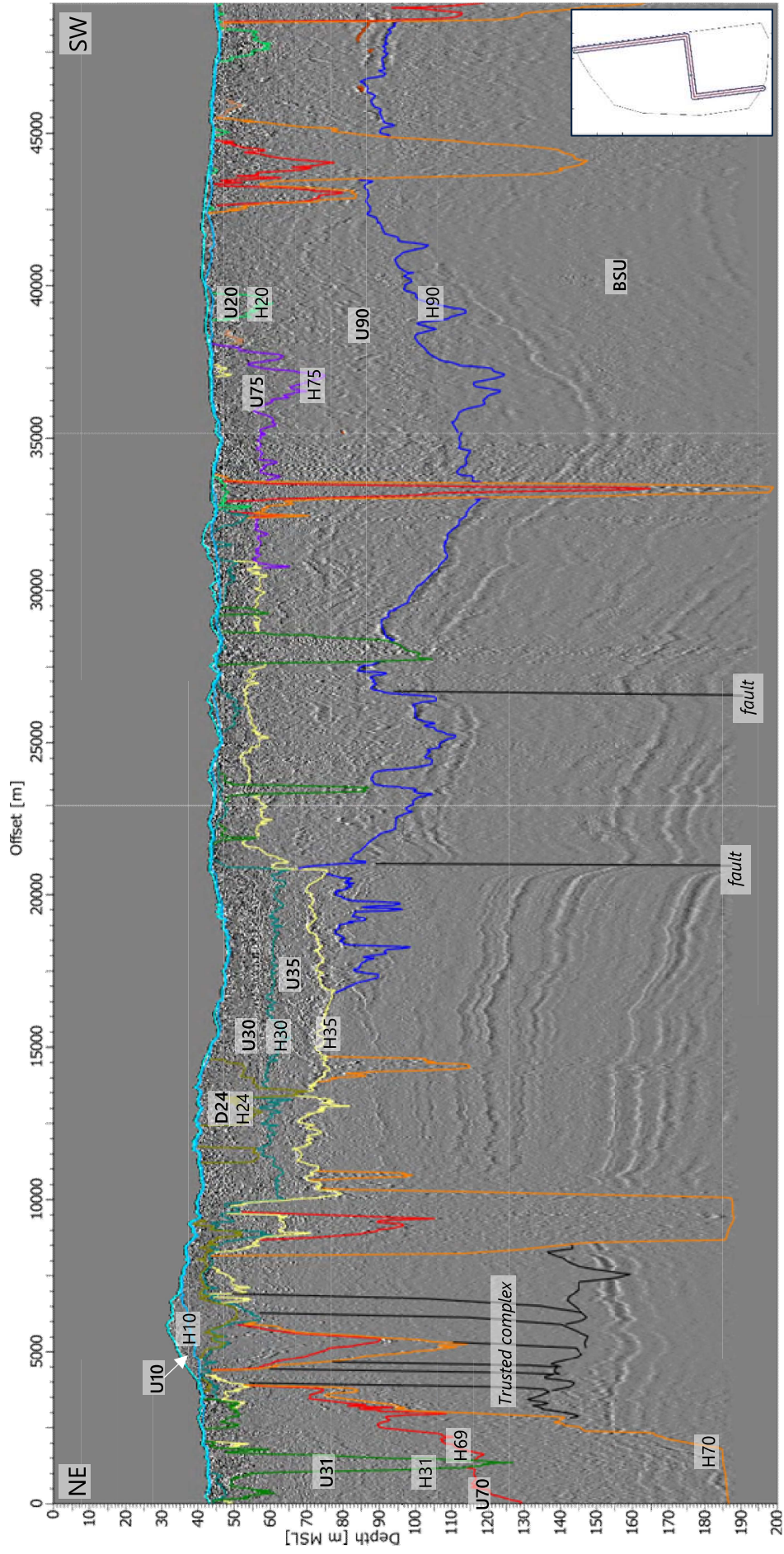
Figure 4.44: Overview of the horizons and seismostratigraphic units interpreted in the 2D-UUHR seismic data.

The BSU is the deepest interpreted unit within the depth of penetration of the 2D-UUHR data and is present throughout the site except where it is cut by valleys of Unit U70.

Internally, the BSU is stratified. The parallel reflectors are dipping gently towards the west. Towards the top of the unit, the stratification becomes less defined (Figure 4.45).

The boundary between the BSU and the overlaying Unit U90 is not marked by a clear reflector and often coincides with the first seafloor multiple. The boundary is depicted by the change of the seismic character between the two units. In the north-east of the site, where the BSU is overlain by Unit U35, the top of the BSU is a well-defined positive reflector (horizon H35). In the north of the site, the BSU is deformed what is indicated by thrust faults dipping towards the north (more information in section 4.4.2). In the rest of the site, normal faults and an inverted normal fault are present in this unit (more information in section 4.4.4).

In previous studies, this unit was considered as the bedrock of Miocene age (Ramboll., 2021). It is interpreted that the BSU are coarsening upward pro-delta clay to delta-front sand deposits of Miocene age of the Eridanos River delta (Figure 4.1). The westward dip of the strata may be a structural dip or clinoforms of the delta (Overeem et al., 2001; Gibbard and Lewin, 2016).

Figure 4.45: Line EAX2277P01.MIG. 2D-UUHR data example of Units U90 and BSU.

4.3.1.3   Unit U90

Unit U90 has a sheet-like geometry and always overlies the BSU (Figure 4.45). The unit is present throughout most of the site, except in the north and where it is cut out by valleys of Unit U70. It has a thickness of up to 87 m (Figure 4.46). The base of Unit U90 is marked by horizon H90, which has a flat to irregular geometry.

Internally, Unit U90 has a complex seismic character, including transparent, chaotic intervals and local stratification, with horizontal to inclined parallel reflectors. Locally, internal erosion surfaces are present (Figure 4.47). Locally, amplitude anomalies with a reverse polarity are present (more information in section 4.4.1), which may represent beds of peat and/or organic clay. The internal erosion surfaces and inclined stratification may represent fluvial channel and bar deposits.

It is interpreted that Unit U90 forms Early to Middle Pleistocene fluvial delta-top deposits of the Cenozoic delta system of the Eridanos River (Figure 4.1; Overeem et al., 2001; Gibbard and Lewin, 2016; COWI, 2021).

Figure 4.46: Left: Depth to horizon H90 (base of Unit U90). Right: Thickness of Unit U90.
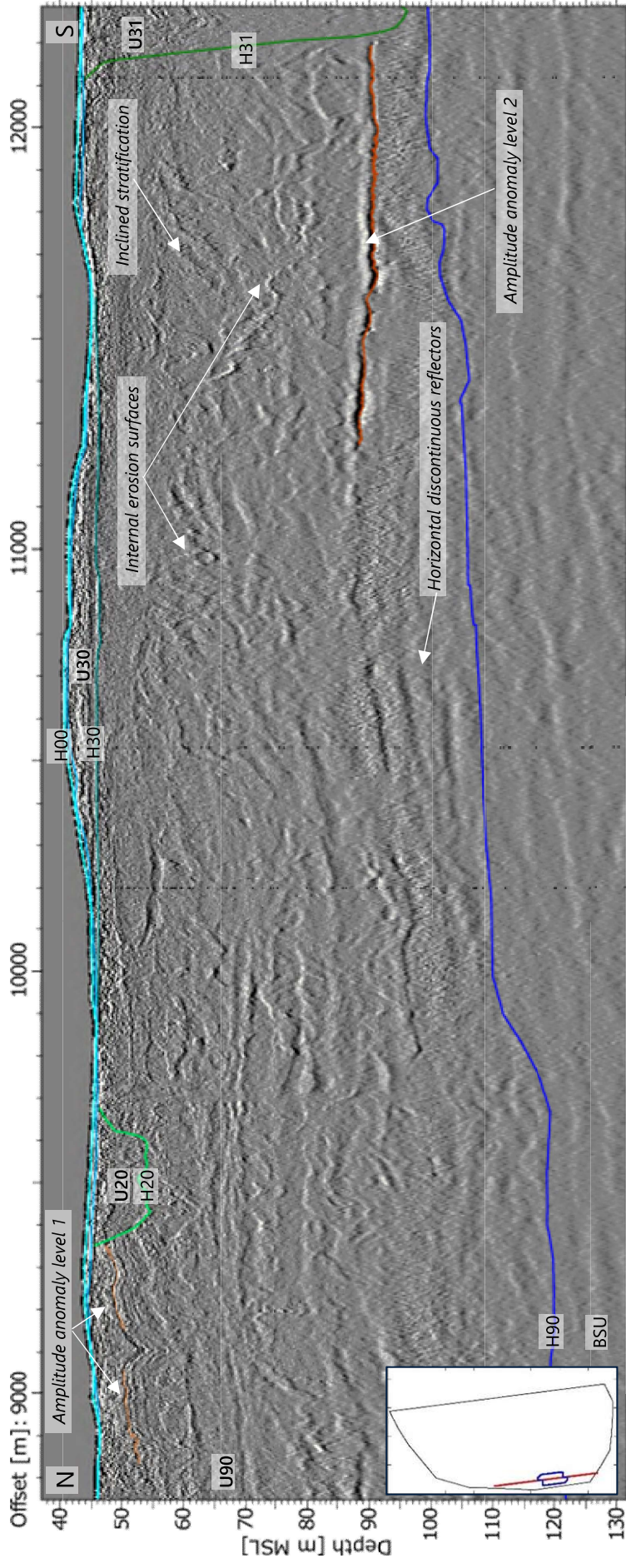
Figure 4.47: Line EAC6025P01.MIG. 2D-UUHR data example of Unit U90.

4.3.1.4 Unit U75

Unit U75 has a sheet-like geometry and always overlies Unit U90. The unit is only locally present in the west-central part of the site and at the same stratigraphical level as Unit U35. The unit has a thickness of up to 31 m (Figure 4.48). The base of Unit U75 is marked by horizon H75, which has an irregular to locally channelised geometry.

Internally, Unit U75 has a complex seismic character. The internal seismic character includes acoustically transparent intervals, stratified intervals, inclined stratified intervals, and internal erosion surfaces (Figure 4.49). The seismic character is similar to the underlying Unit U90 and the overlaying Unit U35. The basal horizon H75 is a clearly distinguishable medium-amplitude, positive reflector. Horizon H75 and Unit U75 are interpreted separate from horizon H35 and Unit U35. This is because horizon H35 is an unconformity, which is always younger than the valleys of Unit U70. In contrast, horizon H75 is truncated by the valleys of Unit U70 (Figure 4.49).

It is interpreted that the internal erosion surfaces and inclined stratification may be fluvial channel and bar deposits.

Figure 4.48: Left: Depth to horizon H75 (base of Unit U75). Right: Thickness of Unit U75.
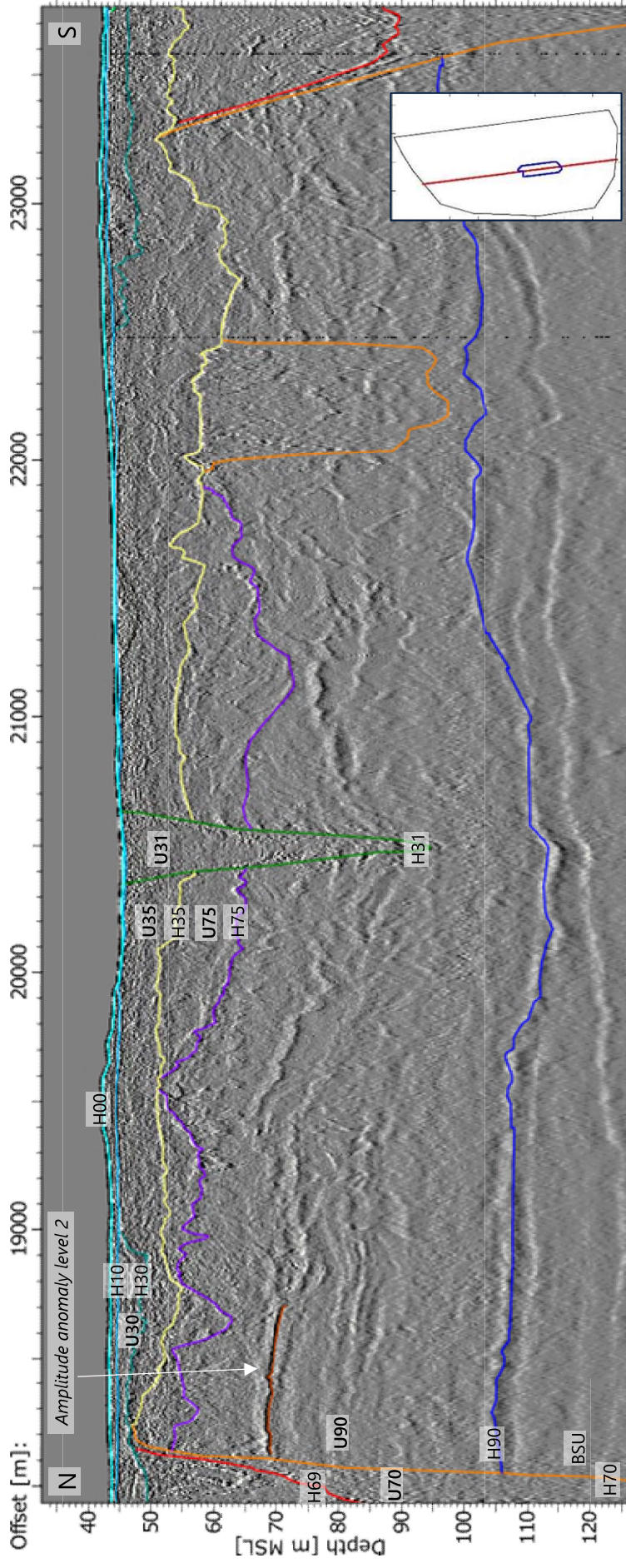
Figure 4.49: Line EAK2129P01.MIG. 2D-UUHR data example of Unit U75.

Unit U70 forms the infill of deep valleys with a north-east to south-west orientation (Figure 4.51). The base of these valleys is marked by horizon H70, which often lies deeper than the maximum penetration of the 2D-UUHR seismic data (i.e., approximately 200 m below MSL).

Two seismic facies are observed in Unit U70. The lower part of the valley-fill is often acoustically chaotic to transparent, whereas towards the top the valley-fill is stratified (Figure 4.52). At the base of the stratified interval a clear reflector is often observed, which is interpreted as horizon H69 (Figure 4.50, Figure 4.52). Internal horizon H69 is not always present in Unit U70.

Unit U70 is interpreted to be the syn- to post-glacial infill of glacial valleys, which were eroded during the Elsterian and/or Saalian glaciations (Figure 4.2; Huuse and Lykke-Andersen, 2000; COWI, 2021; Kirkham et al., 2021).
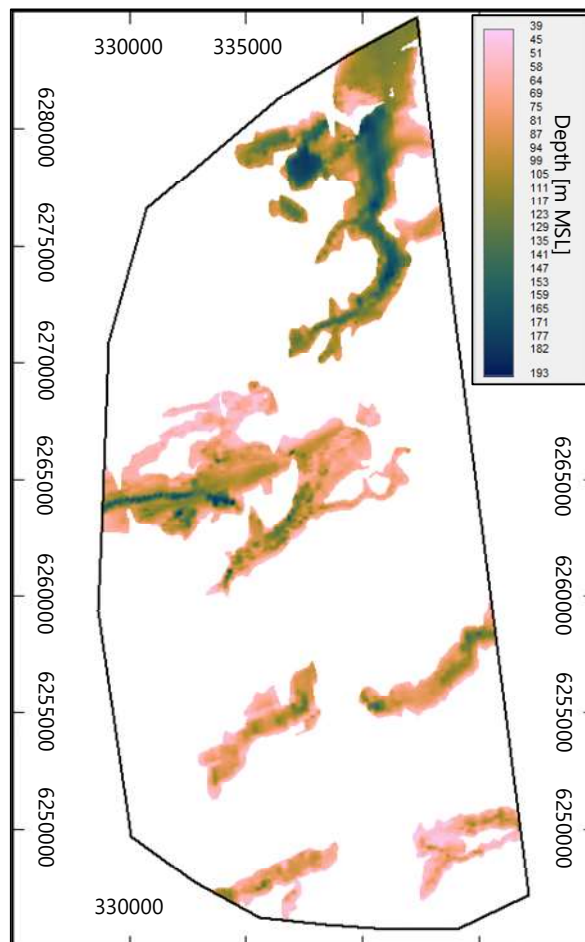
Figure 4.50: Depth to horizon H69 (internal horizon in Unit U70).

Figure 4.51: Left: Depth to horizon H70 (base of Unit U70). Right: Thickness of Unit U70.
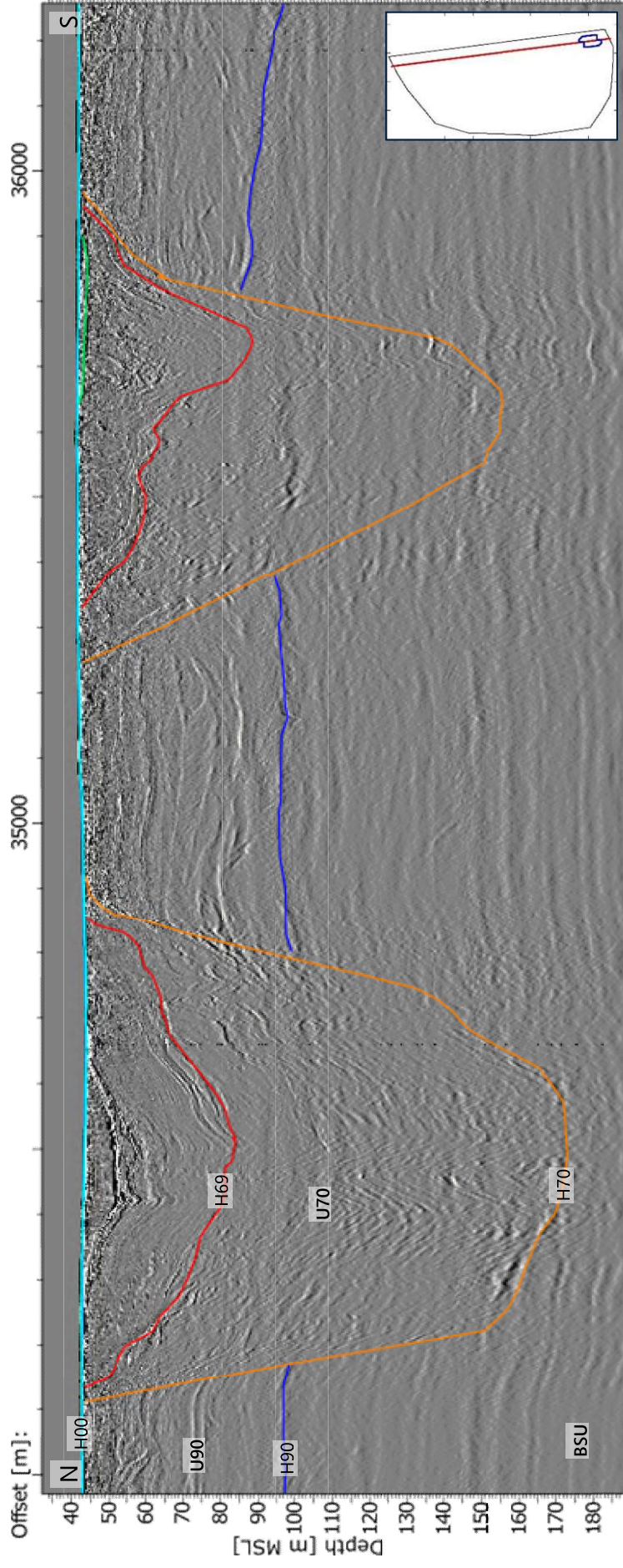
Figure 4.52: Line EAU6241P01.MIG. 2D-UUHR data example of Unit U70 with internal horizon H69.

4.3.1.6   Unit U35

Unit U35 has a sheet-like geometry with flat to undulating base and locally steep erosional margins. The basal horizon H35 forms an angular unconformity with the underlaying units, most notably Unit U70. The thickness of this unit reaches up to 58 m (Figure 4.53).

The unit forms an infill of two broad valleys/depressions with an east-west orientation. These valleys have well-defined steep margins. The steep margins are sometimes associated with a deeper incision of horizon H35 compared to the centre of the depression. The distribution of Unit U35 correlates with the distribution of Unit U30 and deformed Unit U24.

Internally, Unit U35 has a complex acoustic character from locally stratified, to acoustically transparent to chaotic. The chaotic intervals comprise of discontinuous, high amplitude reflectors with sharp to transitional terminations. Complexities include also internal erosion surfaces and inclined reflectors (Figure 4.54).

It is possible that the stepped character of the flanks of Unit U35 are river terraces. The valley-margins associated with the increased depth of the base of this unit suggests that the valleys were eroded by a meandering channel. River terraces may form during relative sea-level drops such as at the beginning of an ice-age or during isostatic rebound after a glaciation.

It is interpreted that the internal erosion surfaces are formed by fluvial channels and that the inclined stratification are fluvial bar deposits. The areas with inclined stratification are relatively local. Therefore, these are interpreted to be bars deposited in a braided river. The horizontal stratification is interpreted to be overbank deposits.

Unit U35 is younger than Unit U70, which is interpreted to be Elsterian and/or Saalian in age and older than Unit U30, which is interpreted to be Eemian to Weichselian in age. Based on the stratigraphic position, this unit could be between late Elsterian and early Weichselian in age.

The scale of the valleys (approximately 10 km wide) resembles the river terraces of the Lower Rhine Valley (Erkens et al., 2011). Therefore, the valleys may be palaeo-valleys of the Eridanos River, which was similar in scale to the Rhine.

The fluvial deposits of Unit U35 may correspond to the remnants of the Saalian palaeo-landscape ('Bakkeøer'), which is recognized in the nearshore areas and onshore Jutland (Larsen and Andersen, 2005; GEUS and Orbicon, 2010; Ramboll, 2021).
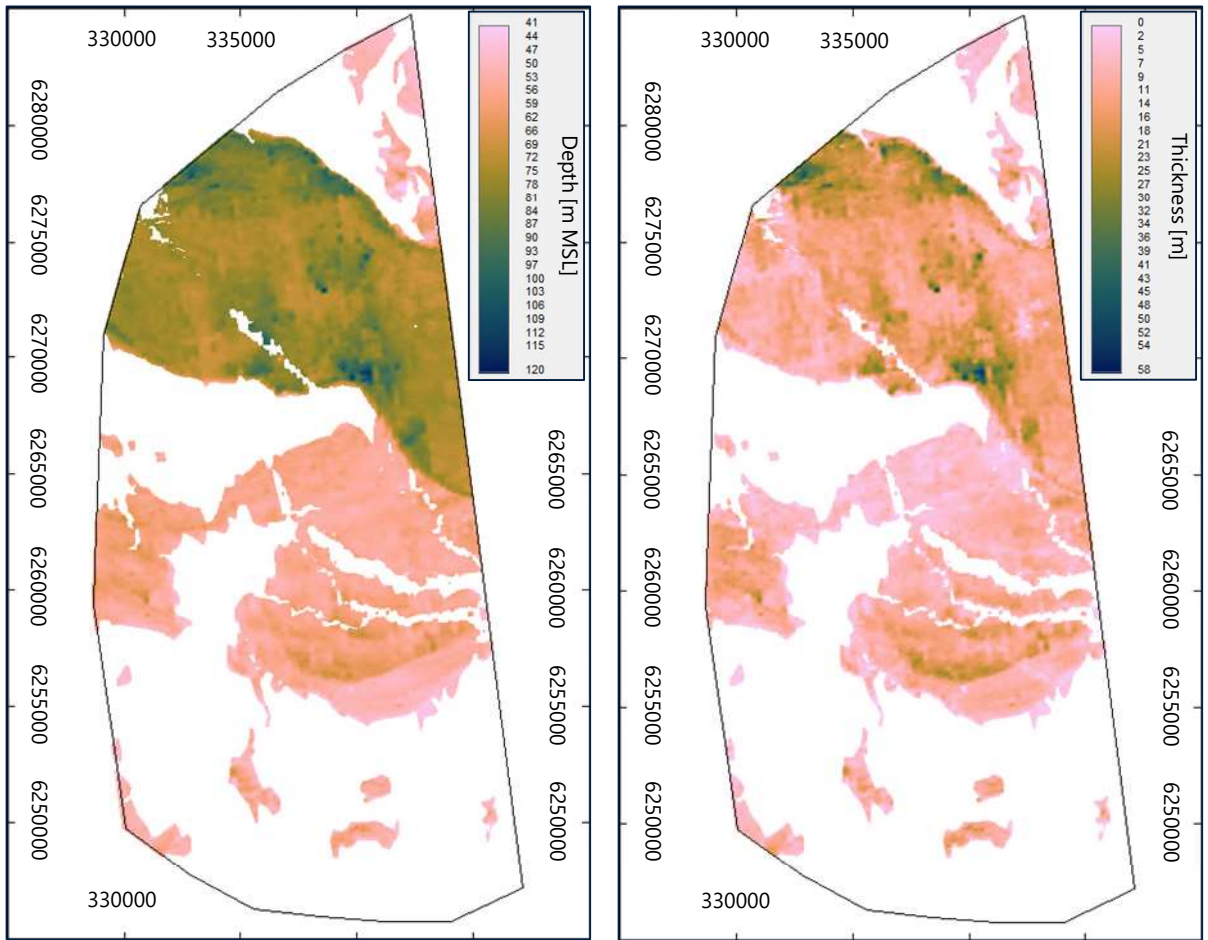
Figure 4.53: Left: Depth to horizon H35 (base of Unit U35). Right: Thickness of Unit U35.
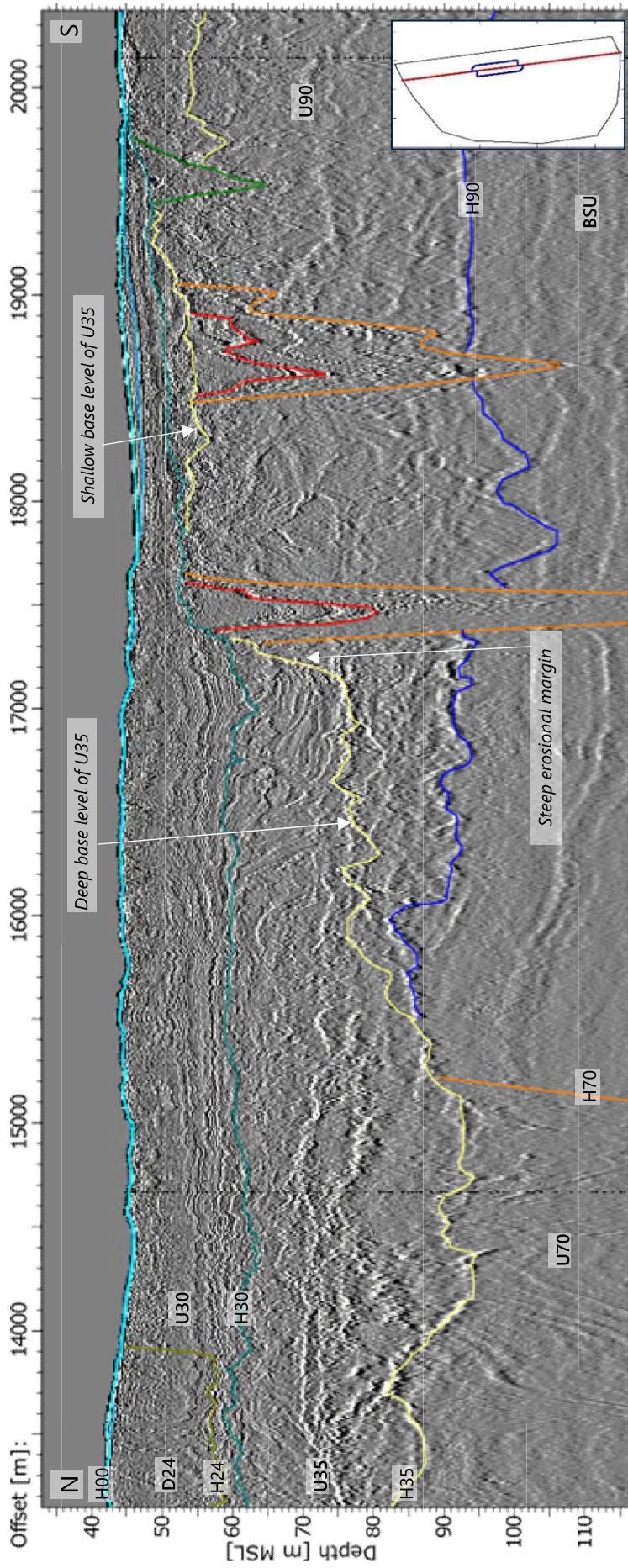
Figure 4.54: Line EAT2221P02.MIG. 2D-UUHR data example of Unit U35.

4.3.1.7 Unit U31

Unit U31 forms the infill of deep channels, up to 119 m deep (Figure 4.55). The base of Unit U31 is marked by horizon H31, which often cuts into Units U35 and U90 The top of Unit U31 is often truncated by horizon H30.

In planar view, this unit shows wide meandering channel system with tributary channels. Internally, this unit is acoustically chaotic (Figure 4.56) or locally stratified with low to high amplitude reflectors, parallel to the base of the channel. The seismic character is similar to the deep channel of Unit U20 and the deep valleys of Unit U70. However, the stratigraphical position of Unit U31 indicates an older age than Unit U30 and a younger age than Unit U35.

The unit is interpreted as late- to post-glacial fluvial and estuarine deposits. From the stratigraphic position this could be from the Elsterian to Holsteinian or Saalian to Eemian deglaciation.
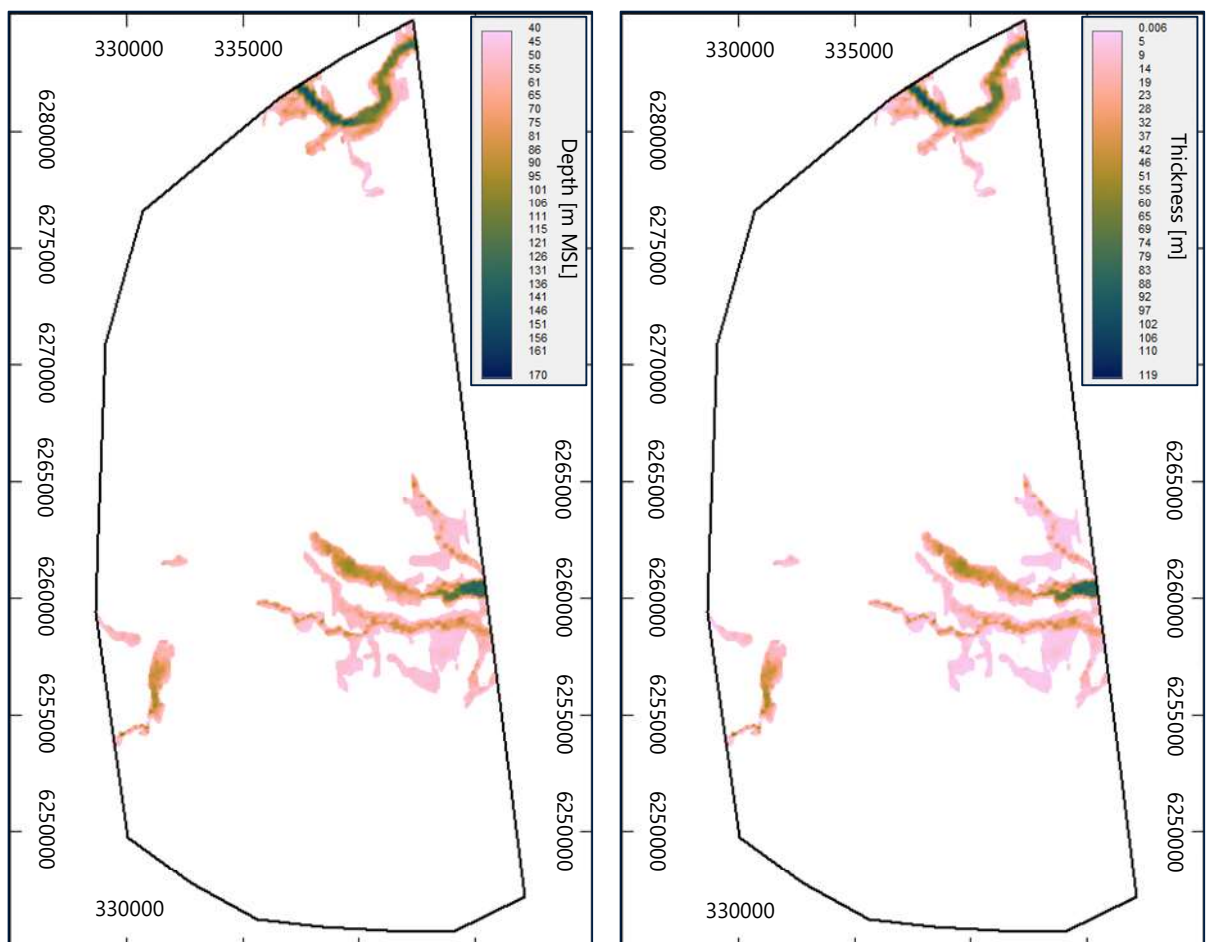
Figure 4.55: Left: Depth to horizon H31 (base of Unit U31). Right: Thickness of Unit U31.
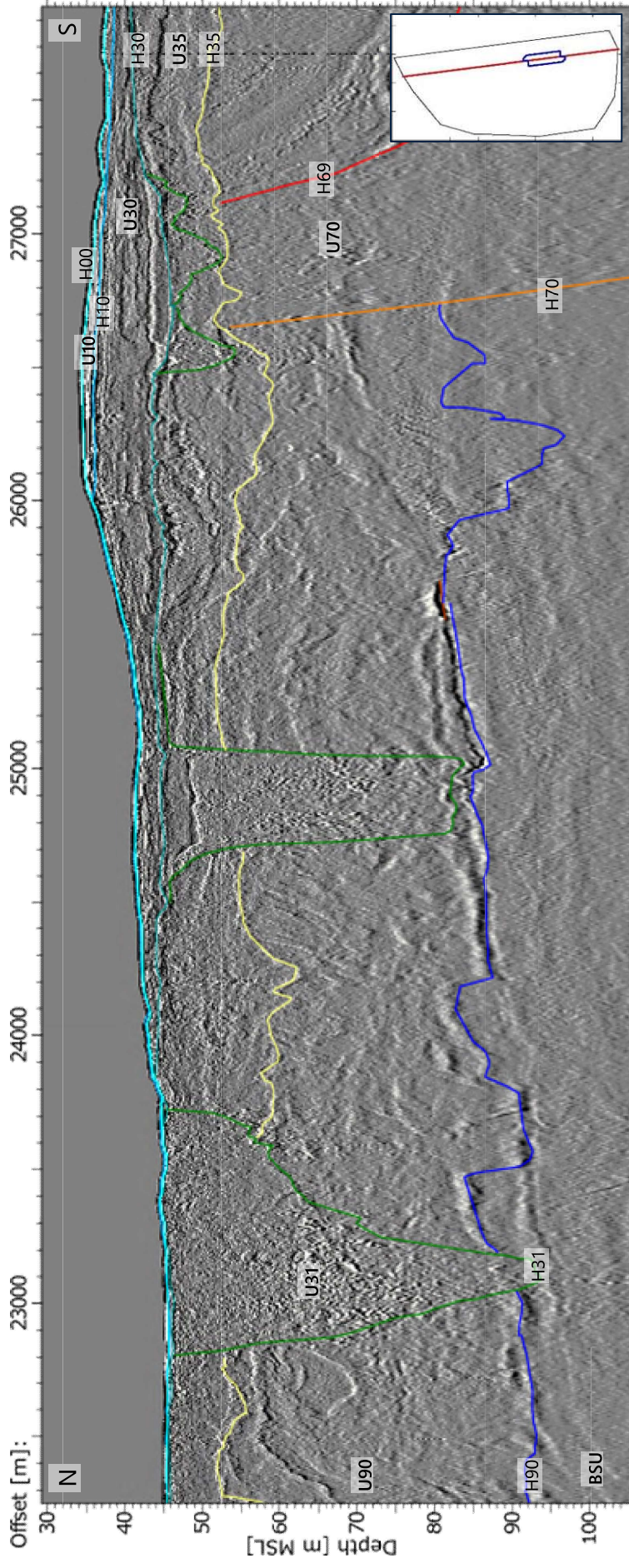
Figure 4.56: Line EAS2213P01.MIG. 2D-UUHR data example of Unit U31.

4.3.1.8 Unit U30

Unit U30 has a sheet-like geometry with a horizontal to undulating base and steep erosional margins. The unit reaches a maximum thickness up to 33 m (Figure 4.57). The base of Unit U30 is marked by horizon H30, a low to medium amplitude positive amplitude reflector. The distribution of Unit U30 is associated with the distribution of Unit U35 and deformed unit D24.

Internally, the unit is stratified with horizontal medium to high amplitude, closely spaced parallel reflectors (Figure 4.58). Locally, in the east of the site, internal channels with acoustically transparent infill are present in this unit, especially in the upper part.

It is interpreted that the stratified Unit U30 was deposited in a (glacio-) marine or (glacio-) lacustrine environment (Larsen and Andersen, 2005; GEUS and Orbicon, 2010; Ramboll, 2021). The stratigraphic position of this unit (underneath Unit D24) indicates an Weichselian or older age.

Unit U30 may correlate to the Ling Bank Formation and/or Dogger Bank Formation in the British sector of the North Sea. The Ling Bank Formation may be of Eemian age, the Dogger Bank Formation is Weichselian in age (Fyfe, 1986; Jeffrey et al., 1991).
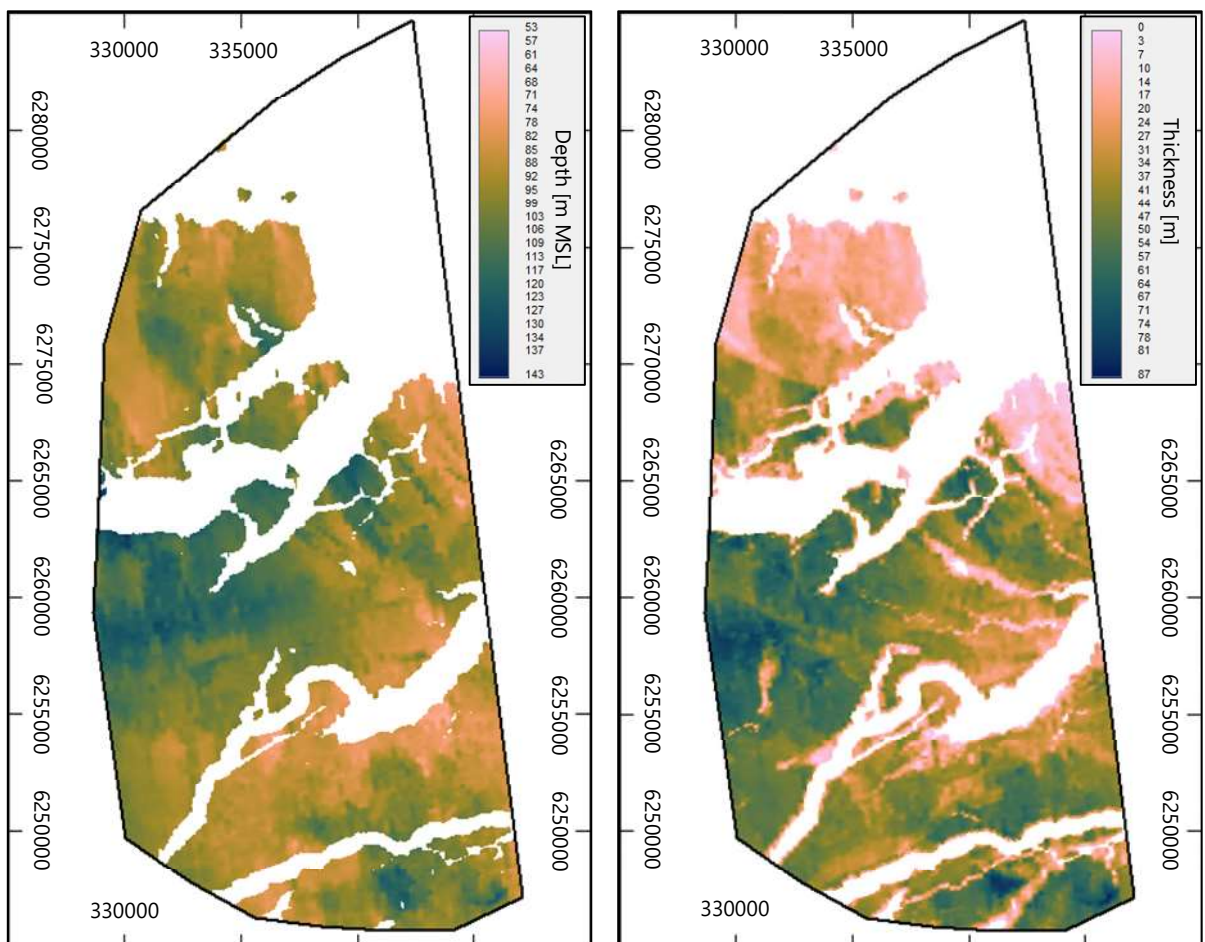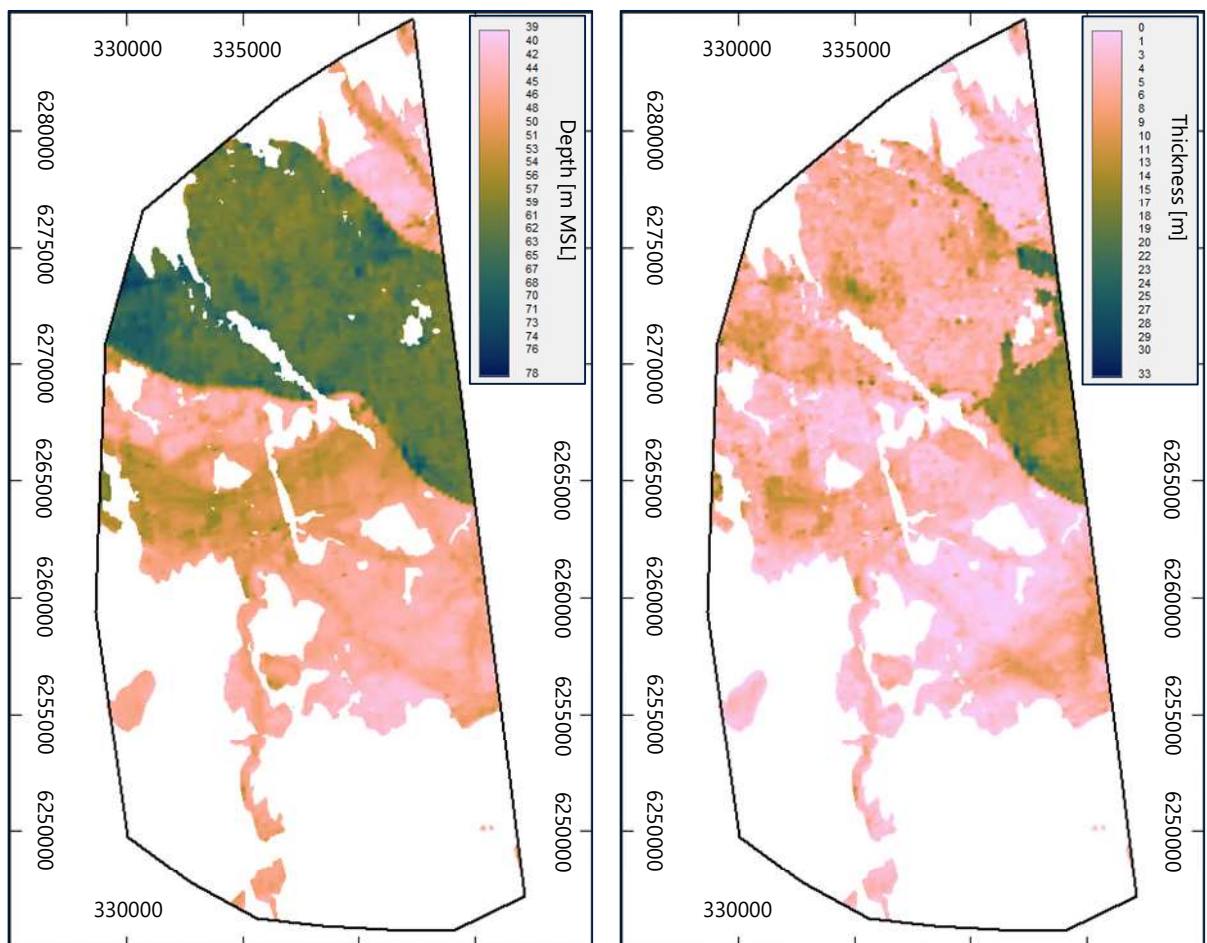

Figure 4.57: Left: Depth to horizon H30 (base of Unit U30). Right: Thickness of Unit U30

FUGRO
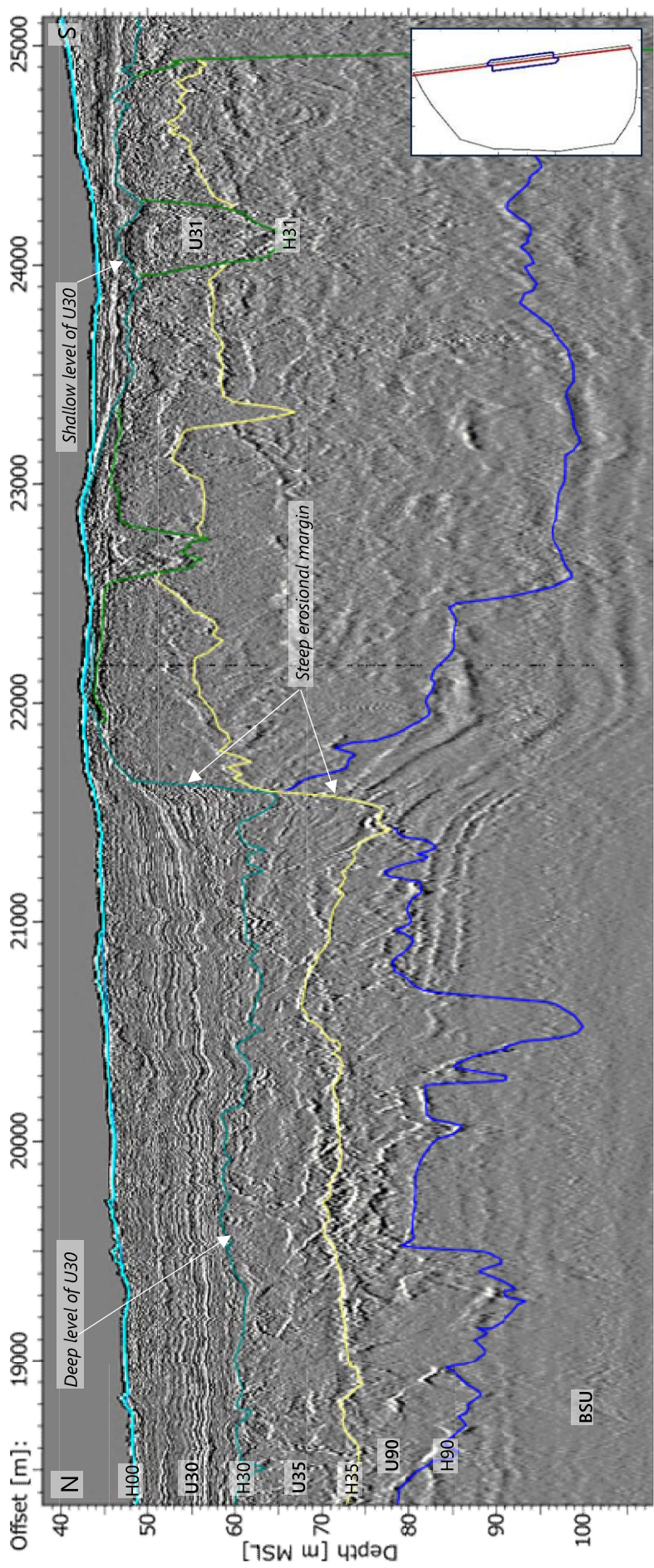
Figure 4.58: Line EAY2261P01.MIG. 2D-UUHR data example of Unit U30.

4.3.1.9   Unit D24

Unit D24 has a sheet-like geometry with a horizontal to undulating base. The unit has a thickness of up to 45 m (Figure 4.59). The base is marked by horizon H24. The unit is present in the northern valley and its distribution correlates with the distribution of Unit U30. It is interpreted that Unit D24 is the same material as Unit U30, but Unit D24 is glacially deformed.

Internally, the unit shows evidence for deformation (Figure 4.60). In areas where the unit is less deformed, the original stratification is still visible but folded. Where this unit is more deformed, northward dipping thrust-faults are observed. Transparent seismic character observed in some areas may indicate strongly deformed sediments, e.g., a complete loss of the original stratification (if any).

It is interpreted that this unit is deformed material of mostly Unit U30, and locally incorporates beds of deeper units. The maximum ice extent during the Weichselian was situated within the northern part of the site (Figure 4.2; GEUS and Orbicon, 2010; Ramboll, 2021). Therefore, it is interpreted that this unit may be a push-moraine formed during the Weichselian.
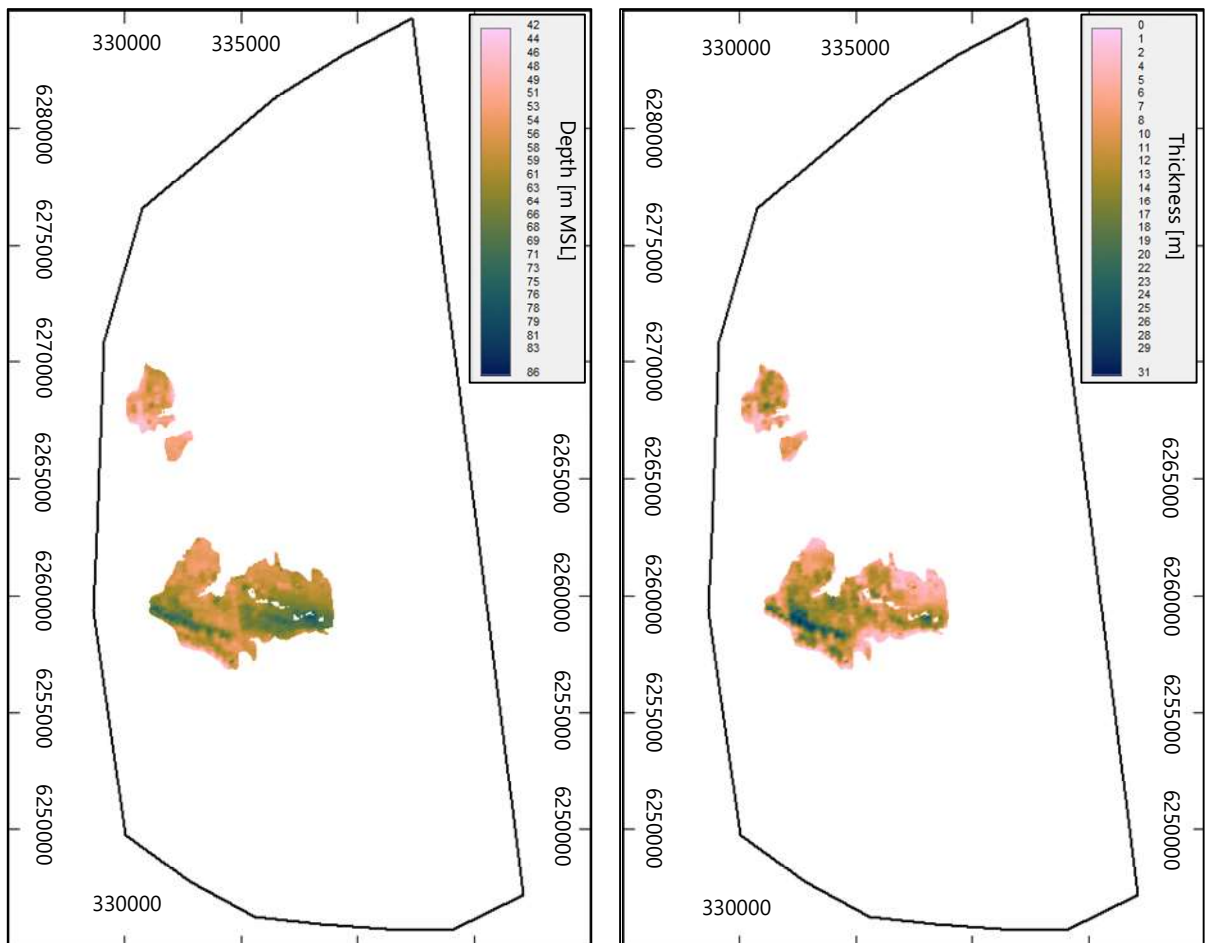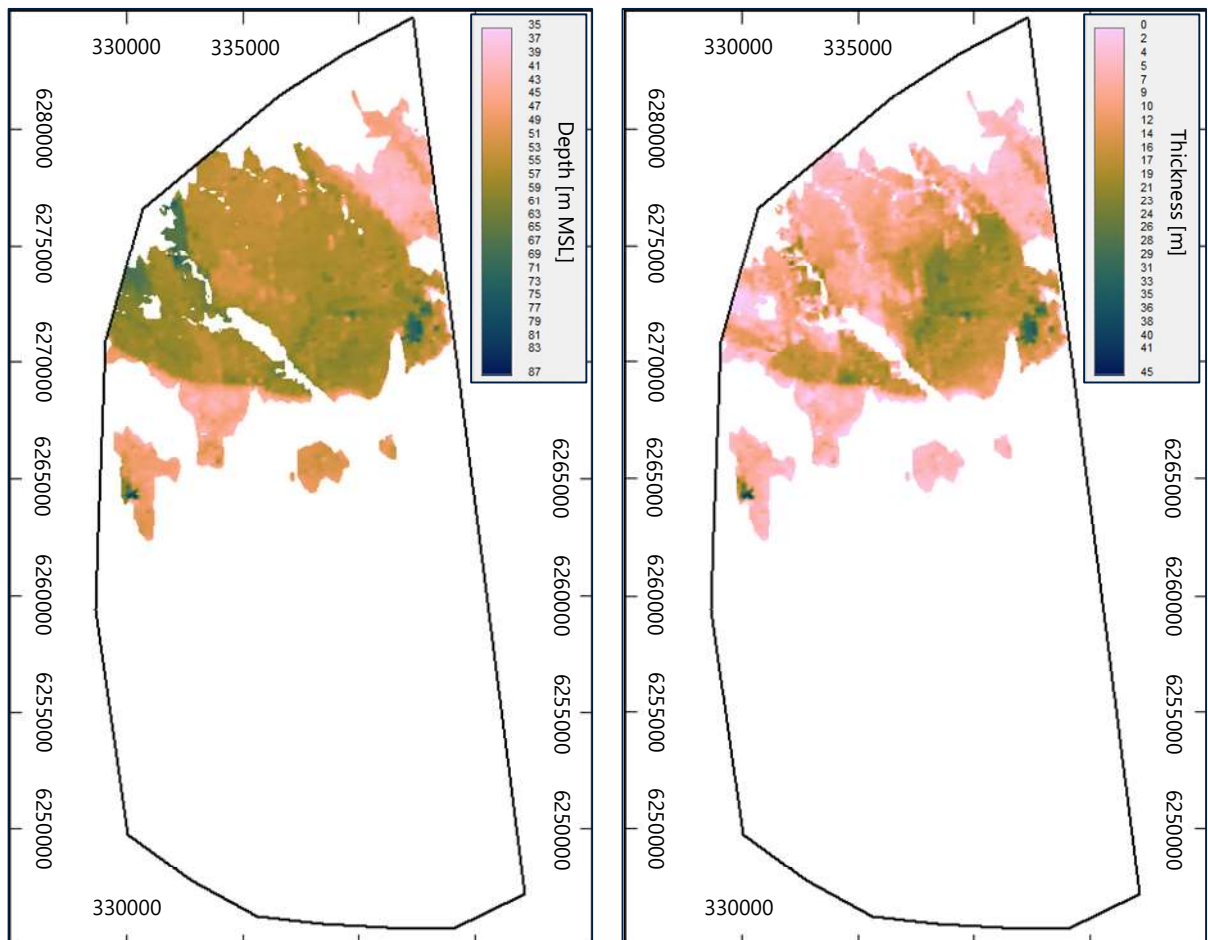

Figure 4.59: Left: Depth to horizon H24 (base of Unit D24). Right: Thickness of Unit D24.
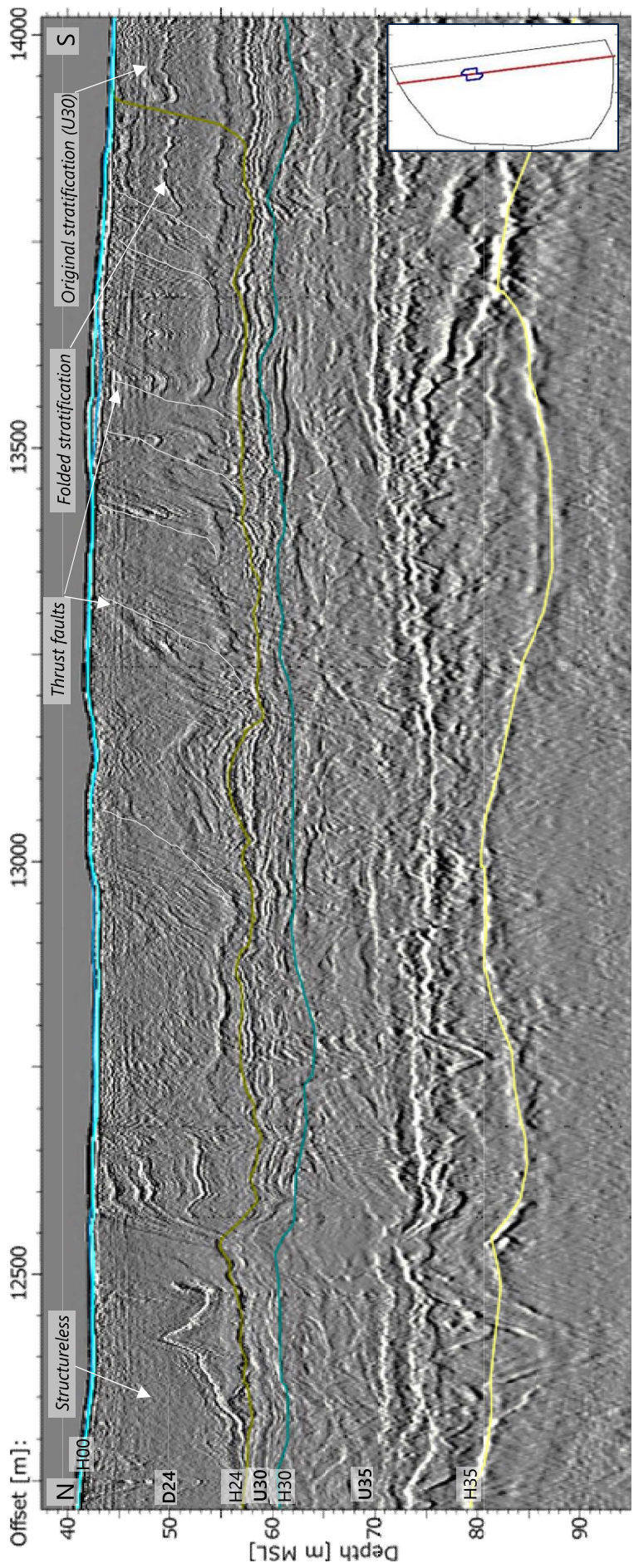
Figure 4.60: Line EAT2221P02.MIG. 2D-UUHR data example of deformed Unit D24.

4.3.1.10   Unit U20

Unit U20 forms the infill of spatially variable (in depth and size) channels. The maximum thickness reaches approximately 120 m (Figure 4.61). The base of Unit U20 is marked by horizon H20, a low to high amplitude positive reflector, or a change in seismic character.

Internally, the unit contains low to high amplitude stratification parallel to the base of the channel. Locally this unit is seismically transparent or chaotic. In the southern part of the site, the unit forms one large channel with a west-south-west to east-north-east orientation connected with many small channels forming a tributary network (Figure 4.61, Figure 4.62). In the northern part of the site the unit forms one deep, narrow channel with a north-west to south-east orientation, and smaller channels parallel to the deep channel (Figure 4.61, Figure 4.63). These channels are associated with some smaller tributary channels. In the north-west of the site, Unit U20 has in general a sheet-like geometry (Figure 4.61, Figure 4.63).

It is interpreted that the unit was deposited in a fluvial and estuarine depositional environment when the site was flooded after the last glacial maximum during the late Weichselian to early Holocene. In the north-west of the site, where Unit U20 forms a relatively thin horizontal layer, this unit was deposited in a coastal environment at the river-mouth, which flowed towards the north-west, where the palaeo-coastline was situated (Leth, 1996; Larsen and Andersen, 2005; Jensen et al., 2008).
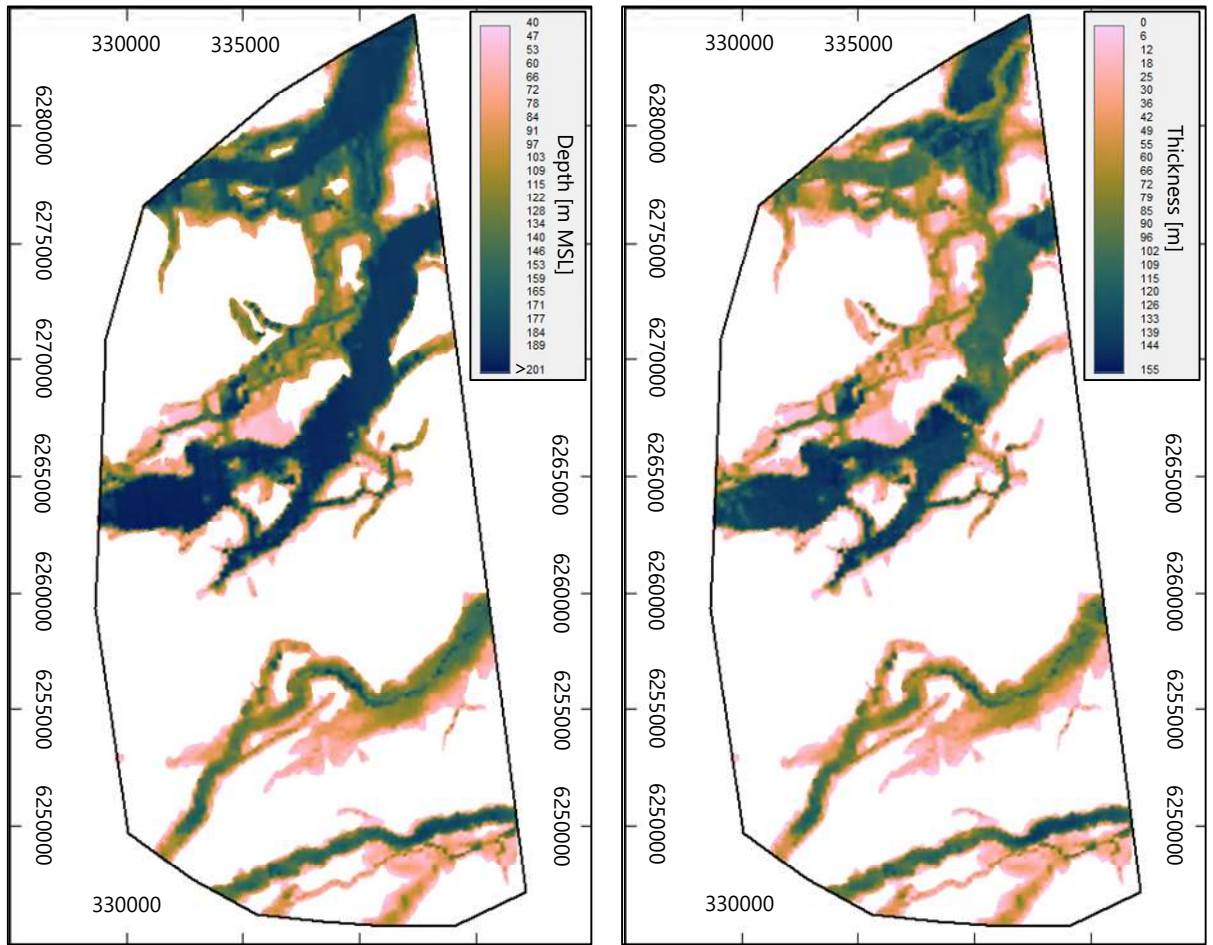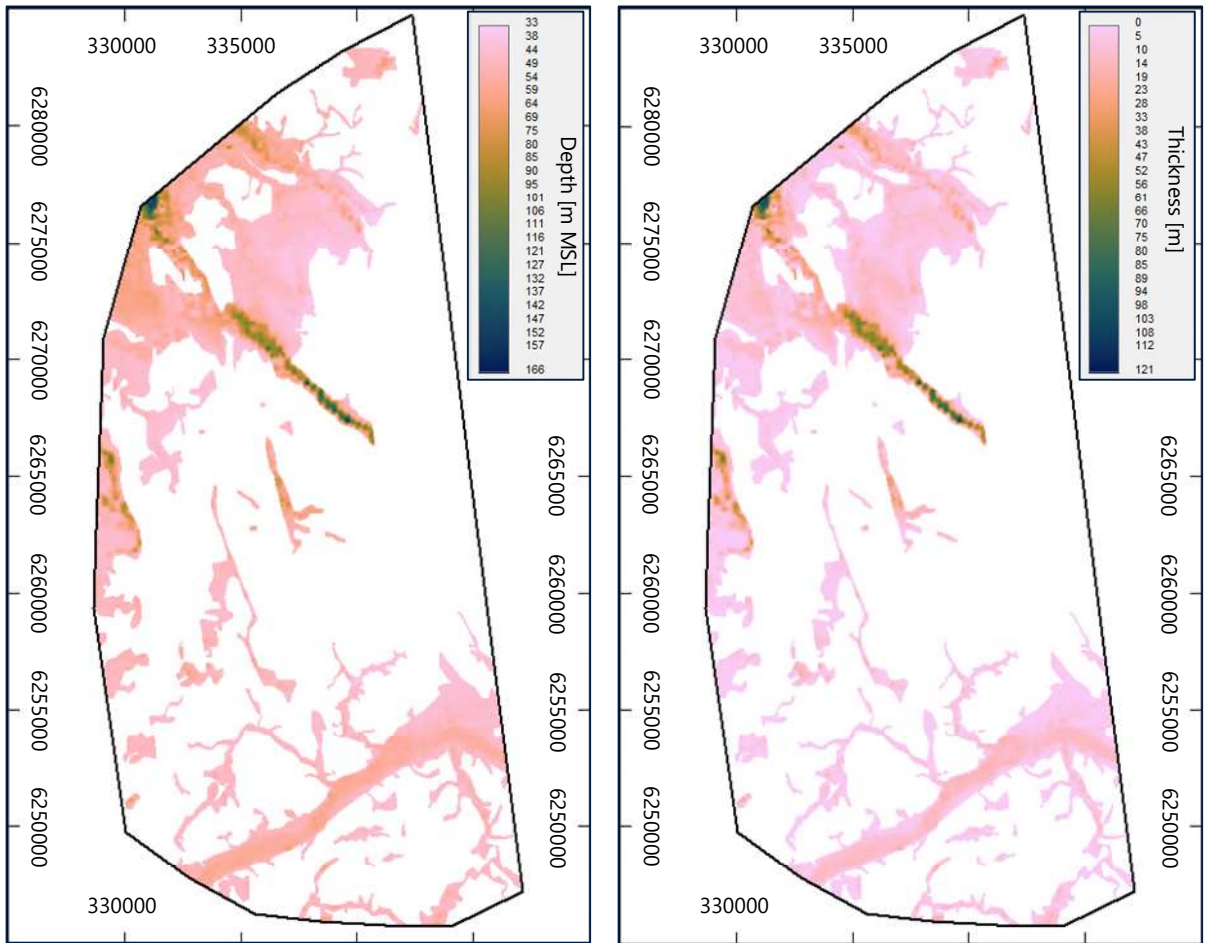
Figure 4.61: Left: Depth to horizon H20 (base of Unit U20). Right: Thickness of Unit U20.
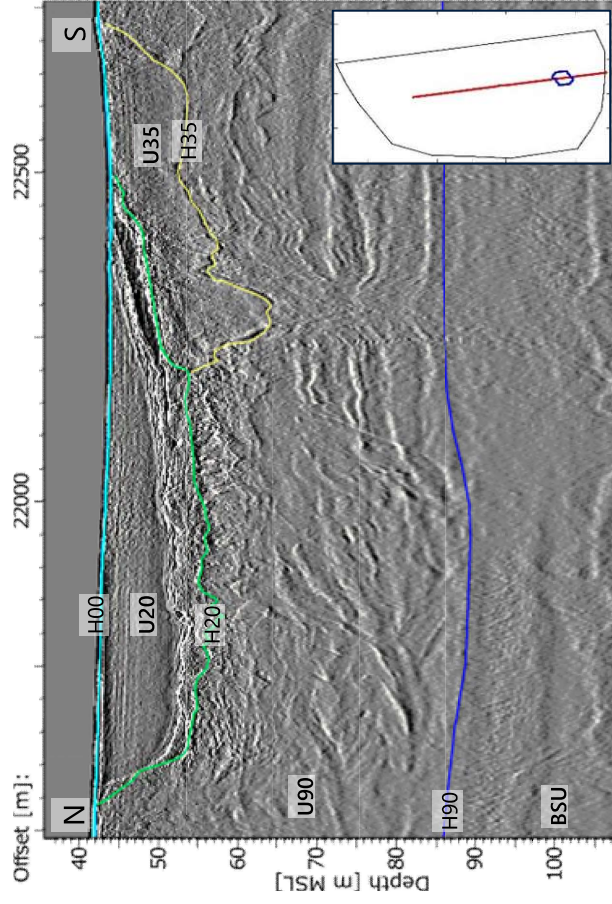
Figure 4.62: Line EAP6169P01.MIG. 2D-UUHR data example of Unit U20.
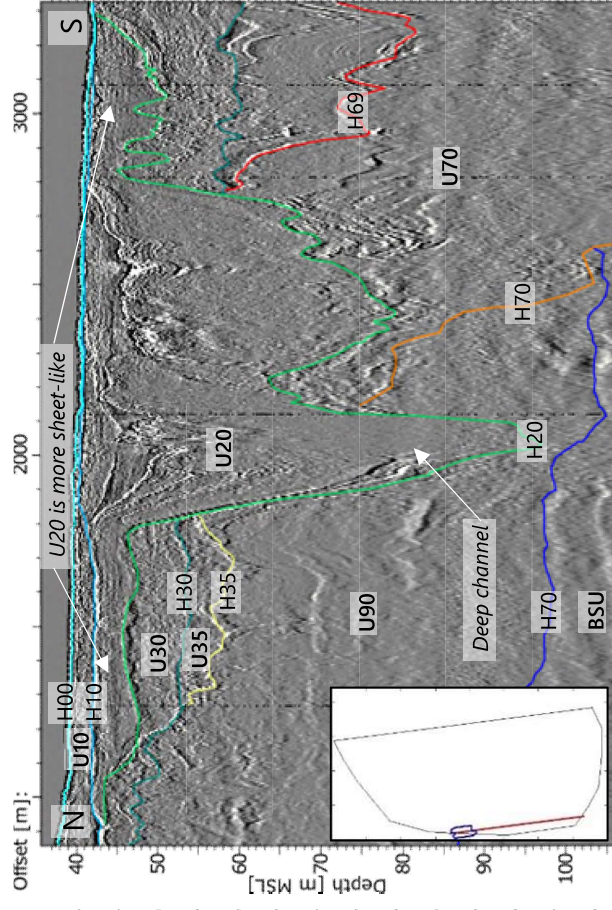
Figure 4.63: Line EAC2021P01.MIG. 2D-UUHR data example of Unit U20.

4.3.1.11 Unit U10

Unit U10 is present across almost the entire site and is generally less than 5 m thick (Figure 4.66, Figure 4.67). In the north of the site, Unit U10 is thicker, reaching a maximum thickness of 22 m in the north-west of the site (Figure 4.66, Figure 4.68). The area where Unit U10 is thicker corresponds to the northern flank of a bathymetric shallow area.

Locally, the base of Unit 10 (horizon H10) may be within the seafloor pulse of the SBP data. It should be noted that the seismic data cannot resolve a top layer thinner than 0.3 m (Peuchen and Westgate, 2018). Therefore, the areas where Unit U10 is interpreted to be absent, a thin layer (<0.3 m) of Unit U10 may be present.

The basal horizon H10 has a horizontal to undulating geometry and is generally a medium to high amplitude positive reflector. Where Unit U10 overlies Unit U20 or Unit U30, horizon H10 can be a low amplitude positive or negative reflector. The basal horizon H10 has been interpreted on the 2D-UUHR and SBP datasets.

In the area where Unit U10 is thin, i.e., less than approximately 5 m, its internal seismic character is acoustically transparent on 2D-UUHR data and acoustically transparent to chaotic on the SBP data (Figure 4.67).

In the north, where Unit U10 is thicker, two internal horizons H05 and H06 were observed on the SBP data (Figure 4.64, Figure 4.65). These internal horizons form respectively the top and base of an interval with clinoforms dipping towards the north (Figure 4.68). The interval above H05 is acoustically transparent to chaotic. The interval between H10 and H06 is acoustically transparent to complex with internal reflectors. In the far north of the site, the interval between H10 and H06 comprises high amplitude stratified to chaotic reflectors.

It is interpreted that the unit represents Holocene marine sediments, which were deposited during and after the Holocene transgression. The internal inclined stratification in the north may represent a short period of coastline progradation of spits or barrier-islands in the early Holocene.
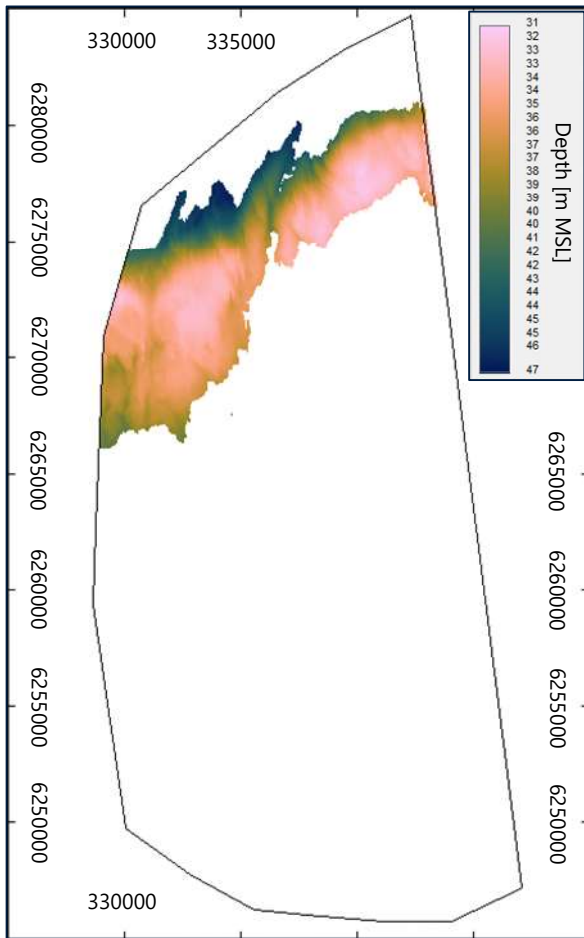
Figure 4.64: Depth to horizon H05 (internal horizon in of Unit U10).
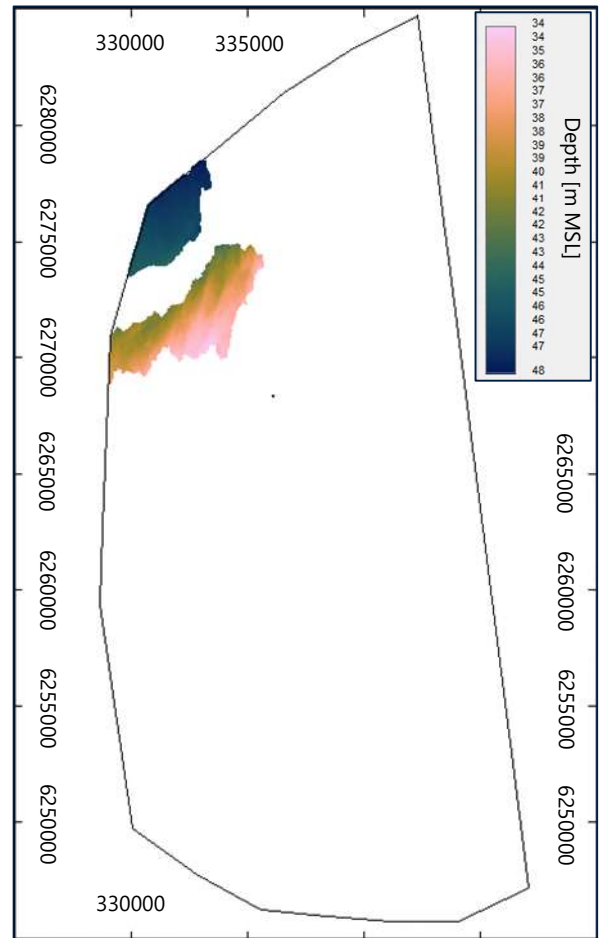
Figure 4.65: Depth to horizon H06 (internal horizon in of Unit U10).
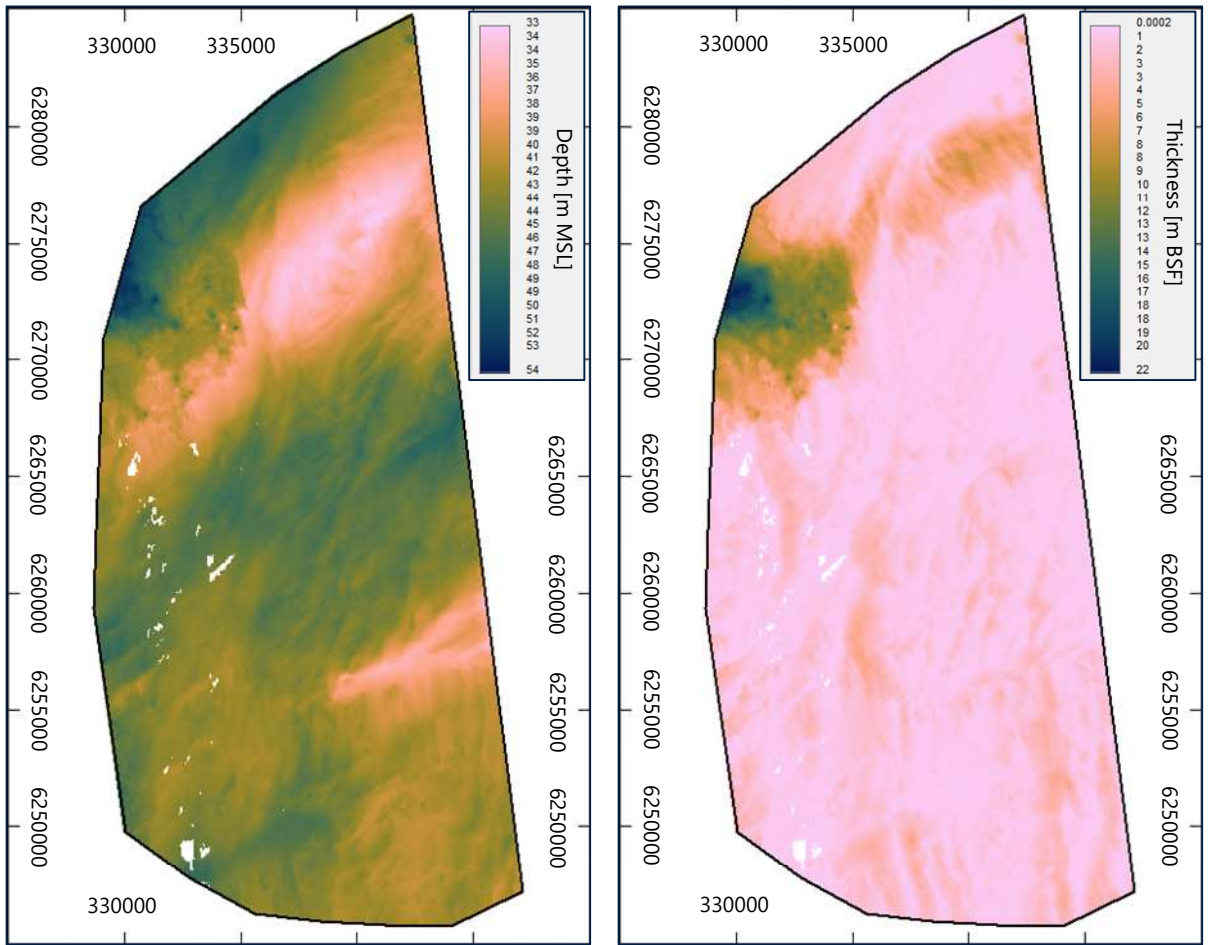
Figure 4.66: Left: Depth to horizon H10 (base of Unit U10). Right: Thickness of Unit U10.
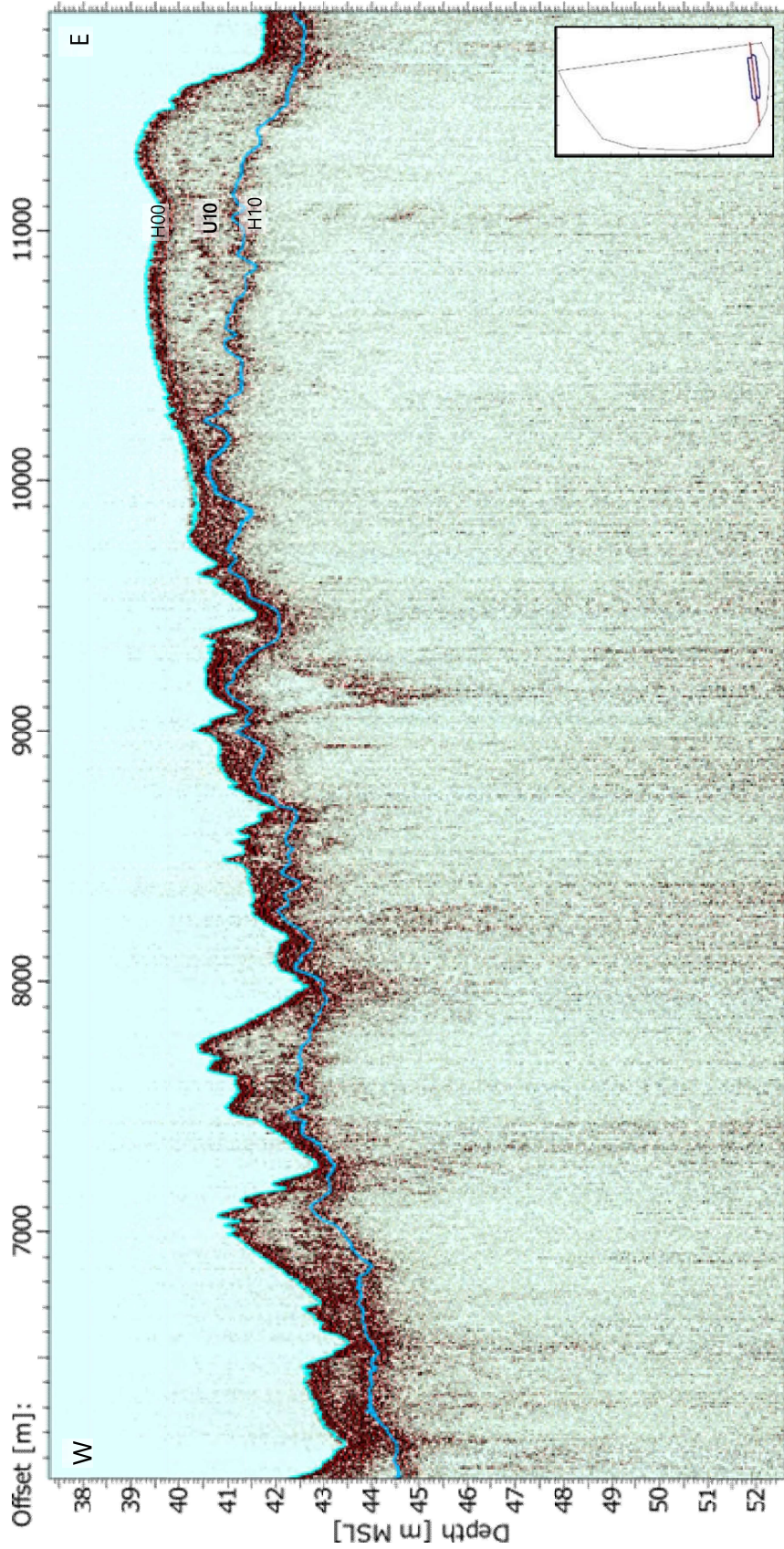
Figure 4.67: Line SBP_EAX2273P01_PRC. SBP data example of Unit U10.
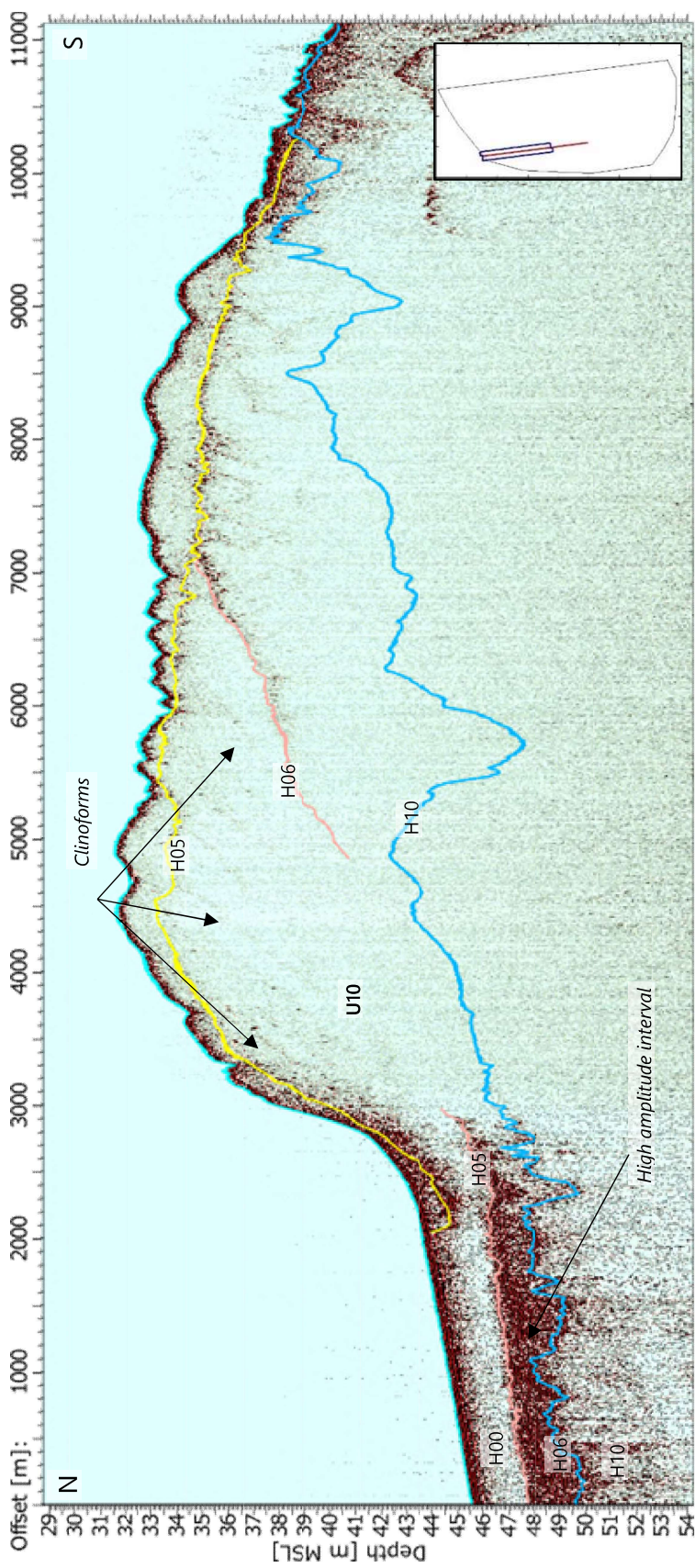
Figure 4.68: Line SBP_EAF1080P02_PRC. SBP data example of Unit U10.

4.4 Geological Features

4.4.1 Amplitude Anomalies

Seismic anomalies in form of high amplitude and reserve polarity are present at two levels (level 1 and level 2) between 0 and 67 m BSF in Unit U90 (Figure 4.69, Figure 4.70, Figure 4.71). No acoustic blanking is associated with these anomalies. These seismic anomalies may be the result of beds /laminae of peat or organic rich clay.

4.4.2 Acoustic Blanking

Acoustic blanking and/or signal distortion was observed below some (limited) amplitude anomalies (Figure 4.72). These features were typically present between 4 m and 16 m BSF and were associated with channels of Unit U20 (Figure 4.74). The areas where they are present have been mapped as "acoustic blanking" (Appendix B). The degree of signal distortion and/or blanking may vary slightly between neighbouring seismic lines. The acoustic blanking can be due to the presence of gas in the soil.

4.4.3 Glacial Deformation

Glacial deformation was observed at two levels, in Unit D24 and in BSU.

In the north, Unit D24 is deformed to a various degree. Deformation includes folding and thrust faults. Acoustic transparency observed locally in the unit may indicate a high degree of disturbance. The base of the deformation is marked as horizon H24 forming the base of Unit D24 (section 4.3.1.9).

In the north, the BSU contains well-defined thrust-faults forming a thrusted complex with a detachment surface at approximately 140 m MSL (Figure 4.73, Figure 4.75). This deformation is assumed to be the result of ice-push from the north and north-east during the Elsterian and/or Saalian glaciation.

During the Weichselian, the maximum extent of the ice sheet was over the northernmost part of the site (Figure 4.2; GEUS and Orbicon, 2010; Ramboll, 2021). Since the observed deformation features are limited to the shallow sub-surface and the northern part of the site, it is interpreted that the deformation of Unit D24 is the result of Weichselian ice-push.

4.4.4 Faults

Normal faults and an inverted normal fault were observed in the BSU (Figure 4.76, Figure 4.77). They extend locally into the base of the overlying Unit U90. It is interpreted that these normal faults are the result of late Cenozoic extension. The inversion of the normal fault in the east of the site may be related to ice-push during the Elsterian and/or Saalian ice age.
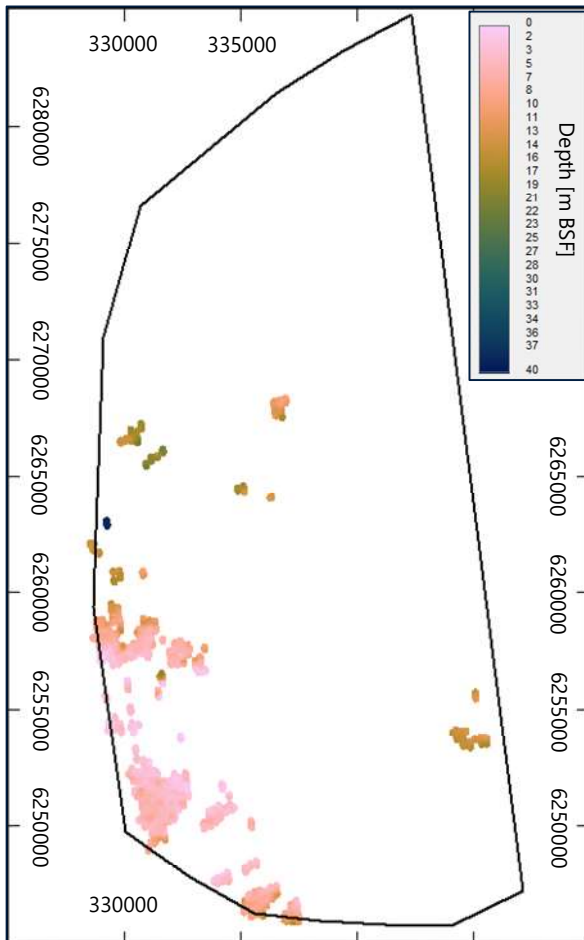
Figure 4.69: Distribution of amplitude anomalies level 1.
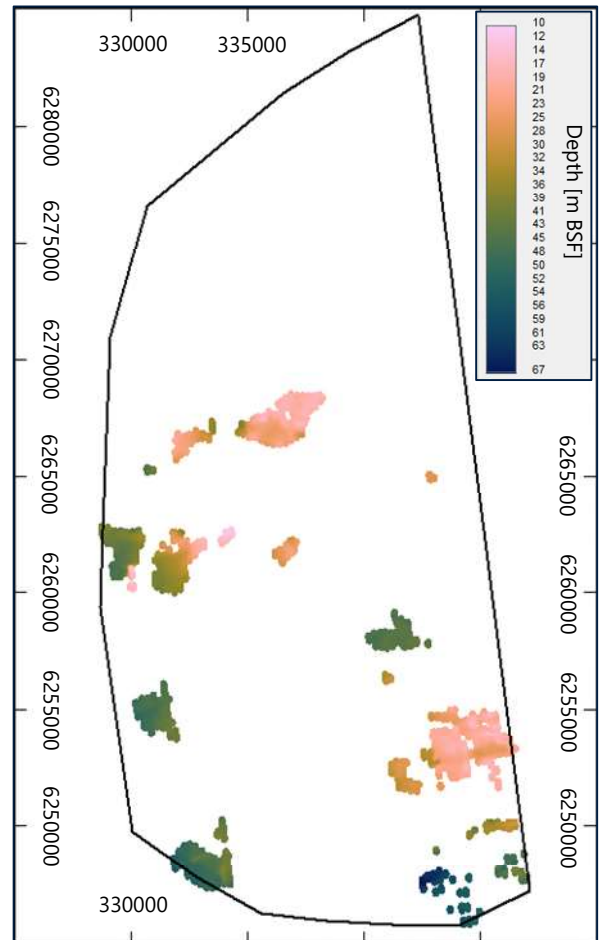
Figure 4.70: Distribution of amplitude anomalies level 2.
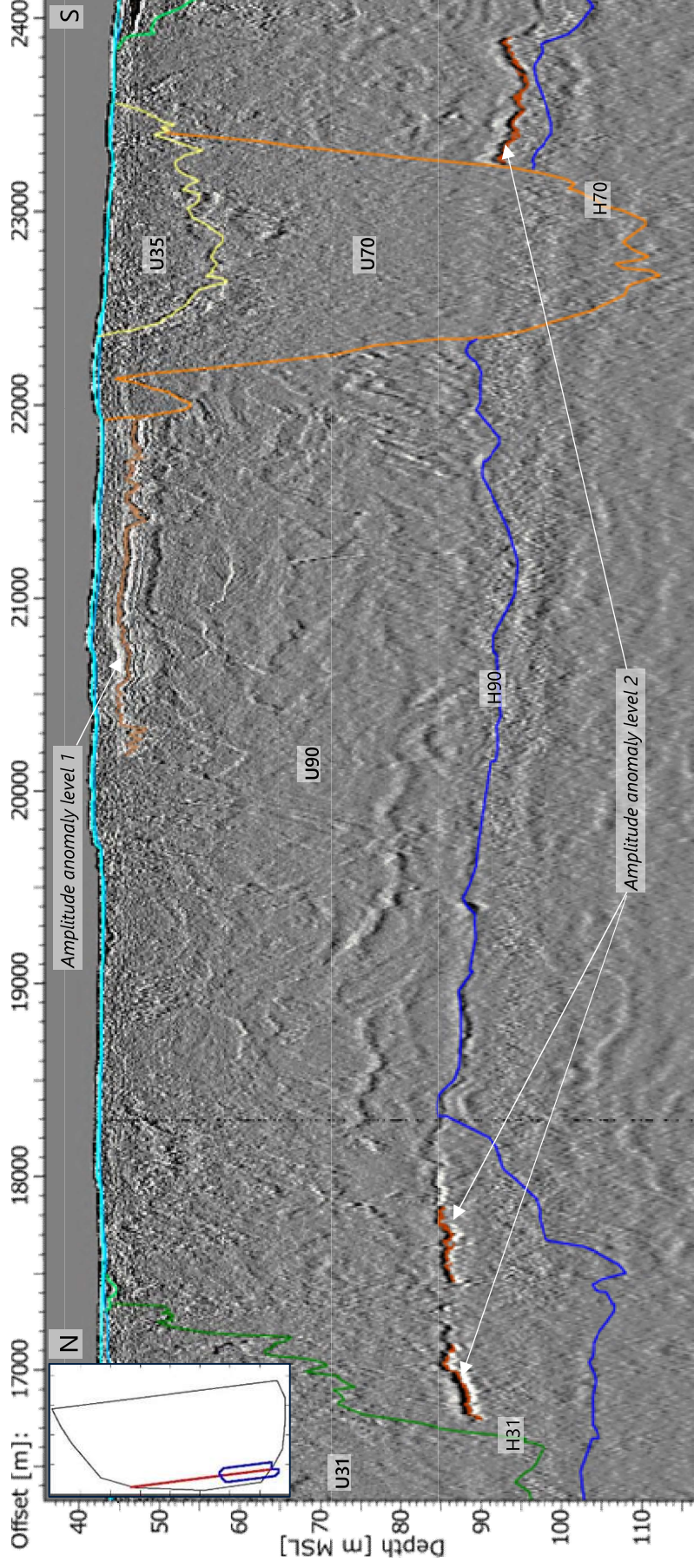
Figure 4.71: Line EAD2033P01.MIG. 2D-UUHR data example of amplitude anomalies.
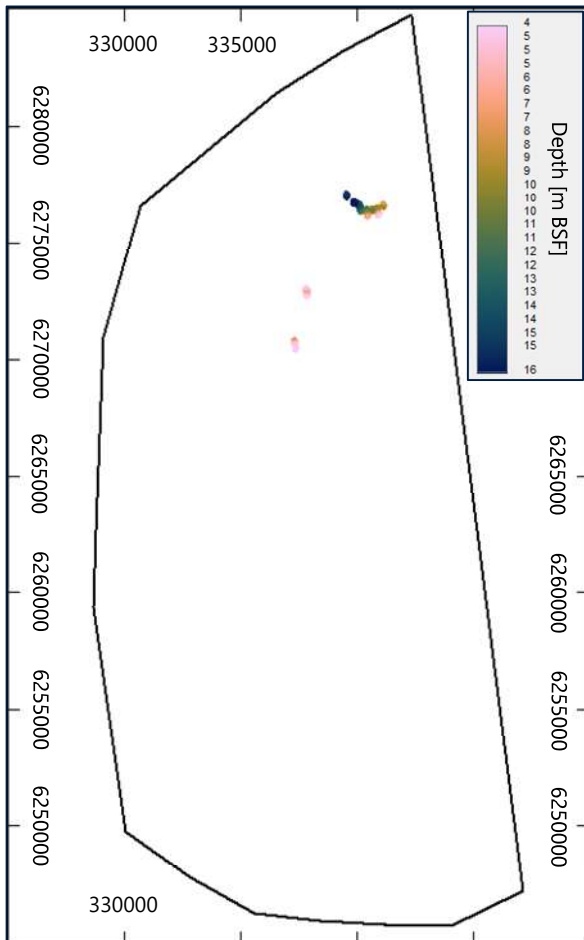
Figure 4.72: Distribution of acoustic blanking.
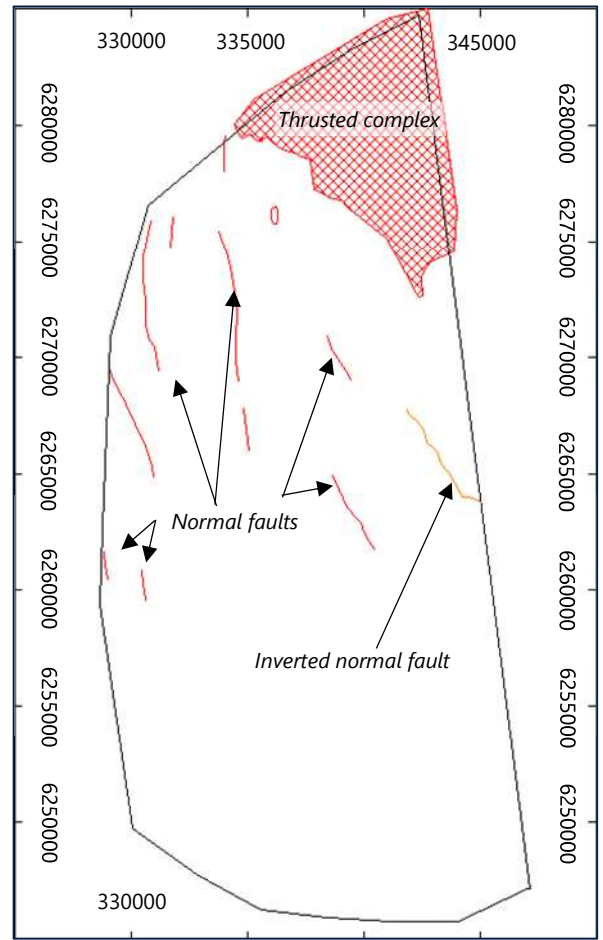
Figure 4.73: Distribution of interpreted faults.
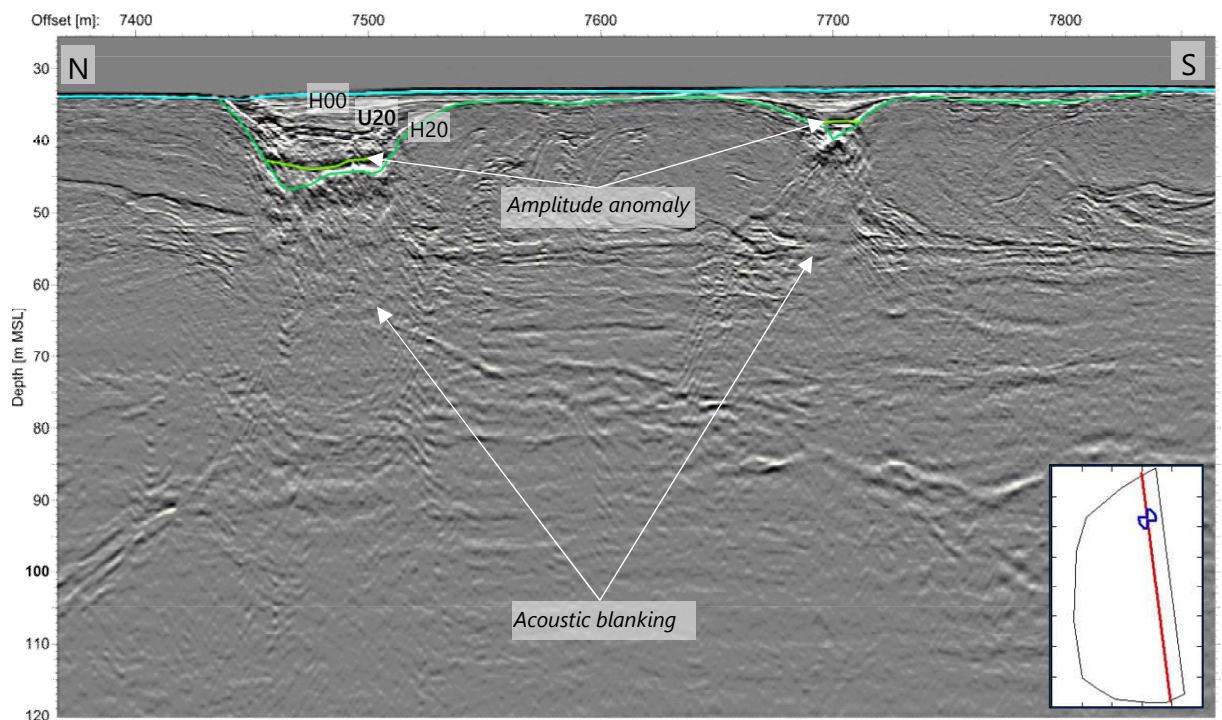
Figure 4.74: Line EAT2229P01.MIG. 2D-UUHR data example of amplitude anomalies with acoustic blanking.

FUGRO
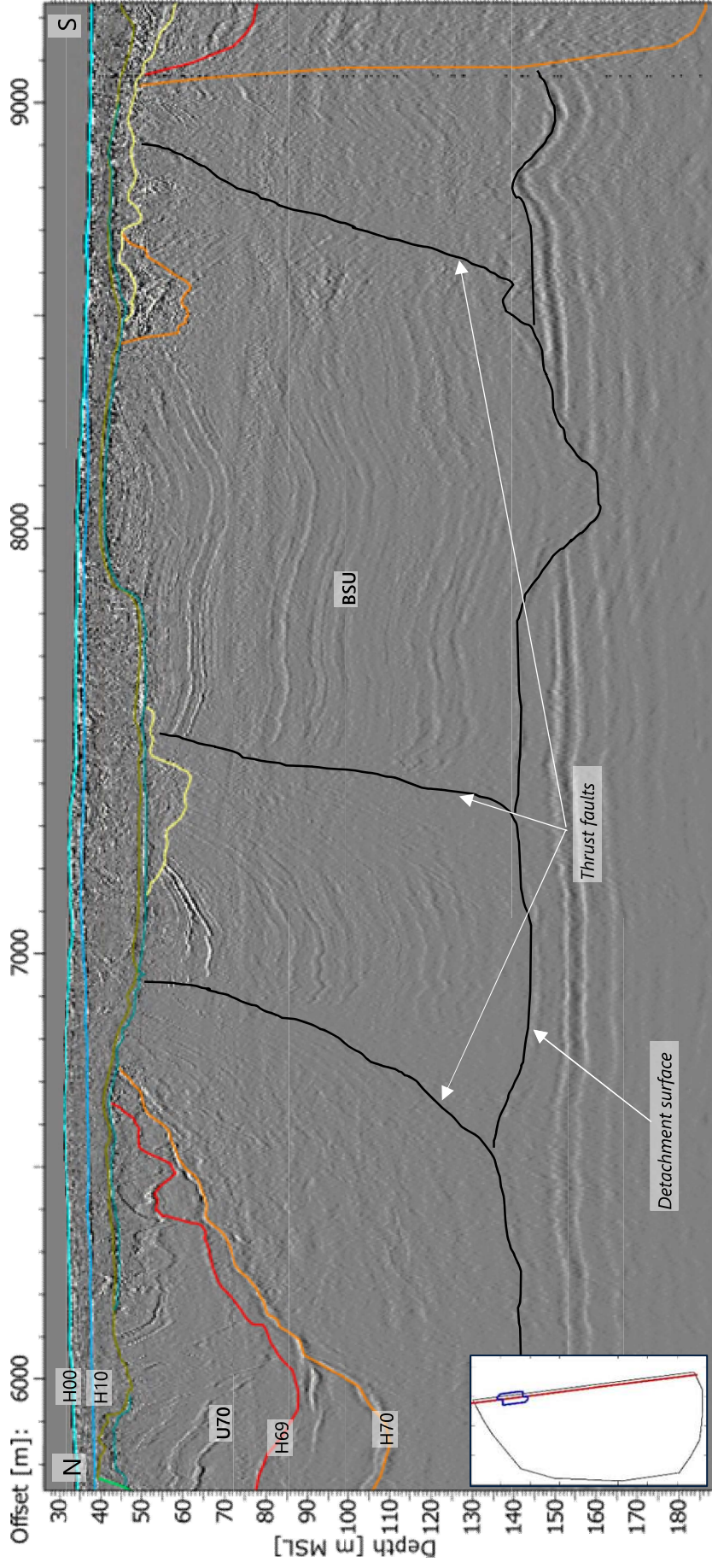
Figure 4.75: Line EAY2261P01.MIG. 2D-UUHR data example of the thrusted complex.
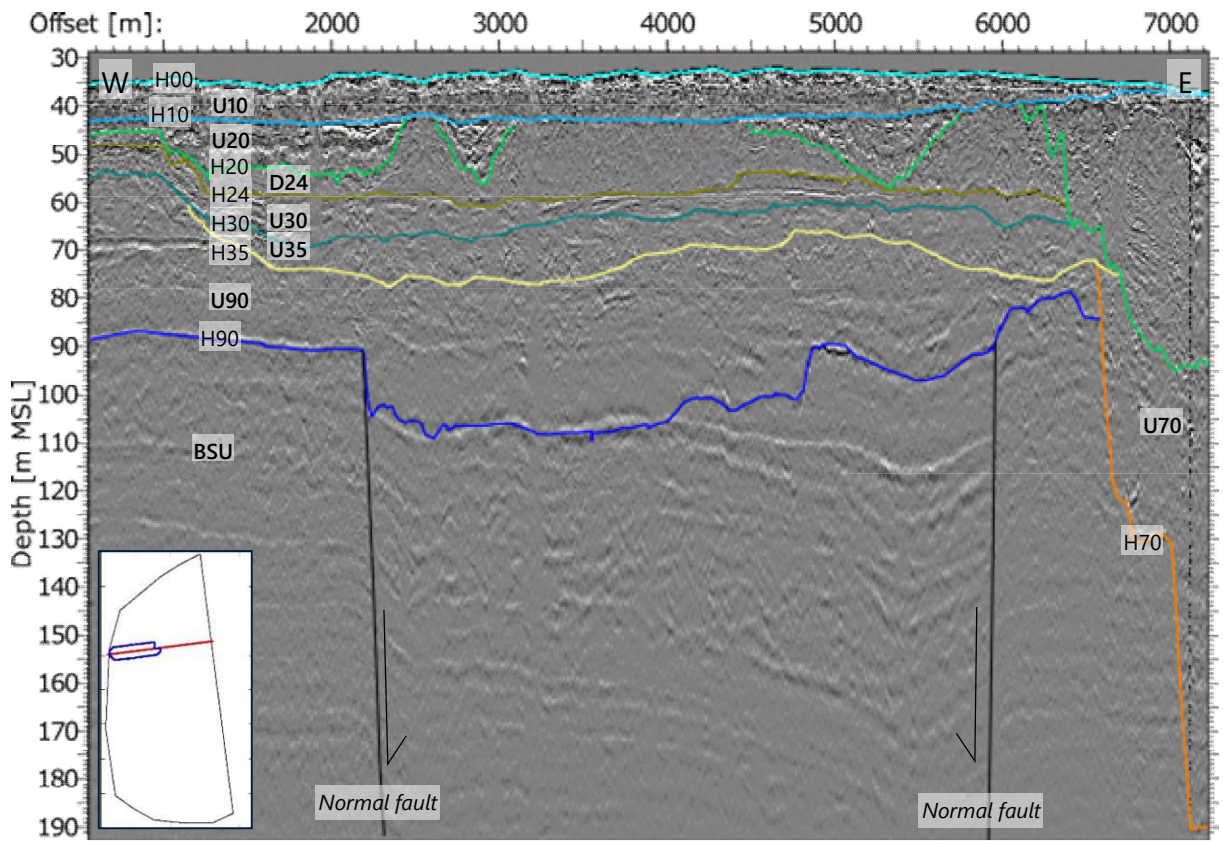
Figure 4.76: Line EAX2296P01.MIG. 2D-UUHR data example of normal faults.
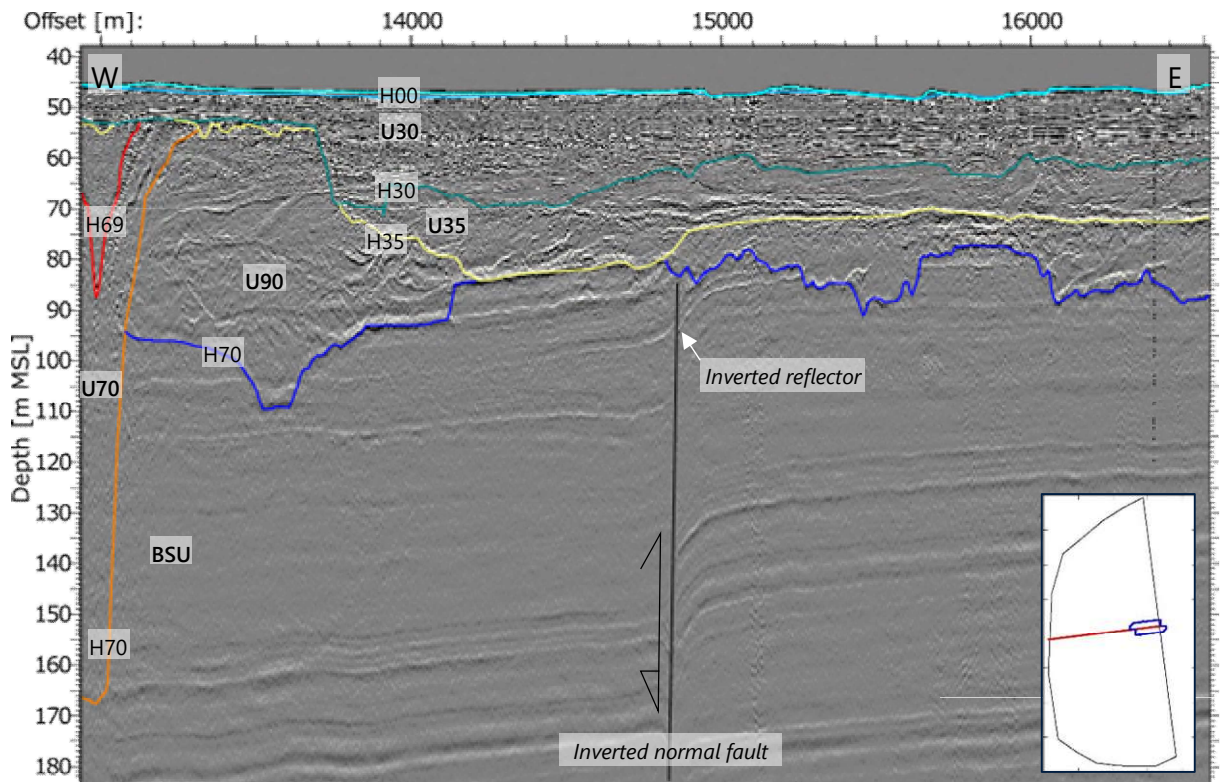
Figure 4.77: Line EAX2290P01.MIG. 2D-UUHR data example of an inverted normal fault.

FUGRO

4.5 Archaeological Findings and Anomalies with Archaeological Potential

Fugro's expertise is limited regarding identification of archaeological findings. Thus, only two objects interpreted as wrecks were classified as archaeological.

Fallwind wreck was observed in the central western part of the site (EA_R_SSS_00580) and surrounded by scattered debris items. A potential wreck marked in ENC database was observed in the northern part of the site (EA_P_SSS_00591). Detailed positions and measurements of the wrecks and debris items are presented in Table 4.14. Both wrecks can be seen in SSS, MBES and MAG datasets. Refer to Figure 4.32 and Figure 4.33 for data examples.

Table 4.14: Positions and measurements of wrecks found within the OWF Zone West site.

SSS_ID	Easting [m]	Northing [m]	Length [m]	Width [m]	Height [m]
EA_P_SSS_00591	337224.95	6279528.76	31.5	11.9	0.9
EA_R_SSS_00580	340612.44	6263664.83	73.4	20.6	3.9
Notes: -all the numbers in the table were rounded to one decimal point					

In Block Q and N four (4) features were identified as possible pingo remnants (section 4.2.2.3). Due to the regular circular shape these features are marked also as anomalies with archaeological potential. Detailed positions and measurements are presented in Table 4.15. Data example is shown in Figure 4.17 in section 4.2.2.3.

Table 4.15: Positions and measurements of (potential) archaeological findings within the OWF Zone West site.

Easting [m]	Northing [m]	Length [m]	Width [m]	Height [m]
338943.9	6257793.4	10.7	7.2	0.3
338992.0	6257800.1	16.5	7.0	0.2
339003.6	6257818.6	12.7	7.6	0.2
339026.7	6272222.6	38.5	25.2	0.5
Notes: -all the numbers in the table were rounded to one decimal point				

Fugro cannot exclude or confirm archaeological potential of the identified seafloor targets supplied in the GIS database as part of the final deliverables.

5. Processing and Interpretation Methodology

5.1 Positioning and Navigation

All raw DGPS data were edited to remove erroneous fixes. No smoothing filters were applied to the position data during acquisition.

The antenna position was corrected to the vessel common reference point position (CRP) using measured offsets, during the acquisition of data. The position of the antenna during the analogue programme was corrected for layback of each towed instrument by applying the offset along the vessel track.

Real-time logging of navigation was done using Fugro's StarfixNG navigation system. Bathymetric sounding (water depth) data was logged in Kongsberg SIS software.

The processing of the acquired navigation data was carried out using Starfix VBAProc software.

The data were processed using offsets from the vessel datum for all sensors. Equipment offsets from the CRP position are presented in the Operations Report (*F176286-REP-OPS-001 (02)*).

5.2 Multibeam Echosounder

5.2.1 Data Quality

Multibeam echosounder data quality overall was well within desired specification for the entire OWF Zone West site.

The spatial accuracy achieved for MBES sensor fulfils the requirements. The data was gridded and provided at resolution of 0.25 m and 1.0 m. Standard deviation (2 sigma) was <0.2 for 99.994% of the data, in rare cases marginal standard deviation (2 sigma) was noticed between overlapping blocks in isolated areas (Figure 5.1). THU was <0.5 m and TVU are depth dependent values, and the results were satisfying IHO special order 44. Block based MBES QC reports were supplied to the OCR and are presented in the operations reports.
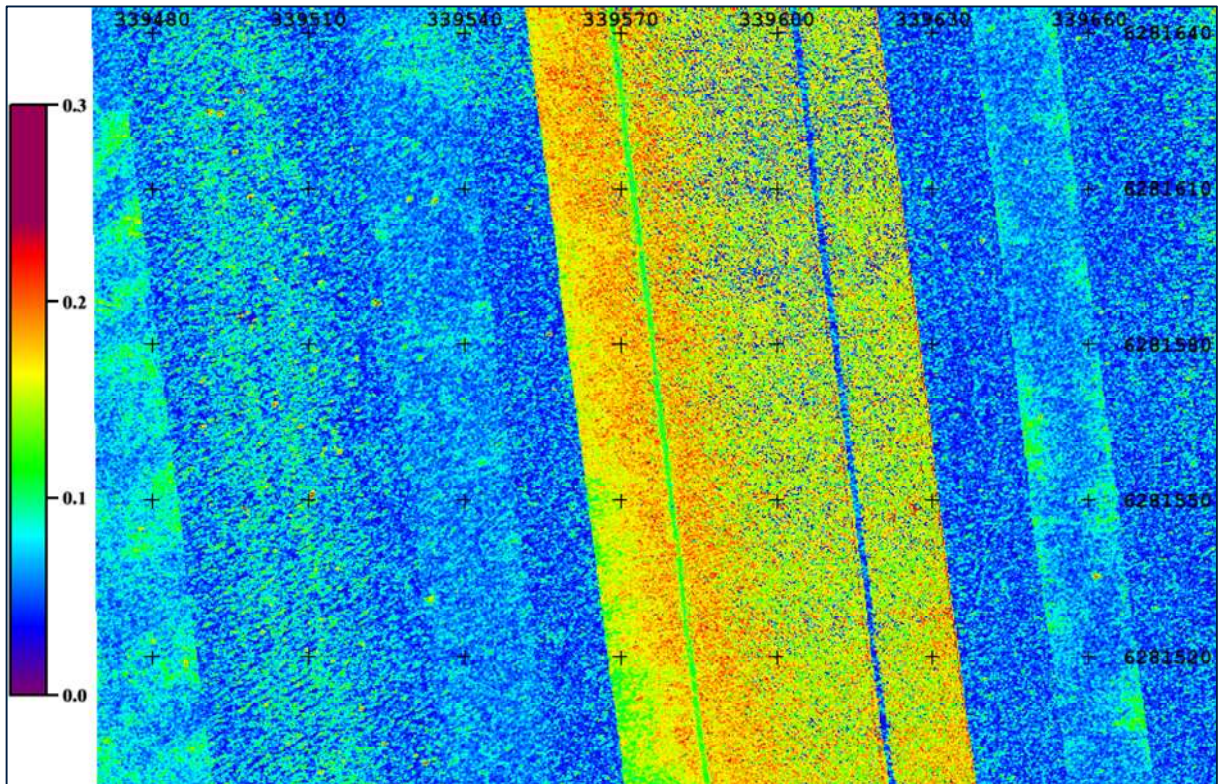
Figure 5.1: Example of the standard deviation (2 Sigma) within the overlap area between blocks S and T in the northern part of the site.

Full coverage was achieved except for a few areas in the eastern and northern part of the site where planned infills were deemed not required by Energinet.

5.2.2   Data Processing

Bathymetry data collected from the hull mounted dual head Kongsberg EM2040 multibeam echo sounder onboard the survey vessel were processed with CARIS Hydrographic Information Processing System and Sonar Information Processing System (HIPS and SIPS) software (Version 11.3/11.4). The CARIS HIPS and SIPS general workflow is presented in Table 5.1. Neighbouring blocks were systematically merged towards completion of data processing.

Table 5.1: CARIS HIPS and SIPS bathymetry processing workflow.

CARIS HIPS Work Step	Description
1. Raw MBES data	MBES raw data as logged by SIS, in combination with data input from StarfixNG
2. HIPS vessel file	Before data were converted into Caris HIPS, a so-called HIPS Vessel File (HVF) was defined. This HVF contains all relevant sensor definitions with information regarding offsets, correction values and system configurations. The HVF defines amongst others: ■ Offsets relative to the centre of gravity (COG); ■ Sound velocity information;

FUGRO

CARIS HIPS Work Step	Description
	■ Dynamic MBES motion (heading, roll, heave, pitch);
	■ Static corrections for gyro heading and error for roll, heave and yaw heading alignment of the multibeam system;
	■ Static TPU (total propagated uncertainty) settings including offsets and survey equipment standard deviations (based on technical specifications).
3. Data conversion to HIPS	The multibeam raw data exported from the online software was converted into HIPS format. Positioning information included in the raw data is based on geographical co-ordinates.
4. Quality control (navigation, attitude data)	Navigation and attitude data were checked for spikes. This is done manually or by using self-defined filters. Spikes were marked and flagged as 'not to be used for further calculation.' The resulting gaps were interpolated over time by calculating new values. Secondary (backup) systems for navigation and attitude data could be added to the HIPS and SIPS project if required.
5. Swath filter	Depth information of one survey line was filtered for spurious values and data not to be used. Filter settings for flagging data as rejected can include the following settings: ■ Min-max. accepted depth range; ■ Distance off nadir; The filters are applied according to the encountered morphology, weather conditions etc. The applied values may vary from area to area. Nevertheless, each line was checked separately, and the filter parameters were adapted if necessary.
6. Tide reduction	All depths were reduced to MSL using the DTU21 MSS model within Caris HIPS & SIPS. Navigation, motion and Starfix.G2+ GNSS elevation data were processed using Fugro Starfix.VBAProc. Ellipsoidal heights of the GNSS antennas were corrected for motions. The heights were reduced to the water line using draught and dimensional offset measurements. Waterline elevations are further reduced to the vertical datum (MSL) by means of DTU21 MSS model. A smooth tide curve was created to reduce MBES data to datum.
7. Sound velocity correction	Each trackline line was corrected for sound velocity.
8. Calculation of final position and depth for each beam (georeferenced bathymetry)	For each individual beam a position and a depth value were calculated with respect to vessel (gyro) heading, tide data (including dynamic draft) and sound velocity correction using time as correlation. In addition, the TVU and THU for each sounding was calculated.
9.TVU-THU filtering[1]	For TVU an IHO Special Order filter was run to remove erroneous soundings exceeded project requirements. For THU a filter was run to remove erroneous soundings exceeded project requirements (0.50 m).

FUGRO

CARIS HIPS Work Step	Description
10. Create work surface	The pre-checked data were used to calculate a CUBE (Combined Uncertainty and Bathymetric Estimator) surface.
11. Surface filter using CUBE	The CUBE algorithm creates a hypothesis for the depth value of a grid cell from the first depth value that falls into a cell. Every following depth value is checked against this hypothesis and according to a variety of settings selected to contribute to the existing hypothesis, to create a new, second hypothesis or to be rejected. A most probable surface is resulting from these calculations. This surface is then used as a base for a surface filter, for which a data window of acceptance around this surface has to be specified using certain parameters. The survey data is then checked against these conditions. Data outside the specified window of acceptance were rejected.
12. Create quality control surfaces	New base surfaces are calculated to check the result. Having undergone these procedures, the data is in a final state for delivery. Contour calculation was achieved by using Fugro Starfix Workbench.
13. Quality control	The data quality is mainly checked using the standard deviation, density (hit count), TVU/THU and visual bathymetry inspection. Local anomalies are removed manually or by a locally applied filter.
14. Data export	As a deliverable from HIPS a gridded dataset is produced and exported as ASCII files.

Note 1:

TVU and THU values were calculated using Caris HIPS&SIPS taking into account all contributing factors applicable for the vessels.

TVU and THU are defined as follows by the IHO Standards for Hydrographic Surveys (S-44), 6th Edition:

- Total horizontal uncertainty (THU): Component of total propagated uncertainty (TPU) calculated in the horizontal dimension. THU is a two-dimensional quantity with all contributing horizontal measurement uncertainties included. Total propagated uncertainty (TPU): Three-dimensional uncertainty with all contributing measurement uncertainties included;
- Total vertical uncertainty (TVU): Component of total propagated uncertainty (TPU) calculated in the vertical dimension. TVU is a one-dimensional quantity with all contributing vertical measurement uncertainties included;
- Uncertainty: Estimate characterising the range of values within which the true value of a measurement is expected to lie as defined within a particular confidence level. It is expressed as a positive value.

5.2.3   Data Interpretation

MBES gridded data were exported to GeoTiff format with 0.25 m resolution to complement interpretation of the seafloor sediments, substrate and morphology. Also, it was used in determining the position of the seafloor targets during the SSS data interpretation in SonarWiz.

The intensity of acoustic reflectivity data such as backscatter and SSS is represents the type and grain size of the sediments present on the seabed. It allows distinction between different substrates and identification of certain morphologies (e.g. small-scale structures) and benthic habitats. A semi-automatic classification was performed in ArcMap on the backscatter,

FUGRO

bathymetry, and their derivative datasets, and successively validated by correlation with the collected grab samples. The semi-automatic classification involves image analysis of backscatter, bathymetry and bathymetric derivatives based on the object identification (Object-Based Image Analysis). Each analysed image is segmented into objects based on the shape of the clusters, their spatial correlation, and the homogeneity within the clusters.

The results of the semi-automatic classification were manually revised. MBES, backscatter and SSS data were used to cross-check and refine the identified boundaries between the various sediment types, and grab samples were used for ground-truthing where available.

The semi-automatic classification is quantitative, repeatable, comparable, more objective, and less time-consuming than the manual interpretation. The semi-automatic approach makes the methodology repeatable, without overlooking the contribution of expert knowledge to the production of the final sediment and morphological map.

5.3 Backscatter

5.3.1 Data Quality

Backscatter data are of high quality for the entire site. The backscatter mosaic was generated after finalisation of the bathymetry point cloud. Local backscatter anomalies associated with the nadir beams of the MBES could not be fully resolved during backscatter processing. The artefacts were amplified using Dual Swath which significantly increases the amount of energy in the water column. The subtle presence of nadir is typically visible on the flat and featureless seabed (Figure 5.2).
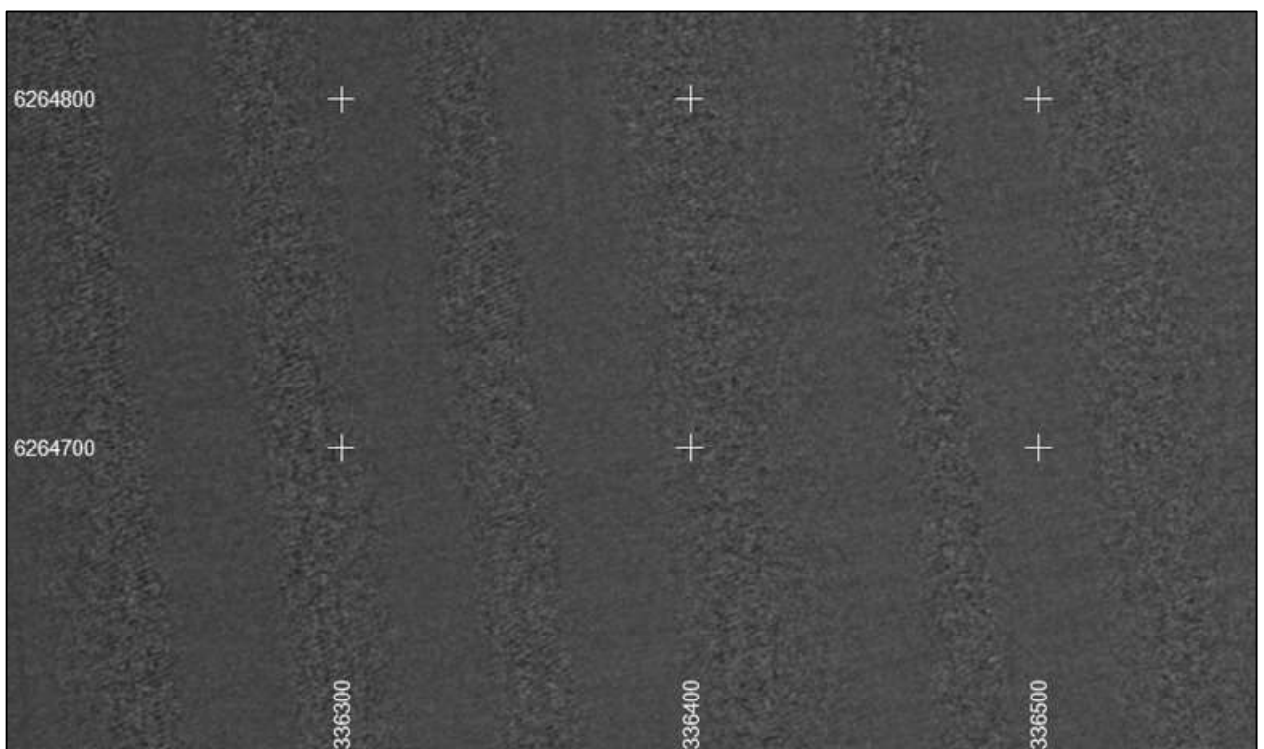
Figure 5.2: OWF Zone West site backscatter, highlighting subtle nadir striping on flat seafloor

5.3.2　Data Processing

Backscatter data collected by the MBES were processed by using Caris HIPS&SIPS (Version 11.3/11.4). Data were initially divided in blocks alike the bathymetry. All blocks were recombined into a single, site-wide 0.5 m backscatter surface.

5.3.3　Data Interpretation

Backscatter data (grid cell size 0.5 m) was imported as raster into a GIS database and used for the seafloor sediments and substrate type classifications. For more detail refer to section 5.2.3.

5.4　Side Scan Sonar

5.4.1　Data Quality

The SSS data quality was monitored throughout the survey and was within the specifications throughout the OWF Zone West site. A localised thermocline affected the far-range areas of the SSS data. This occurred mostly within the northern part of the site where water depths were approximately 29 m – 35 m. The affected segments were clipped and additional SSS infills were run to acquire good quality SSS data coverage in the affected areas. Overall, 200% SSS data coverage including nadir was achieved except for a few areas in the eastern and northern part of the site where 100% coverage was accepted and planned infills were deemed not required by Energinet. The plots presenting areas of 100%, 200% and ≥ 300% coverage were exported from SonarWiz and are included in the GIS deliverables.

During the marginal weather SSS data were observed to be affected by tugging on the cable which manifests as striping artefacts visible in the data. The striping artefacts were observed predominantly within the most western part of the site and were greatly reduced as they survey progressed towards east. The striping artefacts were discussed with the Onboard Client Representatives and if the presence of the striping did not impede the target picking, the data were accepted.

The spatial accuracy achieved for SSS sensor aided by USBL positioning was within +/- 2.0 m. Minimum detected target dimension requirement of 0.5 m in any dimension was met within all survey blocks.

5.4.2　Data Processing

SSS data were recorded in digital formats (.jsf and .xtf) using EdgeTech Discover software.

The .xtf files were imported into Chesapeake SonarWiz software for quality control and subsequent data analysis and interpretation. Each line was checked on import for navigation artefacts and coverage and infills were planned as necessary. Following the Fugro standard procedures, gains were applied using EGN table to normalise the amplitude of a reflected signal across the range. The accuracy of the USBL positioning was carefully assessed throughout the survey by comparing targets observed on reciprocal lines.

FUGRO

For more details on SSS processing procedures refer to Operations Report (*F176286-REP-OPS-001 (02)*).

5.4.3   Data Interpretation

Individual lines were checked on a line-by-line basis for sonar targets and other features in a waterfall display, which provides the highest resolution display of the data. Target picking started offshore as the survey proceeded and was continued later in the office.

A high-frequency dataset was used for the purpose of target picking. Upon the completion of SSS data acquisition for each block, the data were reviewed and polygons marking the boulder fields were drawn in SonarWiz. Individual target picking was conducted outside of the defined boulder fields. SSS targets of at least 1.0 m in any dimension were picked and rationalised against each other (i.e., the same target may be picked from two or more lines) and then checked against MBES data. If a target (e.g., a boulder) had recognisable relief on the DTM, its position was adjusted to the more accurately georeferenced DTM. The rationalisation initially took place in SonarWiz and was finalised in ArcMap. As a result, the target position between SonarWiz and GIS deliverables might differ. Positions in TSG are the final ones.

Targets were assigned the confidence level based on the following criteria:

- Low - target observed on only one SSS line;
- Medium - target observed on multiple SSS lines and/or MBES data;
- High - target confirmed with the background data (i.e. infrastructure, wreck).

Finally, sidescan sonar targets were verified against database information (e.g., known wrecks and other seafloor features) and against the magnetometer data.

SSS mosaics were used to complement the MBES and backscatter datasets during the seafloor features and sediments interpretation.

5.5   Magnetometer

5.5.1   Data Quality

The magnetometer data were acquired along the survey lines except for cross lines orientated in approximately west-east direction. The magnetometer data quality was monitored throughout the survey and was deemed to be of high quality. Noisy data sections were flagged by the offline team and further confirmed by Fugro QHD processors. Infills were planned and acquired where necessary. OCR also reviewed the data quality and noise interference in the magnetometer data. Several areas of strong background geological noise were observed within the site.

Generally, the data were free from noise and therefore within the specified noise levels (±1 nT). The noise level in the magnetic data was constantly monitored to achieve the required specifications. Sections of noisy data were flagged, analysed, and infills were

acquired where necessary. Sparker noise was removed by applying narrow linear filter to the raw magnetic field acquired along the 2D-UUHR survey lines. Several areas were found to be associated with strong geological background noise, occasionally exceeding 2 nT amplitude. These areas were observed across the site except for the shallowest part in the north. An additional QC was conducted where the signal strength value dropped below 100: in none of the cases the magnetic field showed evidence of being distorted or affected.

As single magnetometer was being used during the survey, the coverage was assessed along each line within specified survey blocks of the site. The magnetometer was towed at a consistent altitude of less than 5.0 m (mostly 3 m) above the seafloor, throughout the survey. Any areas where the altitude was outside of this permitted range were removed from the magnetometer gridded dataset. Infills were planned and completed except for the fishing gear areas and a few areas in the eastern and northern part of the site where planned infills were deemed not required by Energinet.

5.5.2   Data Processing

The navigational data were merged with raw magnetometer data in Fugro Starfix VBA Proc processing software and exported as a single ASCII file per line. The position of the magnetometer was calculated by applying offset from the USBL beacon to the magnetometer sensor. In VBA Proc, USBL beacon positions were manually de-spiked, and after applying offsets to the magnetometer, the navigation was interpolated. Where an USBL gap exceeded 10 seconds, the magnetic data were not considered, and an infill was planned.

The required cut-off altitude value was 5 m for most of the site with the exception of the fishing gear areas where the cut-off altitude was 7 m. All the magnetic data with an altitude greater than 5 m (7 m inside fishing gear areas) were masked out from the calculation of the residual grid. Outliers (data spikes) in altimeter readings were removed manually. Resultant gaps of up to 30 fiducials were interpolated.

Due to extensive presence of the fishing gear during the first weeks of acquisition, Energinet granted a concession for altitude gaps occurring for the following reasons:

- Altitude exceeds 5.0 m (up to 5.5 m) for less than 100 m outside the fishing gear areas;
- Altitude exceeds 5.0 m within the fishing gear areas;
- Altitude exceeds 5.0 m on run-in/ run-out from the fishing gear areas.

The fishing gear areas were shifted several times during the survey. The overview in Figure 5.3 presents the cumulative area of approximately 173 km^2 within the site where the fishing gear was observed.
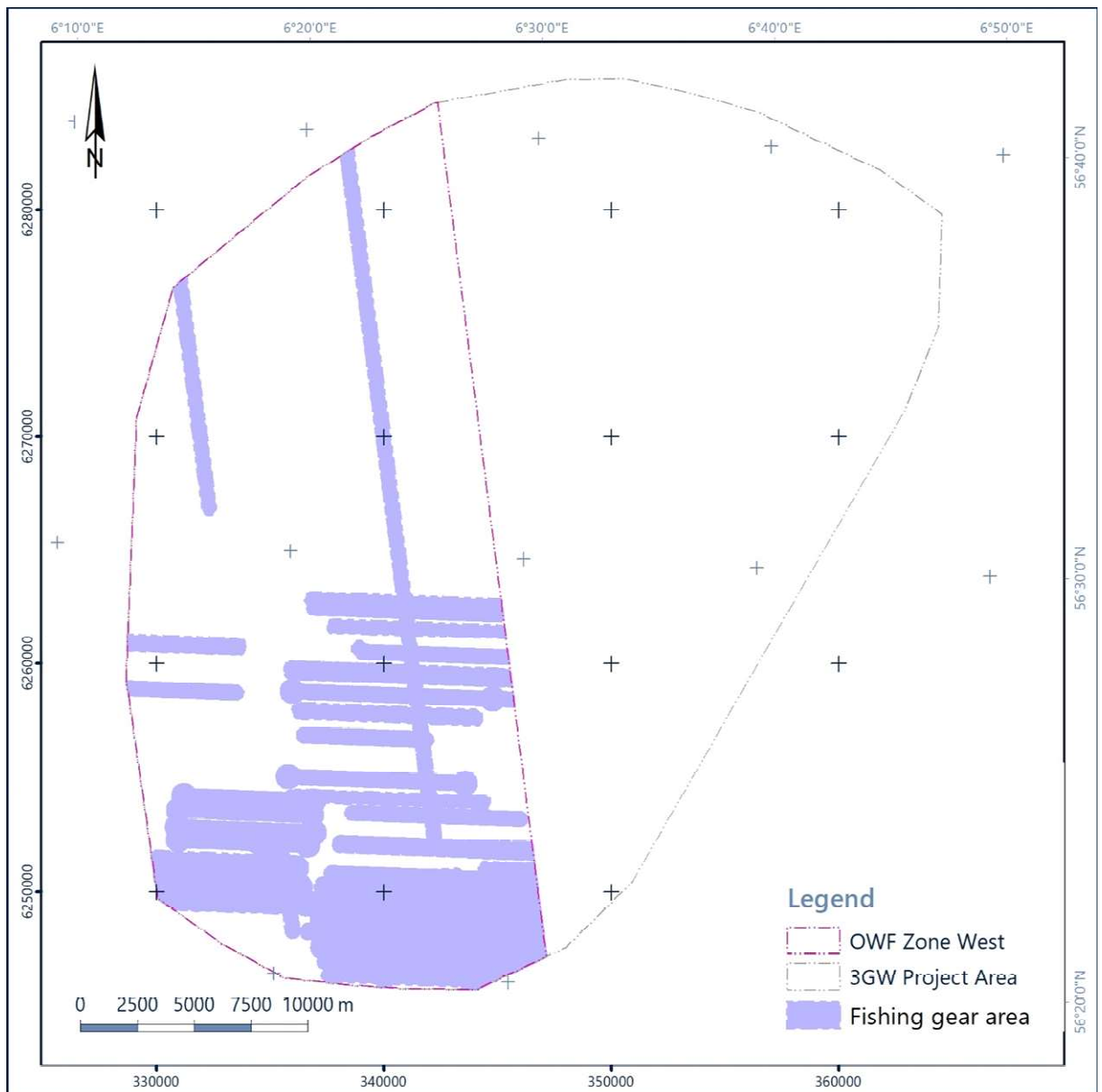
Figure 5.3: Overview of the fishing gear areas in the OWF Zone West site.

Spikes in the magnetometer data were manually removed and magnetometer data were not interpolated but replaced by a dummy which was not displayed in the profile or plan view. High-frequency and low-amplitude noise was removed from the despiked magnetometer data by applying a B-spline filter.

Long-wavelength variations in the magnetic field were removed in order to isolate the shorter wavelengths which make up the residual magnetic field. After de-spiking and noise removal, as described above, the sequence of non-linear filters was applied to the magnetometer data in order to obtain a magnetic residual field representing any ferrous or magnetic objects on the seafloor or at shallow burial depth.

5.5.3   Data Interpretation

Magnetometer data were processed and interpreted using Oasis Montaj software.

The magnetometer target picking was performed using the Blakely test method on the analytical signal grid with a cut-off value of 3 nT/m. Duplicates from the automatically picked targets were removed and the remaining target was manually measured on the magnetic residual field. This was done to remove targets smaller than 10 nT peak-to-peak amplitude as well as to avoid targets being picked multiple times due to their complexity. Magnetometer target positions were moved either to the centre of the maximum inflection points (dipoles), the highest point of the residual peak-to-peak value (monopoles) or anomaly midpoints (complex anomalies).

5.6 Parametric Sub-Bottom Profiler

5.6.1 Data Quality

SBP data quality was monitored throughout the survey and generally deemed to be high. The technical requirements of the survey with regards to resolution, penetration and trigger rate were met throughout the survey. Penetration varied across the survey area depending on the geology, however in general a minimum penetration of 10 m below seafloor was achieved as per technical requirements with a maximum observed penetration of approximately 25 m. Vertical data resolution was 0.3 m as per the specification requirements. Ping rate was monitored with respect to vessel speed during real-time survey to avoid multiple effect in SBP data.

Positioning of the SBP data was checked to ensure that it remained within the project specification of +/- 1 m. Features present within the survey site were used to check the SBP positioning against the MBES and SSS data.

Although data quality of sub-bottom profiler was generally good for the entire survey, some lines exhibited vertical noise and cavitation caused by marginal weather conditions. During the 2D-UUHR survey, the electrical/sparker noise was visible. These noise artefacts were reduced using burst noise removal during processing. Interpretability is not affected by this noise as it is only apparent as vertical artefacts in the data that are dissimilar to real reflectors. Areas of cavitation in sub-bottom profiler data were assessed with collaboration of OCR. Reruns were completed when required except for a few areas in the eastern and northern part of the site where planned infills were deemed not required by Energinet.

5.6.2 Data Processing

The SBP data were logged using SESWIN software recording files in .ses3 format. Vessel heave at the SBP transducer location was recorded and applied during the acquisition. The recorded .ses3 files were converted to .sgy format and processed in RadExPro. Processing steps applied offshore consisted of:

- Amplitude correction to compensate for spherical spreading and anelastic losses during the propagation of acoustic waves;
- Bandpass filtering to remove noise from the data (Butterworth filter 5000 Hz – 15000 Hz);
- Burst noise removal to remove exceptionally high amplitudes from the data.

Subsequently, the .sgy files were imported into IHS Kingdom software, where navigation was checked for artefacts and data quality was assessed. Where extensive cavitation due to bad weather occurred, data was consulted with the Onboard Client Representative and infills were planned as required.

Processing of the SBP data continued in the office where the following processing was done:

- Tide and draft correction;
- Automatic seabed pick;
- Time–depth conversion;
- Correctly formatted text header inserted into .sgy files.

The result of automated seabed pick was injected into byte 61–64 in .sgy files and imported into IHS Kingdom as a horizon, where it was compared with seismic and MBES data. For the time–depth conversion a two-layer model was used, separating water column and subsurface, with sound velocities of 1481 m/s up to 1509 m/s for the water column (varying between lines based on the average of the water column profiles as measured by the SVP) and 1600 m/s for the shallow soils, respectively.

5.6.3 Data Interpretation

The following strategy was applied for SBP data interpretation:

- Compiling historical geotechnical, geophysical and geological data from client-provided sources and Fugro database as well as from available literature;
- Interpretation of seismically distinct units and horizons in the time-domain, verified by available historical shallow geotechnical data and literature;
- Identification and interpretation of key geological features, which can be potential hazards (geohazards) for offshore infrastructure;
- Time–depth conversion of horizons and geological features by the utility of a two-layer velocity model, identical to the velocity model applied to the SBP data;
- Gridding (and contouring) of soil unit boundaries/horizons in metres BSF and in metres below MSL; isochore unit thicknesses in metres.

The following needs to be considered for the SBP data:

- The line spacing for the SBP data was 62.5 m. Potential features smaller than this distance may not have been detected where present in between seismic lines;
- Gridding of horizons was performed within IHS Kingdom Suite 2020. All gridding was done with the 'flex gridding' algorithm and parameters were kept the same among all SBP horizons. The cell size was set to 5 m by 5 m. The search distance was set to 50 m, to make sure there were no gaps in the grids due to line spacing variations. Minimum curvature was applied, and smoothness was set to halfway (6).

FUGRO

5.7 Multichannel 2D-UUHR Seismic

5.7.1 Data Quality

2D-UUHR (MCS) data quality was monitored throughout the survey and generally deemed to be high. The technical requirements of the survey with regards to resolution were met throughout the survey for the entire site. Penetration was achieved to at least 100 m below seafloor. Vertical resolution at or near the seabed is better than 0.3 m and approximately 0.7 m at about 100 m below seabed. This resolution range is achieved through a processed data bandwidth of 200 Hz to 3400 Hz with a dominant frequency of approximately 1500 Hz at or near the seafloor.

Positioning of the 2D-UUHR data (MCS) was checked to ensure that it remained within the project specification of +/- 7 m for 95% of the line. Infills / reruns were run for the sections of the lines / complete lines as and when required to adhere with the required survey specification and deemed data quality. OCR was involved for respective data acceptance of the survey blocks.

Although data quality of 2D-UUHR (MCS) data was generally good for the entire survey blocks, some lines had vertical noise and cavitation caused by marginal weather condition acquisitions. This noise was reduced during further processing.

Some lines had noise at bottom of the stacks, which was caused by overlapping of the shots due to high vessel speed. These shots were muted during processing.

5.7.2 Data Processing

Detailed description of the processing flow applied to the 2D-UUHR seismic data collected during the survey is presented in the seismic processing report (F176286-REP-PROC-001 (01)) attached to the Operations Report (F176286-REP-OPS-001 (02)).

5.7.3 Data Interpretation

The following strategy was applied for 2D-UUHR data interpretation:

- Compiling historical geotechnical, geophysical and geological data from client-provided sources and Fugro database as well as from available literature;
- Interpretation of seismically distinct units and horizons in the time-domain, verified by available historical shallow geotechnical data and literature;
- Identification and interpretation of key geological features, which can be potential hazards (geohazards) for offshore infrastructure;
- Time–depth conversion of horizons, grids and geological features used the RMS velocities, which were picked as stacking velocities. For more details see the seismic processing report (F176286-REP-PROC-001);
- Where a horizon is not picked, it is interpreted to be not present;

FUGRO

- In the areas where horizon H70 is interpreted to be deeper than the maximum depth of penetration of the seismic data, the horizon is picked at the base of the available seismic profile;
- Gridding (and contouring) of soil unit boundaries/horizons in metres BSF and in metres below MSL; isochore unit thicknesses in metres.

The following needs to be considered for the 2D-UUHR data:

- The quality of the 2D-UUHR data was good with a typical penetration depth of 200 m MSL;
- The line spacing for the 2D-UUHR data is 250 m. Potential features smaller than this distance may not be detected where present in between seismic lines;
- Gridding of horizons was performed within IHS Kingdom Suite 2020. All gridding was done with the 'flex gridding' algorithm and parameters were kept the same among all 2D-UUHR horizons. The cell size was 5 m by 5 m. Polygons were used to limit the extent of the produced grids. The search distance was set to 150 m, to make sure there were no gaps in the grids due to line spacing variations. Minimum curvature was applied, and smoothness was set to halfway (6).

5.8   Grab Samples

Grab samples were collected at the agreed locations within the OWF Zone West site. Each sample was weighed, as per specification, with a minimum of 3 kg of sediment collected per grab.

Initial visual analysis was recorded, and high-resolution photographic images were taken of each sample. The grab samples were sealed and stored in separate boxes to maintain the integrity of each sample and for safety during transit. Samples were offloaded during a port call at the soonest opportunity and transported to the onshore geotechnical lab for further, in-depth analysis.

All the grab samples were analysed in the laboratory. The results of the organic matter content and particle size distribution tests are supplied as part of the final deliverables.

Based on the results of the laboratory testing, the grab samples were classified following the Danish standard (Larsen et al., 1995). For the purpose of seafloor sediment classification GEUS terminology was required (Leth, J.O. (ed.) et al., 2014: Danmarks digitale havbundssedimentkort 1:250.000).

5.9   Automatic Boulder Picking

Due to large number of boulders observed in the SSS data automatic boulder picking was performed using Fugro developed tool – GAIA.Automation. This section details the processing routine and analysis of the results.

The aim of the automatic boulder picking is to produce a boulder density map presenting spatial distribution of the boulder fields. To achieve this objective Fugro performed the following:

1. All accepted SSS data were processed using the automatic boulder picking tool.
2. The output picks were deduplicated and filtered.
3. Final QC and manual cleaning of the filtered results was performed, and density map was created.

GAIA.Automation workflow can be broken down into 4 steps:

- Processing and merging correct navigation with the SSS data (.xtf);
- Automatic target picking using artificial intelligence (AI). Output file (.shp) contains point features;
- Determination and application of optimal filtering to increase picking accuracy;
- Analysis and interpretation of targets and boulder field distribution.

5.9.1 Automatic Target Picking

Once all the .xtf files are merged with processed navigation, computation starts, and targets are automatically picked by AI within the GAIA.Automation software. This process forms the underlying basis of the complete workflow.

The software can process multiple input files at the same time and performs calculations on a file-by-file basis.

Once completed, a GIS compatible shapefile file containing all targets and their coordinates, dimensions and areas is generated from the software.

Details of the automatic picking process described below:

- The AI algorithm is based on 'machine learning' (ML) developed over the past number of years on sample datasets collected across the world;
- Being a computationally heavy tool, .xtf files and the resulting shapefiles are stored and analysed in the cloud;
- All targets are then automatically generated, and their specific attributes measured:
  - Targets with a shadow extending out of the SSS range are assigned a height value of -999;
  - If the AI picking algorithm did not detect a shadow at all, the value will be 0.

An example of the raw output from the automatic boulder picking tool with all measured attributes is presented in Figure 5.4.
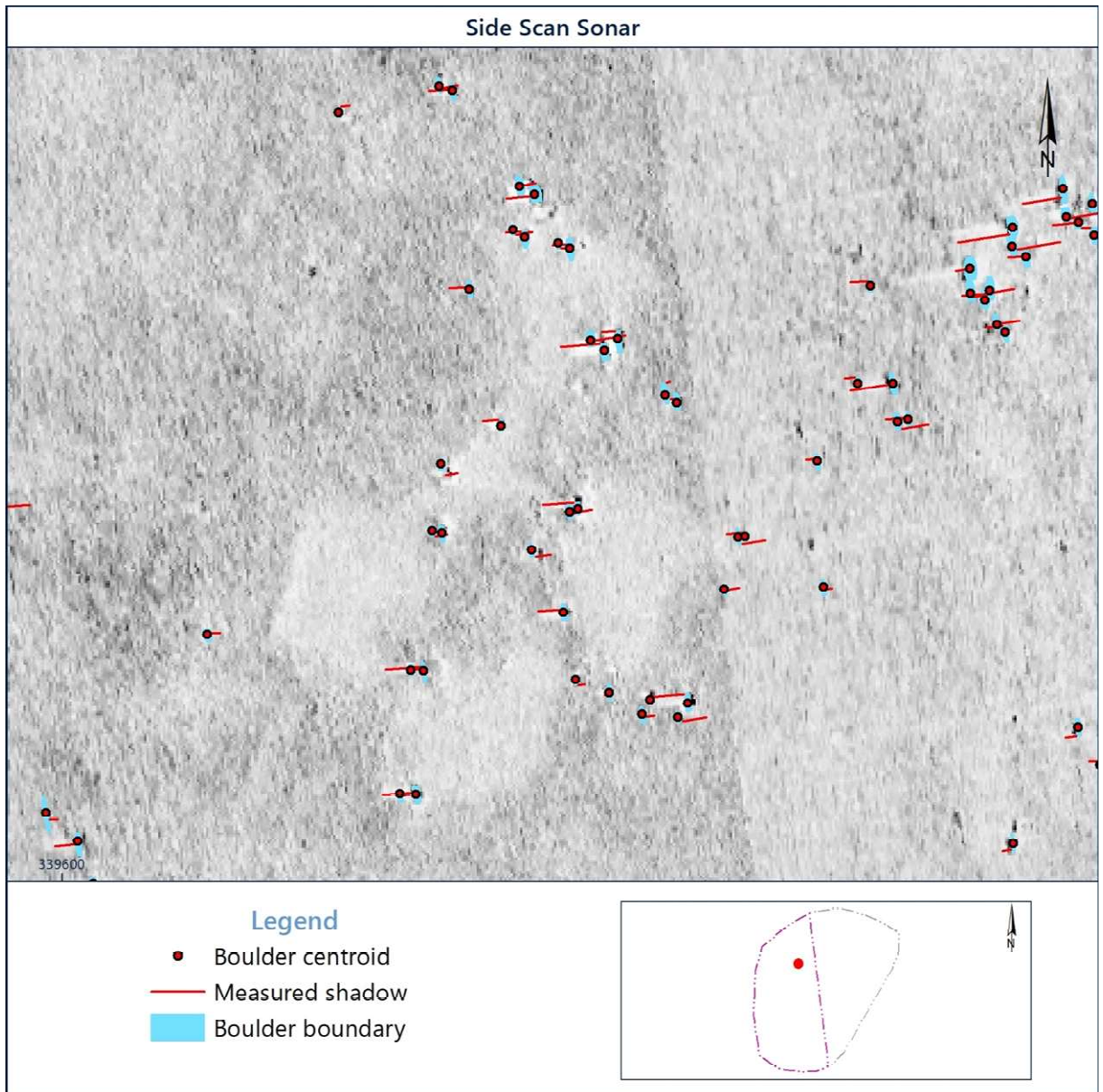
Figure 5.4: Unfiltered results of the automatic boulder picking tool.

5.9.2 Filtering

The output shapefile is automatically generated and initially contains a number of false picked targets (i.e., double picked targets and false positives) depending primarily on the original data quality. As such, deduplication and application of a robust set of filters ensures the presentation of more representative results. Ultimately, the filter settings selected are chosen to balance the over-picking and under-picking of targets whilst keeping in mind the aims of the project – creating boulder density map.

Particular attention is paid to the following filter options:

- Confidence level

- Confidence level is a default output of the AI algorithm. Values range from 0 to 1, with values near 1 representing targets that match well with the AI's machine learned datasets.
- Dimensions
  - Length and width (calculated on the pixel area occupied by the specific target);
  - Height (calculated from the fish altitude and the shadow length of the target);
  - Filtering by dimensions minimises the errors induced by noise and other data artefacts.

Where there is an overlap between the adjacent side scan sonar lines, targets are required to be deduplicated. The targets are deduplicated by considering only one line in case of coverage overlap. The line used is the line visible in the side scan mosaic (i.e., the line appearing on top when constructing the side scan mosaic).

5.9.3 Creating Density Map

Fugro's default method for the visualisation and analysis of the high number of resulting targets is through the creation of a density map.

To be able to quickly estimate the boulder distribution, density and average dimension can have an important role in site planning, i.e., micro-rerouting of a cable, planning of geotechnical, environmental or UXO operations.

In summary, the density map offers:

- Instant overview of target distribution;
- Precise estimation of the number of targets per m^2;
- Improved data-driven interpretation.

The density map is produced using a method called Kernel Density Estimation (KDE). In mathematical terms, it is a non-parametric method that attempts to describe population distribution (in this case on how the target are spread) based on a finite number of data samples (the picked targets).

Another key aspect of this method is that the result will not include artefacts related to a fixed searching distance (resolved by using a kernel). Various distribution models can be used (Figure 5.5). The natural distribution of targets is not properly represented using a 'tophat' kernel, motivating the use of a 'gaussian' kernel.
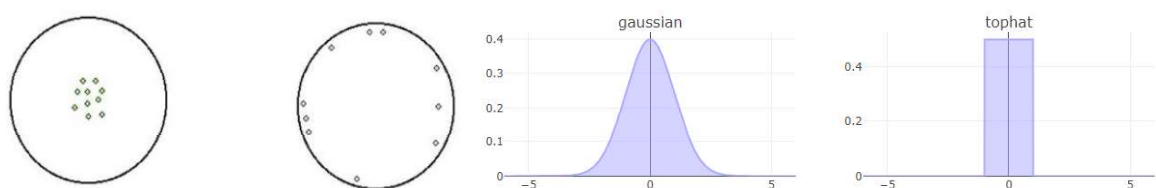
Figure 5.5: Gaussian and 'tophat' distribution model.

5.9.4   Results

Processing of the OWF Zone West site dataset was performed as per the processing flow detailed in the sections above.

To improve the accuracy of the final density map and distribution of boulder fields, two sets of the filtering parameters were applied – one set corresponding to areas where boulder polygons were defined manually and another one for the remaining part of the site. This division allowed to use less conservative filtering in areas where numerous boulders where observed. More conservative approach outside the boulder polygons allowed to remove several false picks related to data artefacts and seabed features other than targets (i.e. ripple marks).

For the purpose of defining the filtering parameters a subset of SSS data including lines spread across the site was used. Based on the statistical analysis of the target attributes provided in the output shapefile, three attributes were selected to guide the filtering:

- Area – picks measuring more than 1.0 m^2 in size were mostly related to false picks within areas of ripple marks outside of boulder polygons. Few real targets of that size were observed inside the boulder polygons and these were kept by setting a high threshold for confidence level;
- Confidence – high confidence is assigned to targets which match well with the AI's machine learned datasets;
- Length and Height – generally, the smaller the height, the higher confidence level is required to validate the pick.

The Table 5.2 presents the filtering parameters defined for the OWF Zone West site dataset.

Table 5.2: Filtering parameters for automatic boulder picking results within the OWF Zone West site.

Inside Boulder Polygons	Outside Boulder Polygons
No modifications done to the target attributes prior to filtering	All targets with **height ≤ 0.1 m** had **confidence lowered by 0.03**
- Targets with the **area ≥ 1.02** require **confidence ≥ 0.98** - Targets with **confidence ≤ 0.85** OR **length ≤ 0.5 m** are removed	- Only the targets with the **area ≤ 1.02** AND **confidence ≥ 0.75** are kept - Targets with the **height ≤ 0.2 m** require **confidence ≥ 0.86** - Targets with the **height ≤ 0.1 m** require **confidence ≥ 0.97**

Once the filtering was completed for the entire dataset, the density map was created at 5 m resolution, using 'kernel density approximation' with a bandwidth of 25 m. The bandwidth influences the overall smoothness of the grid. Its value was chosen based on the expectation of the smoothness of the target distribution. The default unit for the density map is a number of boulders found in an area of 10 m x 10 m. For the purpose of charting and data examples

FUGRO

the density was recalculated to represent number of boulders in an area of 100 m x 100 m according to the requirements.

Although a certain number of predominantly small targets would have been missed in the computation, the general distribution and density of targets were observed to have been preserved.

Most of false picks were observed to occur at features such as ripple marks and edges of the trawl scars. While the AI algorithm is untrained to account for such features, carefully adjusted filtering parameters removed many false picks related to the ripple marks (Figure 5.6). As a result, no false boulder fields were identified within ripple marks areas.
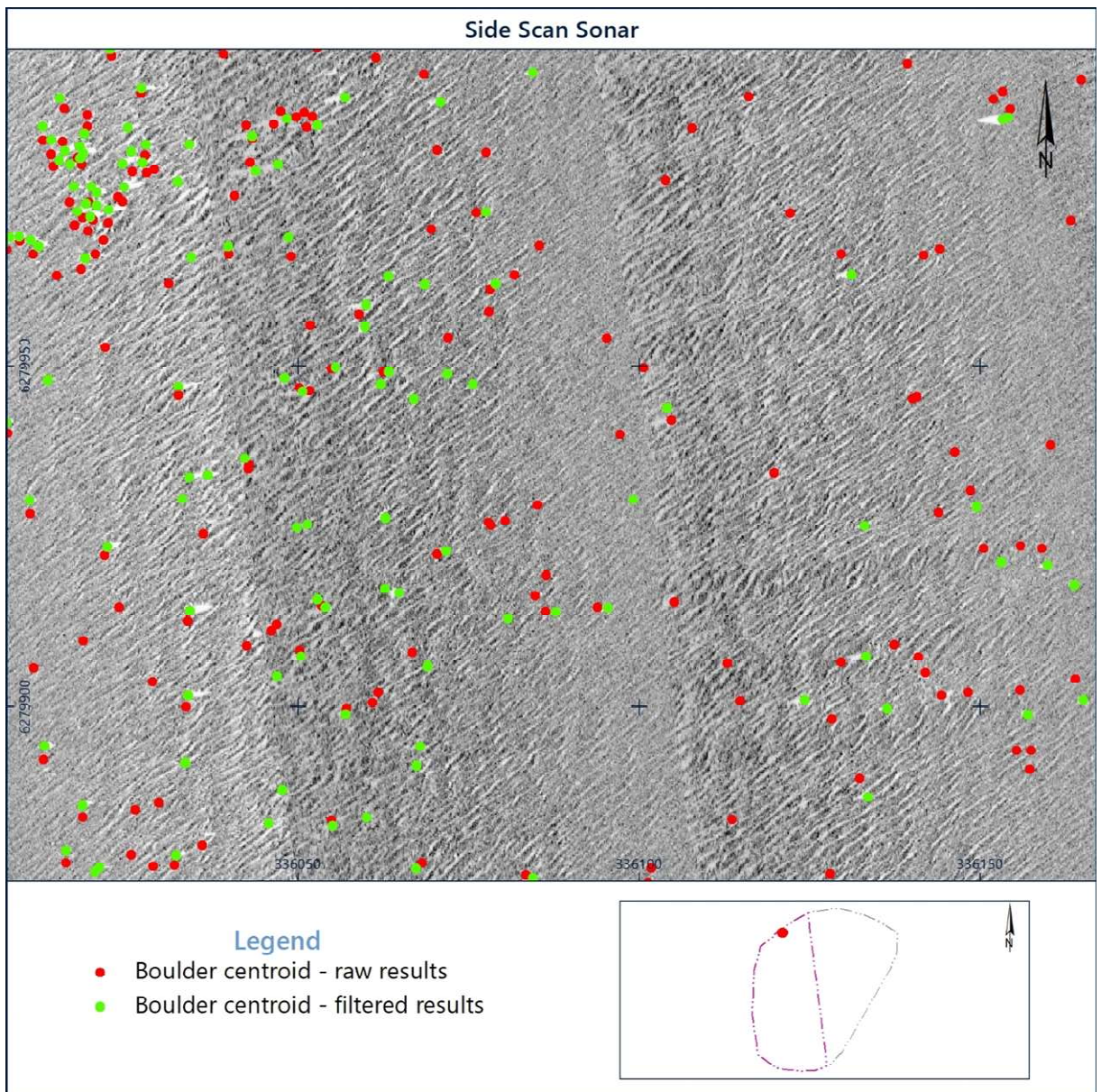
Figure 5.6: Comparison between raw and filtered results of automatic boulder picking tool within the area of ripple marks.

Removing false picks related to trawl scars has proven to be more complicated and, on several occasions, required manual deleting of the picks as they were creating false boulder fields visible in the density map (Figure 5.7).
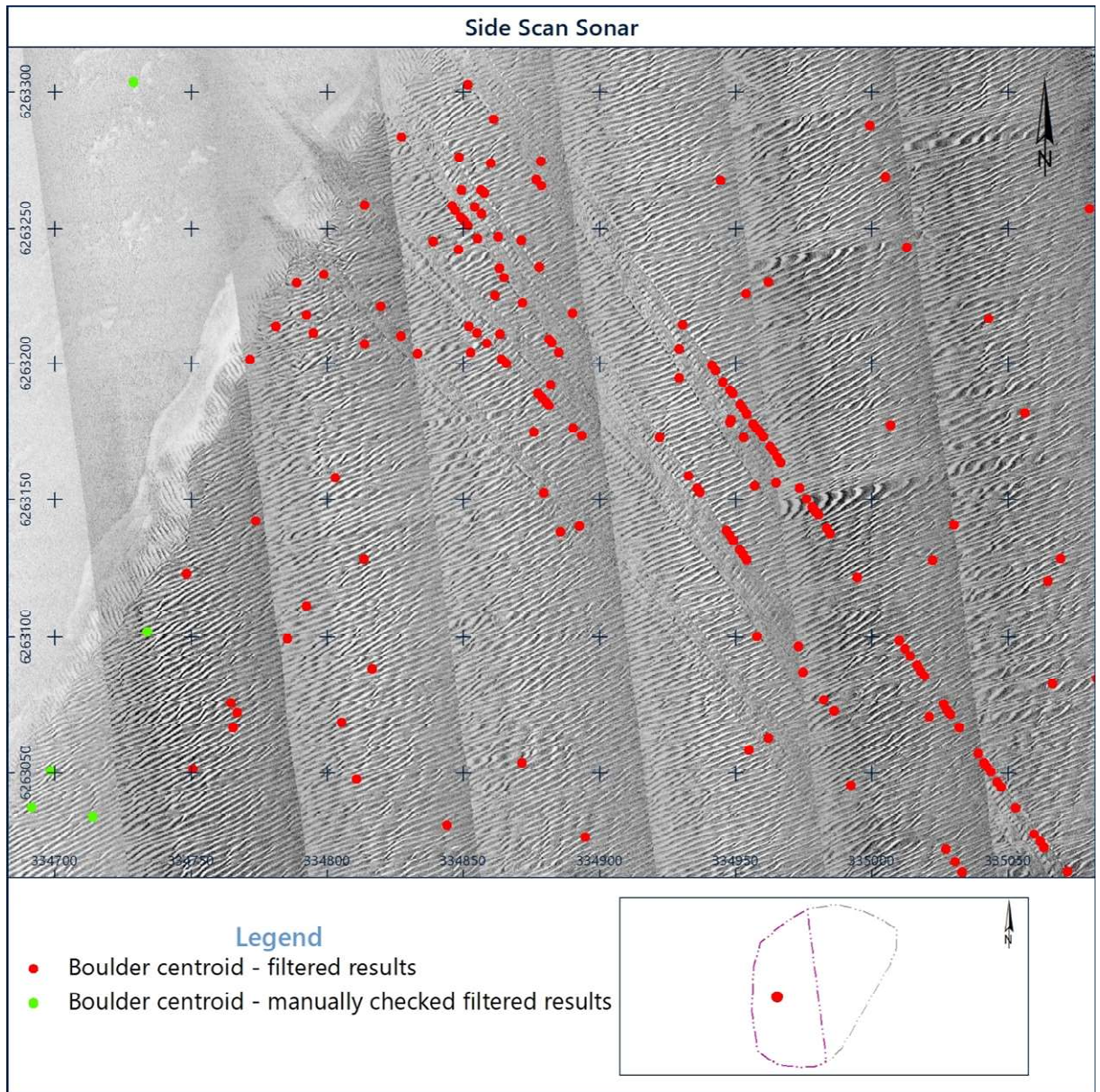
Figure 5.7: Example of an area with trawl marks where false picks were not filtered out and had to be removed manually from the automatic boulder picking tool results.

Lastly, the manually defined boulder polygons were compared with the final density map created from the automatic picking results. Both datasets match very well with very few differences observed (Figure 4.27 and Figure 4.28). Mismatches are mainly caused when:

- An area contains numerous small boulders. Automatic tool recognizes it as a boulder field, while the interpreter decided to pick the targets ≥ 1.0 m manually rather than drawing a boulder polygon (Figure 5.8);

- Boulder density within the area varies, i.e., patches of very low density are surrounded by high density fields. Automatic tool provides precise contours and separates the area into different fields, while the interpreter decided to draw one larger polygon (Figure 5.9).
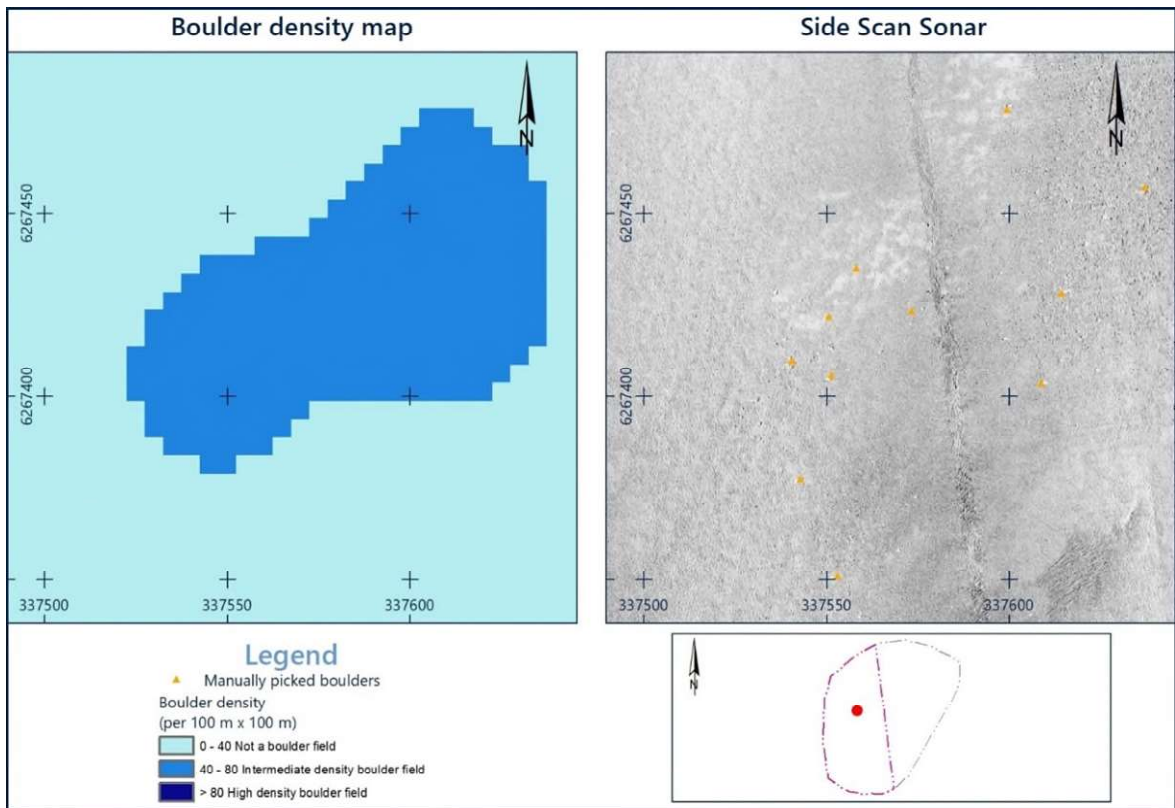
Figure 5.8: Intermediate density boulder field recognized by the automatic boulder picking tool but not defined during manual interpretation.
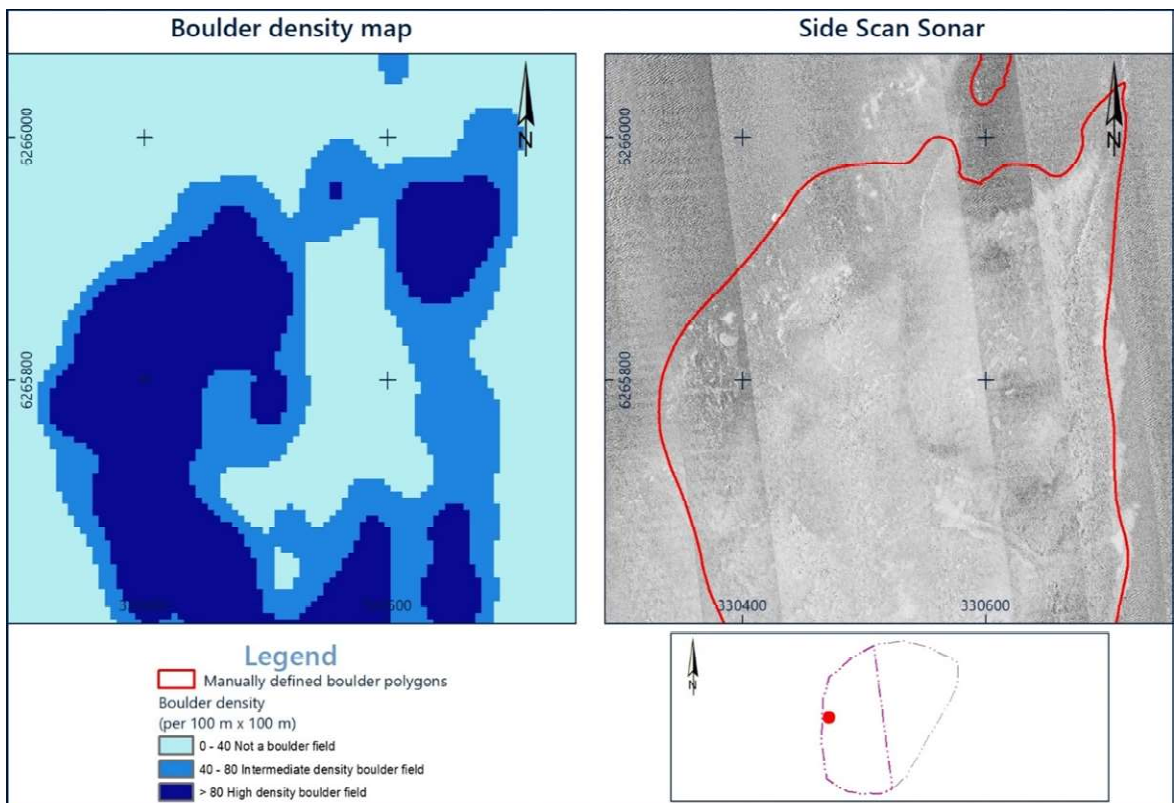
Figure 5.9: Boulder field overestimated in size during the manual interpretation.

6.   References

COWI. (2021). Thor Offshore Wind Farm; Integrated Geological Model (A205839).

Danish Råstofbekendtgørelsen (BEK no. 1680 of 17/12/2018, Phase IB). Received from Energinet as part of the Scope of Services.

Erkens, G., Hoffmann, T., Gerlach, R., and Klostermann, J. (2011). Complex fluvial response to Lateglacial and Holocene allogenic forcing in the Lower Rhine Valley (Germany). *Quaternary Science Reviews 30*(5-6), 611-627. https://doi.org/10.1016/j.quascirev.2010.11.019

Fyfe, J.A. 1986. Fisher, Sheet 56°N 02°E, Quaternary Geology. Keyworth: British Geological Survey, 1:250 000 Series.

GEUS and Orbicon. (2010). Marin råstof- og naturtypekortlægning i Nordsøen, 2010. Naturstyrelsen.

Gibbard, P.L., and Lewin, J. (2016). Filling the North Sea Basin: Cenozoic sediment sources and river styles. *Geologica Belgica, 19*(3-4), 201-217. http://dx.doi.org/10.20341/gb.2015.017

Huuse, M., and Lykke-Andersen, H. (2010a). Large-scale glaciotectonic thrust structures in the eastern Danish North Sea. In Maltman, A.J., Hubbard, B., and Hambrey, M.J. (Eds.), *Deformation of Glacial Material* (pp. 293-305). Geological Society, London, Special Publications, 176.

Huuse, M., and Lykke-Andersen, H. (2000b). Overdeepened Quaternary valleys in the eastern Danish North Sea: morphology and origin. *Quaternary Science Reviews, 19*, 1233-1253. https://doi.org/10.1016/S0277-3791(99)00103-1

Jeffery, D.H., Laban, C., Mesdag, C.S. and Schüttenhelten, R.T.E. 1991. Dogger, Sheet 55°N 02°E, Quaternary Geology. Keyworth: British Geological Survey and Haarlem: Rijks Geologische Dienst, 1:250 000 Series.

Jensen, J.B., Gravesen, P., and Lomholt, S. (2008). Geology of outer Horns Rev, Danish North Sea. *Geological Survey of Denmark and Greenland Bulletin, 15*. 41-44. https://doi.org/10.34194/geusb.v15.5040

Kirkham, J.D., Hogan, K.A., Larter, R.D., Self, E., Games, K., Huuse, M., Stewart, M.A., Ottesen, D., Arnold, N.S., and Dowdeswell, J.A. (2021). Tunnel valley infill and genesis revealed by high-resolution 3-D seismic data. *Geology, 49(12)*, 1516-1520. *https://doi.org/10.1130/G49048.1*

Larsen, B., and Andersen, L.T. (2005). Late Quaternary stratigraphy and morphogenesis in the Danish eastern North Sea and its relation to onshore geology. *Netherlands Journal of Geosciences, 84*(2), 113-128. https://doi.org/10.1017/S0016774600023003

Leth, J.O. (1996). Late Quaternary geological development of the Jutland Bank and the initiation of the Jutland Current, NE North Sea. *NGU Bulletin, 430*, 25-34. https://hdl.handle.net/11250/2674130

MMT. (2021). North Sea OWF and Energy Islands, Geophysical Survey Report, Report No.: 103783-ENN-MMT-SUR-REP-SURVWPA, Rev.2, dated 13 December 2021, reported to Energinet.

Overeem, I., Weltje, G.J., Bishop-Kay, C., and Kroonenberg, S.B. (2001). The Late Cenozoic Eridanos delta system in the Southern North Sea Basin: a climate signal in sediment supply? *Basin Research, 13*, 293-312. https://doi.org/10.1046/j.1365-2117.2001.00151.x

Peuchen, J. and Westgate Z. (2018). Defining geotechnical parameters for surface-laid subsea pile-soil interaction, In Hicks, Pisanò and Peuchen (Eds), *Cone Penetration Testing 2018* (pp. 519-524), CRC Press, Delft University.

Ramboll. (2021). Energy Island; Danish North Sea, Geoarchaeological and Geological Desk Study, Document No.: 1100046209 -1526721553-4, dated 19 April 2021, reported to Energinet.

Appendices

FUGRO

Appendix A

Guidelines on Use of Report

This report (the "Report") was prepared as part of the services (the "Services") provided by Fugro for its client (the "Client") and in accordance with the terms of the relevant contract between the two parties (the Contract") and to the extent to which Fugro relied on Client or third-party information as was set out in the Contract.

Fugro's obligations and liabilities to the Client or any other party in respect of this Report are limited to the extent and for the time period set out in the Contract (or in the absence of any express provision in the Contract as implied by the law of the Contract) and Fugro provides no other representation or warranty whether express or implied, in relation to the use of this Report, for any purpose. Furthermore, Fugro has no obligation to update or revise this Report based on any future changes in conditions or information which emerge following issue of this Report unless expressly required by the provisions of the Contract.

This Report was formed and released by Fugro exclusively for the Client and any other party expressly identified in the Contract, and any use and/or reliance on the Report or the Services for purposes not expressly stated in the Contract, will be at the Client's sole risk. Any other party seeking to rely on this Report does so wholly at its own and sole risk and Fugro accepts no liability whatsoever for any such use and/or reliance."

Appendix B

Charts

FUGRO

Charts (detailed below) have been presented as a separate PDF file.

Chart Type	Chart Name
OVERVIEW CHART	SN2021_013_EnergyIsland_OWF_Lot2_01_NU_250k_OVERVIEW
CRP TRACKS AND GRAB SAMPLE LOCATION CHART	SN2021_013_EnergyIsland_OWF_Lot2_02_NU_25k_CRP_GRAB
CRP TRACKS AND GRAB SAMPLE LOCATION CHART	SN2021_013_EnergyIsland_OWF_Lot2_03_NU_25k_CRP_GRAB
SHADED RELIEF BATHYMETRY CHART	SN2021_013_EnergyIsland_OWF_Lot2_04_NU_25k_SHR_BTY
SHADED RELIEF BATHYMETRY CHART	SN2021_013_EnergyIsland_OWF_Lot2_05_NU_25k_SHR_BTY
BACKSCATTER MOSAIC CHART	SN2021_013_EnergyIsland_OWF_Lot2_06_NU_25k_BKS
BACKSCATTER MOSAIC CHART	SN2021_013_EnergyIsland_OWF_Lot2_07_NU_25k_BKS
SEAFLOOR CLASSIFICATION - GEOLOGY CHART	SN2021_013_EnergyIsland_OWF_Lot2_08_NU_25k_SBC_GEOLOGY
SEAFLOOR CLASSIFICATION - GEOLOGY CHART	SN2021_013_EnergyIsland_OWF_Lot2_09_NU_25k_SBC_GEOLOGY
SEAFLOOR CLASSIFICATION - MORPHOLOGY CHART	SN2021_013_EnergyIsland_OWF_Lot2_10_NU_25k_SBC_MORPHOLOGY
SEAFLOOR CLASSIFICATION - MORPHOLOGY CHART	SN2021_013_EnergyIsland_OWF_Lot2_11_NU_25k_SBC_MORPHOLOGY
SEAFLOOR CLASSIFICATION - SUBSTRATE TYPE CHART	SN2021_013_EnergyIsland_OWF_Lot2_12_NU_25k_SBC_SUBSTRATE
SEAFLOOR CLASSIFICATION - SUBSTRATE TYPE CHART	SN2021_013_EnergyIsland_OWF_Lot2_13_NU_25k_SBC_SUBSTRATE
SEABED OBJECTS CHART	SN2021_013_EnergyIsland_OWF_Lot2_14_NU_25k_SBO
SEABED OBJECTS CHART	SN2021_013_EnergyIsland_OWF_Lot2_15_NU_25k_SBO
SEABED FEATURES CHART	SN2021_013_EnergyIsland_OWF_Lot2_16_NU_25k_SBF
SEABED FEATURES CHART	SN2021_013_EnergyIsland_OWF_Lot2_17_NU_25k_SBF
DEPTH TO HORIZON H10 (METRES BSF) - BASE OF UNIT U10	SN2021_013_EnergyIsland_OWF_Lot2_18_NU_25k_SBG_BSF_H10
DEPTH TO HORIZON H10 (METRES BSF) - BASE OF UNIT U10	SN2021_013_EnergyIsland_OWF_Lot2_19_NU_25k_SBG_BSF_H10
DEPTH TO HORIZON H20 (METRES BSF) - BASE OF UNIT U20	SN2021_013_EnergyIsland_OWF_Lot2_20_NU_25k_SBG_BSF_H20
DEPTH TO HORIZON H20 (METRES BSF) - BASE OF UNIT U20	SN2021_013_EnergyIsland_OWF_Lot2_21_NU_25k_SBG_BSF_H20
DEPTH TO HORIZON H24 (METRES BSF) - BASE OF UNIT D24	SN2021_013_EnergyIsland_OWF_Lot2_22_NU_25k_SBG_BSF_H24
DEPTH TO HORIZON H24 (METRES BSF) - BASE OF UNIT D24	SN2021_013_EnergyIsland_OWF_Lot2_23_NU_25k_SBG_BSF_H24
DEPTH TO HORIZON H30 (METRES BSF) - BASE OF UNIT U30	SN2021_013_EnergyIsland_OWF_Lot2_24_NU_25k_SBG_BSF_H30
DEPTH TO HORIZON H30 (METRES BSF) - BASE OF UNIT U30	SN2021_013_EnergyIsland_OWF_Lot2_25_NU_25k_SBG_BSF_H30

Chart Type	Chart Name
DEPTH TO HORIZON H31 (METRES BSF) - BASE OF UNIT U31	SN2021_013_EnergyIsland_OWF_Lot2_26_NU_25k_SBG_BSF_H31
DEPTH TO HORIZON H31 (METRES BSF) - BASE OF UNIT U31	SN2021_013_EnergyIsland_OWF_Lot2_27_NU_25k_SBG_BSF_H31
DEPTH TO HORIZON H35 (METRES BSF) - BASE OF UNIT U35	SN2021_013_EnergyIsland_OWF_Lot2_28_NU_25k_SBG_BSF_H35
DEPTH TO HORIZON H35 (METRES BSF) - BASE OF UNIT U35	SN2021_013_EnergyIsland_OWF_Lot2_29_NU_25k_SBG_BSF_H35
DEPTH TO HORIZON H69 (METRES BSF) – INTERNAL HORIZON IN UNIT U70	SN2021_013_EnergyIsland_OWF_Lot2_30_NU_25k_SBG_BSF_H69
DEPTH TO HORIZON H69 (METRES BSF) - INTERNAL HORIZON IN UNIT U70	SN2021_013_EnergyIsland_OWF_Lot2_31_NU_25k_SBG_BSF_H69
DEPTH TO HORIZON H70 (METRES BSF) - BASE OF UNIT U70	SN2021_013_EnergyIsland_OWF_Lot2_32_NU_25k_SBG_BSF_H70
DEPTH TO HORIZON H70 (METRES BSF) - BASE OF UNIT U70	SN2021_013_EnergyIsland_OWF_Lot2_33_NU_25k_SBG_BSF_H70
DEPTH TO HORIZON H75 (METRES BSF) - BASE OF UNIT U75	SN2021_013_EnergyIsland_OWF_Lot2_34_NU_25k_SBG_BSF_H75
DEPTH TO HORIZON H75 (METRES BSF) - BASE OF UNIT U75	SN2021_013_EnergyIsland_OWF_Lot2_35_NU_25k_SBG_BSF_H75
DEPTH TO HORIZON H90 (METRES BSF) - BASE OF UNIT U90	SN2021_013_EnergyIsland_OWF_Lot2_36_NU_25k_SBG_BSF_H90
DEPTH TO HORIZON H90 (METRES BSF) - BASE OF UNIT U90	SN2021_013_EnergyIsland_OWF_Lot2_37_NU_25k_SBG_BSF_H90
DEPTH TO HORIZON H10 (METRES MSL) - BASE OF UNIT U10	SN2021_013_EnergyIsland_OWF_Lot2_38_NU_25k_SBG_MSL_H10
DEPTH TO HORIZON H10 (METRES MSL) - BASE OF UNIT U10	SN2021_013_EnergyIsland_OWF_Lot2_39_NU_25k_SBG_MSL_H10
DEPTH TO HORIZON H20 (METRES MSL) - BASE OF UNIT U20	SN2021_013_EnergyIsland_OWF_Lot2_40_NU_25k_SBG_MSL_H20
DEPTH TO HORIZON H20 (METRES MSL) - BASE OF UNIT U20	SN2021_013_EnergyIsland_OWF_Lot2_41_NU_25k_SBG_MSL_H20
DEPTH TO HORIZON H24 (METRES MSL) - BASE OF UNIT D24	SN2021_013_EnergyIsland_OWF_Lot2_42_NU_25k_SBG_MSL_H24
DEPTH TO HORIZON H24 (METRES MSL) - BASE OF UNIT D24	SN2021_013_EnergyIsland_OWF_Lot2_43_NU_25k_SBG_MSL_H24
DEPTH TO HORIZON H30 (METRES MSL) - BASE OF UNIT U30	SN2021_013_EnergyIsland_OWF_Lot2_44_NU_25k_SBG_MSL_H30
DEPTH TO HORIZON H30 (METRES MSL) - BASE OF UNIT U30	SN2021_013_EnergyIsland_OWF_Lot2_45_NU_25k_SBG_MSL_H30
DEPTH TO HORIZON H31 (METRES MSL) - BASE OF UNIT U31	SN2021_013_EnergyIsland_OWF_Lot2_46_NU_25k_SBG_MSL_H31
DEPTH TO HORIZON H31 (METRES MSL) - BASE OF UNIT U31	SN2021_013_EnergyIsland_OWF_Lot2_47_NU_25k_SBG_MSL_H31

FUGRO

Chart Type	Chart Name
DEPTH TO HORIZON H35 (METRES MSL) - BASE OF UNIT U35	SN2021_013_EnergyIsland_OWF_Lot2_48_NU_25k_SBG_MSL_H35
DEPTH TO HORIZON H35 (METRES MSL) - BASE OF UNIT U35	SN2021_013_EnergyIsland_OWF_Lot2_49_NU_25k_SBG_MSL_H35
DEPTH TO HORIZON H69 (METRES MSL) - INTERNAL HORIZON IN UNIT U70	SN2021_013_EnergyIsland_OWF_Lot2_50_NU_25k_SBG_MSL_H69
DEPTH TO HORIZON H69 (METRES MSL) - INTERNAL HORIZON IN UNIT U70	SN2021_013_EnergyIsland_OWF_Lot2_51_NU_25k_SBG_MSL_H69
DEPTH TO HORIZON H70 (METRES MSL) - BASE OF UNIT U70	SN2021_013_EnergyIsland_OWF_Lot2_52_NU_25k_SBG_MSL_H70
DEPTH TO HORIZON H70 (METRES MSL) - BASE OF UNIT U70	SN2021_013_EnergyIsland_OWF_Lot2_53_NU_25k_SBG_MSL_H70
DEPTH TO HORIZON H75 (METRES MSL) - BASE OF UNIT U75	SN2021_013_EnergyIsland_OWF_Lot2_54_NU_25k_SBG_MSL_H75
DEPTH TO HORIZON H75 (METRES MSL) - BASE OF UNIT U75	SN2021_013_EnergyIsland_OWF_Lot2_55_NU_25k_SBG_MSL_H75
DEPTH TO HORIZON H90 (METRES MSL) - BASE OF UNIT U90	SN2021_013_EnergyIsland_OWF_Lot2_56_NU_25k_SBG_MSL_H90
DEPTH TO HORIZON H90 (METRES MSL) - BASE OF UNIT U90	SN2021_013_EnergyIsland_OWF_Lot2_57_NU_25k_SBG_MSL_H90
GEOLOGICAL FEATURES CHART	SN2021_013_EnergyIsland_OWF_Lot2_58_NU_25k_GEOF
GEOLOGICAL FEATURES CHART	SN2021_013_EnergyIsland_OWF_Lot2_59_NU_25k_GEOF
Seabed Geology Cross-Section Profile	SN2021_013_EnergyIsland_OWF_Lot2_60_PR_25k_SBP_2DUUHR
Seabed Geology Cross-Section Profile	SN2021_013_EnergyIsland_OWF_Lot2_61_PR_25k_SBP_2DUUHR
Seabed Geology Cross-Section Profile	SN2021_013_EnergyIsland_OWF_Lot2_62_PR_25k_SBP_2DUUHR
Seabed Geology Cross-Section Profile	SN2021_013_EnergyIsland_OWF_Lot2_63_PR_25k_SBP_2DUUHR
Seabed Geology Cross-Section Profile)	SN2021_013_EnergyIsland_OWF_Lot2_64_PR_25k_SBP_2DUUHR
Seabed Geology Cross-Section Profile)	SN2021_013_EnergyIsland_OWF_Lot2_65_PR_25k_SBP_2DUUHR
Seabed Geology Cross-Section Profile)	SN2021_013_EnergyIsland_OWF_Lot2_66_PR_25k_SBP_2DUUHR
Seabed Geology Cross-Section Profile	SN2021_013_EnergyIsland_OWF_Lot2_67_PR_25k_SBP_2DUUHR
Seabed Geology Cross-Section Profile)	SN2021_013_EnergyIsland_OWF_Lot2_68_PR_25k_SBP_2DUUHR
Seabed Geology Cross-Section Profile	SN2021_013_EnergyIsland_OWF_Lot2_69_PR_25k_SBP_2DUUHR
Seabed Geology Cross-Section Profile	SN2021_013_EnergyIsland_OWF_Lot2_70_PR_25k_SBP_2DUUHR
Seabed Geology Cross-Section Profile	SN2021_013_EnergyIsland_OWF_Lot2_71_PR_25k_SBP_2DUUHR
Seabed Geology Cross-Section Profile	SN2021_013_EnergyIsland_OWF_Lot2_72_PR_25k_SBP_2DUUHR
Seabed Geology Cross-Section Profile	SN2021_013_EnergyIsland_OWF_Lot2_73_PR_25k_SBP_2DUUHR
Seabed Geology Cross-Section Profile	SN2021_013_EnergyIsland_OWF_Lot2_74_PR_25k_SBP_2DUUHR
Seabed Geology Cross-Section Profile	SN2021_013_EnergyIsland_OWF_Lot2_75_PR_25k_SBP_2DUUHR
Seabed Geology Cross-Section Profile	SN2021_013_EnergyIsland_OWF_Lot2_76_PR_25k_SBP_2DUUHR
Seabed Geology Cross-Section Profile	SN2021_013_EnergyIsland_OWF_Lot2_77_PR_25k_SBP_2DUUHR
Seabed Geology Cross-Section Profile	SN2021_013_EnergyIsland_OWF_Lot2_78_PR_25k_SBP_2DUUHR

FUGRO

Appendix C
Digital Deliverables

Deliverable Type	Sensor	Deliverable ID	Deliverable Content	Format
Final Deliverable	MBES	01	Un-gridded Soundings	XYZ
Final Deliverable	MBES	02	Gridded data, 0.25 m	ASCII XYZ
Final Deliverable	MBES	03	Gridded data, 0.25 m	GeoTIFF
Final Deliverable	MBES	04	Gridded data, 1.00 m	ASCII XYZ
Final Deliverable	MBES	05	Gridded data, 1.00 m	GeoTIFF
Final Deliverable	MBES	06	Gridded data, 5.00 m	ASCII XYZ
Final Deliverable	MBES	07	Gridded data, 5.00 m	GeoTIFF
Final Deliverable	MBES	08	Bathymetric Contours (0.5 m)	Vector Geodatabase
Final Deliverable	MBES	09	Bathymetry Vessel Tracks	Vector Geodatabase
Final Deliverable	MBES	10	TVU (1.00 m)	ASCII XYZ
Final Deliverable	MBES	11	TVU (1.00 m)	GeoTIFF
Final Deliverable	MBES	12	THU (1.00 m)	ASCII XYZ
Final Deliverable	MBES	13	THU (1.00 m)	GeoTIFF
Final Deliverable	MBES	14	Backscatter	GeoTIFF
Final Deliverable	SVP	15	Processed data	xlsx
Final Deliverable	MBES	16	Target List	Vector Geodatabase
Final Deliverable	SSS	17	HF XTF Files	XTF
Final Deliverable	SSS	18	LF XTF Files	XTF
Final Deliverable	SSS	19	Navigation Files	CSV
Final Deliverable	SSS	20	SSS instrument tracks	Vector Geodatabase
Final Deliverable	SSS	21	SSS Target List	Vector Geodatabase
Final Deliverable	SSS	21a	Target Catalogue	xlsx
Final Deliverable	SSS	22	SonarWiz Projects	
Final Deliverable	MAG	23	MAG measurements	CSV
Final Deliverable	MAG	24	MAG instrument tracks	Vector Geodatabase

Deliverable Type	Sensor	Deliverable ID	Deliverable Content	Format
Final Deliverable	MAG	25	MAG Anomaly target list	Vector Geodatabase
Final Deliverable	SBP & 2DUHRS data	26a	Processed SBP recordings	SEGY
Final Deliverable	SBP & 2DUHRS data	26b	Processed UHRS recordings	SEGY
Final Deliverable	SBP & 2DUHRS data	26c	Velocity model UHRS	SEGY
Final Deliverable	SBP & 2DUHRS data	27a	Processed SBP recordings	PDF
Final Deliverable	SBP & 2DUHRS data	27b	Processed UHRS recordings	PNG
Final Deliverable	SBP & 2DUHRS data	28	SBP and UHRS instrument tracks	Vector Geodatabase
Final Deliverable	SBP & 2DUHRS data	29	SBP and UHRS Anomaly target list	Vector Geodatabase
Final Deliverable	SBP & 2DUHRS data	30	Interpretation of the processed seismic data	CSV
Final Deliverable	SBP & 2DUHRS data	31a	Generated elevation grids relative to vertical datum for each interpreted horizon in 5 m resolution	GeoTIFF
Final Deliverable	SBP & 2DUHRS data	31b	Generated elevation grids relative to vertical datum for each interpreted horizon in 5 m resolution	ASCII XYZ
Final Deliverable	SBP & 2DUHRS data	32a	Generated depth below seabed (BSB) grids for each interpreted horizon in 5 m resolution	GeoTIFF
Final Deliverable	SBP & 2DUHRS data	32b	Generated depth below seabed (BSB) grids for each interpreted horizon in 5 m resolution	ASCII XYZ
Final Deliverable	SBP & 2DUHRS data	33a	Generated Isochore (layer thickness) grids for each interpreted soil unit in 5 m resolution	GeoTIFF
Final Deliverable	SBP & 2DUHRS data	33b	Generated Isochore (layer thickness) grids for each interpreted soil unit in 5 m resolution	ASCII XYZ

Deliverable Type	Sensor	Deliverable ID	Deliverable Content	Format
Final Deliverable	SBP & 2DUHRS data	34	Kingdom project	v2020
Final Deliverable	Grab sampling data	35	Grab sample positions	Vector Geodatabase
Final Deliverable	Grab sampling data	36	Grab sample classification	xlsx
Final Deliverable	Grab sampling data	37	Grab sample laboratory analysis	xlsx
Final Deliverable	Integrated seabed interpretation data	38	Seabed Surface Geology, as polygons	Vector Geodatabase
Final Deliverable	Integrated seabed interpretation data	39	Seabed Surface Point Features	Vector Geodatabase
Final Deliverable	Integrated seabed interpretation data	40	Seabed Surface Line Features	Vector Geodatabase
Final Deliverable	Integrated seabed interpretation data	41	Seabed Surface Polygon Features	Vector Geodatabase
Final Deliverable	Integrated seabed interpretation data	42	Seabed Substrate type	Vector Geodatabase
Final Deliverable	Integrated seabed interpretation data	43	Man-Made-Objects	Vector Geodatabase
Final Deliverable	Integrated seabed interpretation data	44	Man-Made-Objects	Vector Geodatabase
Final Deliverable	Integrated seabed interpretation data	45	Man-Made-Objects	Vector Geodatabase
Final Deliverable	Report	46	Operations Report	PDF
Final Deliverable	Report	47	Geophysical site survey Report (charts as enclosures)	PDF